

2011

## The Design and Synthesis of Molecular Imaging Probes Using A Novel Peptide Hormone Ghrelin

Mark Steven McFarland

Follow this and additional works at: <https://ir.lib.uwo.ca/digitizedtheses>

---

### Recommended Citation

McFarland, Mark Steven, "The Design and Synthesis of Molecular Imaging Probes Using A Novel Peptide Hormone Ghrelin" (2011). *Digitized Theses*. 3556.  
<https://ir.lib.uwo.ca/digitizedtheses/3556>

This Thesis is brought to you for free and open access by the Digitized Special Collections at Scholarship@Western. It has been accepted for inclusion in Digitized Theses by an authorized administrator of Scholarship@Western. For more information, please contact [wlsadmin@uwo.ca](mailto:wlsadmin@uwo.ca).

THE UNIVERSITY OF WESTERN ONTARIO

**The Design and Synthesis of Molecular Imaging Probes Using A Novel Peptide Hormone Ghrelin**

CERTIFICATE OF EXAMINATION

**(Spine title: The Design and Synthesis of Ghrelin Molecular Imaging Probes)**

(Thesis format: Monograph)

by Dr. Robert Fiedler

Dr. Robert Fiedler

**Mark Steven McFarland**

Dr. Robert Fiedler

Graduate Program in Chemistry

*The Design*

A thesis submitted in partial fulfillment  
of the requirements for the degree of  
Master of Science

The Design and Synthesis of Molecular Imaging Probes Using A Novel

School of Graduate and Postdoctoral Studies  
The University of Western Ontario  
London, Ontario, Canada

© Mark Steven McFarland 2011

Chair of the Thesis Examination Panel

THE UNIVERSITY OF WESTERN ONTARIO  
SCHOOL OF GRADUATE AND POSTDOCTORAL STUDIES

**CERTIFICATE OF EXAMINATION**

Supervisor:

Examiners:

\_\_\_\_\_  
Dr. Leonard G. Luyt

\_\_\_\_\_  
Dr. Robert Hudson

\_\_\_\_\_  
Dr. Michael Kerr

\_\_\_\_\_  
Dr. Dwayne Jackson

The thesis by

**Mark Steven McFarland**

entitled:

**The Design and Synthesis of Molecular Imaging Probes Using A Novel  
Peptide Hormone Ghrelin**

is accepted in partial fulfillment of the  
requirements for the degree of  
Master of Science

Date \_\_\_\_\_

\_\_\_\_\_  
Chair of the Thesis Examination Board

## Abstract

Ghrelin is a 28-amino acid peptide hormone that was first discovered in 1999 by Kojima *et al.* Recently, we have developed molecular imaging agents using ghrelin analogues that selectively target the growth hormone secretagogue receptor 1a (GHSR-1a). This is accomplished by placing the imaging component at either the C-terminus of the peptide through a pendant lysine side-chain, or through modification of the Ser-3 residue. Receptor binding assays confirmed that fluorescein ghrelin(1-18) ( $IC_{50} = 9.5$  nM) and non-radioactive fluorine and gallium containing ghrelin analogues ( $IC_{50} = 2.88 - 65$  nM) bound to the GHSR-1a with high affinity. Fluorescein ghrelin(1-18) demonstrated high uptake in the human prostate cancer cell lines PC-3 and LNCaP, as well as *ex vivo* human prostate cancer tissue. This work supported the development of a radiolabelling strategy for incorporating gallium-68 and fluorine-18 into modified ghrelin, for use in PET nuclear imaging.

Keywords: GHSR-1a, Ghrelin, Fluorine-18, Gallium-68, Prostate Cancer, Molecular

Imaging

## Statement of Co-Authorship

Chapter 2: The work presented in this chapter was in collaboration with Dr. Savita Dhanvantari and Dr. John Lewis, Assistant Professors in Medical Biophysics from the University of Western Ontario. The author of this thesis was responsible for the design and synthesis of all analogues contained in this chapter. In the case where the author was not conducting the experiments, credit is given to the appropriate collaborator. Ms. Jill McTavish, an undergraduate student under the supervision of Dr. Dhanvantari, was responsible for conducting the binding assay experiments for all analogues in Table 4 as well as western blot analysis on tissues. Ms. Vanessa Rota, Dr. Dhanvantari's lab technician, was responsible for the serum stability studies in Table 4. The author did contribute to the serum studies by optimizing a C-18 sep-pack procedure, integrating UV HPLC traces and plotting the information on excel. Ms. Rebecca McGir, Dr. Dhanvantari's lab technician, carried out live cell imaging, tissue microscopy and analyzed data.

Dr. Chen Lu, a visiting medical resident working under the supervision of Dr. John Lewis, conducted all imaging experiments with prostate cells lines and *ex vivo* prostate tissue. The Translational Prostate Cancer Research Group conducted pathological analysis for the *ex vivo* prostate tissue study.

Chapter 3: All work presented in this chapter was done solely by the author with the exception of determining the binding affinities for ghrelin analogues in Table 3.3. This was done in collaboration with Dr. Savita Dhanvantari, an Assistant Professor in Medical Biophysics from the University of Western Ontario. Ms. Jill McTavish, a

summer student, and Ms. Vanessa Rota, a lab technician, conducted the binding assay experiments and determined the IC-50 values.

Chapter 4: All work presented in this chapter was done solely by the author with the exception of determining the binding affinities for ghrelin analogues in Table 4.6 and 4.8. This was done in collaboration with Dr. Savita Dhanvantari, an Assistant Professor in Medical Biophysics from the University of Western Ontario. Ms. Jill McTavish, a summer student, and Ms. Vanessa Rota, a lab technician, conducted the binding assay experiments and determined the IC-50 values.

## Acknowledgements

To all who have supported, guided and shared scientific thought over the past two years, thank you. Your input and advice has been invaluable to my success as a student and has allowed me to achieve goals, which I had never thought were possible.

Thank you to Dr. Len Luyt, who has always supported, advised and challenged me. Thank you for giving me the confidence in this “come back” season. I would also like to thank my collaborators and their students: Dr. Savita Dhanvantari, Dr. John Lewis and Dr. Mike Kovacs, for their commitment and valuable input into our project.

A special thanks to the past and present Luyt lab members for their continual support, encouragement, and friendship. All of you have made the last two years a lot easier when chemistry was being chemistry...

Thank you to all my family and friends, for listening and supporting me through the last two years, but above all Mich, for always being there, I couldn't have achieved this without you.

## Table of Contents

CERTIFICATE OF EXAMINATION .....	ii
Abstract .....	iii
Statement of Co-Authorship .....	iv
Acknowledgements .....	vi
Table of Contents .....	vii
List of Tables .....	xi
List of Figures and Illustrations .....	xiii
List of Schemes .....	xvi
List of Abbreviations and Symbols .....	xviii
Introduction .....	1
1.1 Introduction to Molecular Imaging .....	1
1.2 Designing Peptide Based Imaging Probes .....	4
1.3 Fmoc Solid Phase Peptide Synthesis .....	7
1.4 Positron Emission Tomography .....	10
1.5 Radioisotopes used in PET Nuclear Imaging .....	11
1.6 Fluorescence Microscopy .....	14
1.7 Scope of Thesis .....	16
Chapter Two: The Design, Synthesis, and Application of a Fluorescein Labeled Ghrelin Analogue .....	19
2.1 Methods in Diagnosing Early Stage Prostate Cancer .....	19
2.2 Introduction to Imaging G-Protein Coupled Receptors .....	21
2.3 Imaging the Growth Hormone Secretagogue Receptor-1a (GHSR-1a) .....	22
2.3.1 Incorporating an Optical Imaging Agent into a Modified Ghrelin Peptide....	28
2.4 Results and Discussion .....	29
2.4.1 Serum Stability Studies on Ghrelin Analogs .....	33
2.4.2 Binding Assays .....	33
2.4.3 Imaging Probe Studies in Cell and Fixed Tissue .....	35



2.5 Conclusions.....	40
2.6 Experimental.....	41
2.6.1 Materials and Equipment.....	41
2.6.2 General Procedure for Peptide Assembly.....	41
2.6.3 General Procedure for Selective Deprotection's and Resin Cleavage .....	42
2.6.4 [Dpr <sup>3</sup> (Octanoic acid)][Lys <sup>19</sup> (Fluorescein)]ghrelin(1-19)-amide (2.21) .....	43
2.6.5 [Dpr <sup>3</sup> (Octanoic acid)] ghrelin(1-18)-amide (2.22) .....	44
2.6.6 Receptor Binding Assays.....	44
2.6.7 Serum Stability Study <sup>83</sup> .....	45
2.6.8 Tissue Expression of GHSR-1a <sup>83</sup> .....	45
2.6.9 Binding of Fluorescein-ghrelin to heart tissue in situ <sup>83</sup> .....	46
2.6.10 Evaluation of Fluorescein-ghrelin in PC3, LNCaP, and BPH cell lines .....	46
2.6.11 Evaluation of Fluorescein-ghrelin in ex vivo prostate samples <sup>86</sup> .....	47
2.6.12 Quantitative Analysis for ghrelin analogue binding <sup>86</sup> .....	48
 Chapter Three: The Design and Synthesis of a Gallium-68 Labelled Ghrelin Analogue	
for PET Nuclear Imaging.....	49
3.1 Introduction.....	49
3.1.1 The Design and Synthesis of a Gallium Ghrelin Analogue.....	52
3.2 Results and Discussion .....	53
3.2.1 The Design and Synthesis of a Gallium-68 Radiolabelled Ghrelin Analogue .....	57
3.3 Conclusions.....	59
3.4 Experimental.....	60
3.4.1 Materials and Equipment.....	60
3.4.2 General Procedure for Peptide Assembly.....	61
3.4.3 General Procedure for Selective Deprotection and Resin Cleavage .....	61
3.4.4 Dpr <sup>3</sup> (octanoic acid)][Lys <sup>19</sup> (DOTA)]ghrelin(1-19)-amide (3.6) .....	62
3.4.5 [Dpr <sup>3</sup> (octanoic acid)][Lys <sup>19</sup> ( <sup>69/71</sup> Ga-Dota)]ghrelin(1-19)-amide (3.7) .....	63
3.4.6 [Dpr <sup>3</sup> (octanoic acid)][Lys <sup>19</sup> ( <sup>68</sup> Ga-Dota)]ghrelin(1-19)-amide (3.8).....	63
 Chapter Four: The Design and Synthesis of Fluorine Labelled Ghrelin Analogues For use in Positron Emission Tomography .....	
4.1 Introduction.....	64

4.1.1 Fluorine-18 in Recent Drug Developments.....	64
4.1.2 Synthetic Approaches for Incorporating Fluorine-18 into Biomolecular Vehicles.....	65
4.1.3 Production of Fluorine-18 .....	68
4.1.4 Designing a Method for Incorporating Fluorine-18 into Ghrelin Analogues.	69
4.2 Results and Discussion .....	72
4.2.1 The Design of Non-radioactive Fluorine Bearing Ghrelin Analogues.....	72
4.2.2 Designing an Integrated Radiopharmaceutical using Fluorine-18 prosthetic groups.....	77
4.2.3 Incorporating Fluorine-18.....	85
4.2.4 Other Attempts at Designing Non-Radioactive Standards.....	89
4.3 Conclusions.....	91
4.4 Experimental.....	92
4.4.1 Materials and Equipment.....	92
4.4.2 General Procedure for Peptide Assembly.....	93
4.4.3 General Procedure for Selective Deprotection and Resin Cleavage .....	94
4.4.4 General Procedure for Fluorine Bearing Ghrelin(1-18), and [Tyr <sup>8</sup> ]Ghrelin(1-8) Analogues .....	94
4.4.5 [Dpr <sup>3</sup> (fluorobenzoic acid)]Ghrelin(1-18)-amide (4.21) and [Dpr <sup>3</sup> (4-fluoro- 1-naphthoic acid)]Ghrelin(1-18)-amide (4.22) .....	95
4.4.6 [Dpr <sup>3</sup> (fluorobenzoic acid)][Tyr <sup>8</sup> ]Ghrelin(1-8)-amide (4.24), [Dpr <sup>3</sup> (4- fluoro-1-naphthoic acid)][Tyr <sup>8</sup> ]Ghrelin(1-8)-amide (4.25), [Dpr <sup>3</sup> (6-fluoro- 2-naphthoic acid)][Tyr <sup>8</sup> ]Ghrelin(1-8)-amide (4.26) and [Tyr <sup>8</sup> ]Ghrelin(1-8)- amide (4.27) .....	95
4.4.7 General Procedure for Protecting Carboxylic Acids .....	95
4.4.8 2-Ethyl-3-aminonaphthoate (4.32) .....	96
4.4.9 2-Ethyl-6-aminonaphthoate (4.39) .....	96
4.4.10 2-Ethyl-6-fluoronaphthoate (4.45).....	96
4.4.11 1-Ethyl-4-dimethylamino-naphthoate (4.52).....	97
4.4.12 General Procedure for Reductive Amination of Aromatic Amines .....	97
4.4.13 3-Dimethylamino-2-naphthoic acid (4.31) .....	97
4.4.14 2-Ethyl-3-dimethylaminonaphthoate (4.33) .....	97

4.4.15 6-Dimethylamino-2-naphthoic acid (4.37).....	98
4.4.16 2-Ethyl-6-dimethylaminonaphthoate (4.40).....	98
4.4.17 2-Ethyl-3-methylamino-naphthoate (4.34).....	98
4.4.18 General Procedure for Forming a Quaternary Ammonium Salt.....	99
4.4.19 6-(N, N, N-trimethylammonium trifluoromethansulfonyl)-2 naphthoic acid (4.38).....	99
4.4.20 2-ethyl-6-(N, N, N-trimethylammonium trifluoromethansulfonyl)- naphthoate (4.41).....	99
4.4.21 4-(N,N,N-trimethylammonium trifluoromethansulfonyl)-1-naphthoic acid (4.49).....	99
4.4.22 4-dimethylamino-1-naphthoic acid (4.48).....	100
4.4.23 4-dimethylamino-1-naphthaldehyde (4.50).....	100
4.4.24 4-dimethyl-1-naphthoic acid (4.51).....	101
4.4.25 F-18 radiolabelling procedure 2-Ethyl-6- <sup>18</sup> fluoronaphthoate (4.46).....	101
 Chapter Five: Conclusions.....	 103
 Chapter Six: References.....	 108
Appendix A.....	117
Appendix B.....	138
Curriculum Vitae .....	140

## List of Tables

Table 2.1. Alanine scans on truncated human ghrelin. NBA is no binding affinity was observed when alanine was substituted in these positions. Study by Cancraenenbroeck <i>et al.</i> <sup>75</sup> .....	26
Table 2.2. The Importance of Gly <sup>1</sup> and Ser <sup>2</sup> in ghrelin analogs. Study by Matsumoto <i>et al.</i> <sup>73,74</sup> .....	27
Table 2.3. Ghrelin analogs with their purity, calculated, and observed mass.....	33
Table 2.4. Binding affinity and serum stability of ghrelin and analogues. IC <sub>50</sub> values are means ± SEM (n=3-5). Values for serum half-lives represent the time point at which 50% of the peptide remained as assessed by HPLC. ND, not determined.....	35
Table 3.1. [Dpr(octanoyl) <sup>3</sup> , Lys(DOTA) <sup>19</sup> ] ghrelin(1-19)-amide 3.6 calculated and observed exact mass, and purity determined after HPLC purification. ....	55
Table 3.2. [Dpr(octanoyl) <sup>3</sup> , Lys(Ga <sup>69/70</sup> -DOTA) <sup>19</sup> ] ghrelin(1-19)-amide 3.6 calculated and observed exact mass, and purity determined after HPLC purification. ....	56
Table 3.3. Comparing the binding affinities of synthesized ghrelin analogs to native ghrelin. ....	57
Table 4.1. Commonly used positron emitting radionuclides <sup>114</sup> .....	65
Table 4.2. Selected fluorine-18 labelled radiopharmaceuticals in clinical use.....	65
Table 4.3. Various modifications to native ghrelin's Ser <sup>3</sup> side chain and their reported binding affinities. A study by Badnarek <i>et al.</i> .....	70
Table 4.4. Various fluorine bearing ghrelin(1-14)-amide analogs and their reported IC <sub>50</sub> values. N= 1, 4, 7. Study by Rosita <i>et al.</i> .....	71
Table 4.5. Fluorine bearing ghrelin analogues with their calculated and observed exact mass, as well as purity determination after HPLC purification. ....	75
Table 4.6. Comparing the binding affinities of synthesized fluorine bearing ghrelin(1-18)-amide analogs to native ghrelin and hexarelin (mean ± s.d., n= 3).....	75
Table 4.7. Fluorine bearing ghrelin analogues with their calculated and observed exact mass, and purity determined after HPLC purification .....	76
Table 4.8. Binding affinities to the GHSR of low molecular weight [Tyr <sup>8</sup> ]ghrelin(1-8)-amide analogues with varying Dpr <sup>3</sup> side chains. ND = Not determined.....	77
Table 4.9. Various reagents and conditions used for protecting 2-amino-3-naphthoic acid 4.30.....	81

Table 4.10. Summary of fluorinating agents used to displace the quaternary ammonium salt 4.43..... 84

## List of Figures and Illustrations

Figure 1.1. Schematic diagram of the design of molecular imaging probes.....	2
Figure 1.2. (a) Maximum intensity projection of whole body PET scan using the molecular imaging probe $^{18}\text{F}$ -2-Deoxy-D-Glucose ( $^{18}\text{F}$ -FDG) (b) Structure of $^{18}\text{F}$ -FDG. ....	3
Figure 1.3. Principle behind targeting cancer-specific receptors. Signalling source would create a signal to detect the peptide binding to its overexpressed receptor. ....	5
Figure 1.4. Various methods for incorporating radioisotopes for PET nuclear imaging: (a) Direct labeling pendent design (b) Pendent chelate design (c) Prosthetic group design (d) Integrated design. ....	7
Figure 1.5. Structures of commonly used linkers in SPPS. ....	8
Figure 1.6. The interaction of a positron ( $\text{E}^+$ ) emitted from a radioactive source ( $^{18}\text{F}$ -FDG) with an electron ( $\text{E}^-$ ). This annihilation event produces two gamma rays at 180 degrees apart. Both gamma rays are detected by scintillation detectors in a PET instrument, and rendered to display an image. ....	12
Figure 1.7. Fluorescence process: (A) Excitation, (B) Vibrational Relaxation, (C) Emission. ....	15
Figure 1.8. Commonly used fluorophores: (a) FITC, $\lambda_{\text{EX}} \approx 494 \text{ nm}$ , $\lambda_{\text{EM}} \approx 521 \text{ nm}$ (b) Texas Red, $\lambda_{\text{EX}} \approx 589 \text{ nm}$ , $\lambda_{\text{EM}} \approx 615 \text{ nm}$ (c) Cy-5.5, $\lambda_{\text{EX}} \approx 494 \text{ nm}$ , $\lambda_{\text{EM}} \approx 521 \text{ nm}$ . ....	16
Figure 2.1. (a) T2 weighted MRI of advanced PCa (red arrow) on the periphery of the prostate gland. (b) Trans-rectal ultrasound of advanced PCa (red arrow). (c) $^{18}\text{F}$ -FDG PET-CT overlay image showing advanced prostate cancer (red arrow) and surrounding bladder uptake (yellow arrow) (Fig c) <sup>47</sup> . ....	20
Figure 2.2. <i>Top</i> figure represents a patient with early stage PCa. <i>Bottom</i> figure represents a patient with BPH. In both figures, Red arrows show the anatomic location of the tumour (CT scan) and accumulation of $^{18}\text{F}$ -FDG (PET scan). Each patient's condition was confirmed by post-surgical biopsies. ....	21
Figure 2.3. Growth hormone secretagogue receptor indicating the seven trans-membrane domain. <sup>59</sup> ....	22
Figure 2.4. Structure of Human Ghrelin. ....	24
Figure 2.5. Origins of human ghrelin. <sup>69</sup> ....	25
Figure 2.6. $\text{IC}_{50}$ values reported for modified ghrelin(1-28) analogs. Results show the importance of the acylated side chain to the GHSR binding affinity. Positioning the acylated side chain towards the N-terminus (b) shows a loss in binding	

affinity. A substantial decrease in binding affinity is observed in analogs where the side chain is positioned towards the C-terminus (c and d). In the absence of the acylated side chain (e) binding is reduced. Replacing serine with 2,3-diaminopropionic acid (Dpr) (f) shows a relatively small change in binding affinity to the GHSR. ....	28
Figure 2.7. Serum stability studies for fluorescein-ghrelin 2.21 (top) and ghrelin(1-18)-amide 2.22. Half-lives were extrapolated and calculated at 50% (based on line of best fit). ....	34
Figure 2.8. The hapten amplification technique is shown where an anti-fluorescein antibody is incubated with the probe, followed by the addition of Alexa Fluor 647 secondary antibody. This approach amplifies the signal and shifts the detection of the probe to the near infrared spectrum. ....	36
Figure 2.9. Evaluation of fluorescein-ghrelin 2.21 binding and uptake in prostate cancer cells (PC3 and LNCaP) and BPH cells. Nucleus stained with DAPI blue (upper panels). Fluorescence micrograph of probe without overlaid DAPI stain (middle panel) and with (lower panel). Graph shows the quantitative analysis of probe signal intensity in cells lines. ....	37
Figure 2.10. Evaluation of fluorescein-ghrelin 2.21 and uptake in PC3 cells. Fluorescence micrograph of PC3 cells incubated with fluorescein-ghrelin 2.21 in the presence (middle and panels) and absence (upper panels) of excess ghrelin(1-18)-amide 2.22. Negative control (lower panels) contained no fluorescent probe. Graph shows the quantitative analysis of probe signal intensity with and without the presence of unlabelled ghrelin(1-18)-amide 2.22. ....	37
Figure 2.11. Evaluation of fluorescein-ghrelin 2.21 probe in <i>ex vivo</i> human prostate biopsy tissue. Preferential uptake was found in PIN and PCa, as compared to normal prostate and BPH. ....	39
Figure 2.12. <i>In situ</i> binding of fluorescein-ghrelin in murine heart tissue. Binding of fluorescein-ghrelin alone (a), or in the presence of ghrelin (b) or hexarelin (c). Auto-fluorescence shown in (d). ....	40
Figure 3.1. The production of $^{68}\text{Ga}$ through the ( <i>p</i> , 2 <i>n</i> ) reaction with $^{69}\text{Ga}$ . ....	50
Figure 3.2. Temperature stability study of [Dpr(octanoyl) <sup>3</sup> , Lys(DOTA) <sup>19</sup> ] ghrelin(1-19)-amide 3.6. Analogue 3.6 was dissolved in an aqueous solution at room temperature. At ten-minute time intervals, aliquots of 3.6 were taken from the solution and injected onto the HPLC to assess the peptide's stability. UV chromatograms show no decomposition in analogue 3.6 when being exposed to various temperatures based on the peak retention times. ....	58
Figure 3.3. HPLC UV trace of non-radioactive standard 3.7 (bottom) and gamma trace of gallium-68 labelled product 3.8 (top). ....	59

Figure 4.1. Our design approach in modifying ghrelin(1-18) for the incorporation of fluorine-18..... 72

Figure 4.2. Novel Naphthalene prosthetic group targets. .... 79

Figure 4.3. Schematic diagram of the Tracer Lab FX F-E system. Vials contained: Vial 1 (V<sub>1</sub>) a 2mL solution of Kryptofix 2.2.2 and <sup>18</sup>F<sup>-</sup>, Vial 2 (V<sub>2</sub>) a 2ml solution of anhydrous acetonitrile and Vial 3 (V<sub>3</sub>) a solution of Starting Material dissolved in 1mL anhydrous DMSO. Synthesis began by transferring vial 1 contents to the reaction flask. Azeotropic removal of residual water occurred by heating the reaction flask (under vacuum) with acetonitrile from vial 2. Vial 3 was then be added (under helium) to the reaction flask, starting the reaction..... 87

Figure 4.4. HPLC UV trace of non-radioactive standard 4.45 (top) and gamma trace of fluorine-18 labelled product 4.46 (bottom). .... 88

Figure 4.5. HPLC traces of precursor 4.41 (top) and standard 4.45 (bottom). .... 89



## List of Schemes

Scheme 1.1. General peptide synthesis using SPPS. ....	9
Scheme 1.2. Fluorine-18 decay.....	13
Scheme 1.3. Production of Germanium-68 and Gallium-68. ....	14
Scheme 2.1. Design of ghrelin(1-18)-amide peptides. ....	30
Scheme 2.2. Orthogonal Protecting group strategy for the synthesis of [Dpr(octanoyl) <sup>3</sup> , Lys(fluorescein) <sup>19</sup> ] ghrelin(1-19)-amide. ....	31
Scheme 2.3. Synthesis of [Dpr(octanoyl) <sup>3</sup> , Lys(fluorescein) <sup>19</sup> ] ghrelin(1-19)-amide. ....	32
Scheme 3.1. Fmoc-SPPS synthesis of on resin [Dpr(alloc) <sup>3</sup> , Lys(Mtt) <sup>19</sup> ]ghrelin(1-19)-amide 3.1. All other amino acids were protected using standard Fmoc chemistry protecting groups.....	54
Scheme 3.2. Synthesis of [Dpr(octanoyl) <sup>3</sup> , Lys(DOTA) <sup>19</sup> ] ghrelin(1-19)-amide 3.6.....	55
Scheme 3.3. Synthesis of [Dpr(octanoyl) <sup>3</sup> , Lys(Ga <sup>69/70</sup> -DOTA) <sup>19</sup> ] ghrelin(1-19)-amide 3.7.....	56
Scheme 3.4. The gallium-68 radiolabelling synthesis in forming [Dpr(octanoyl) <sup>3</sup> , Lys(Ga <sup>68</sup> -DOTA) <sup>19</sup> ] ghrelin(1-19)-amide 3.8.....	59
Scheme 4.1. An electrophilic fluorination reaction using [ <sup>18</sup> F]acetyl-hypofluorite in the production of [ <sup>18</sup> F]FDG .....	67
Scheme 4.2. Synthetic steps used to reach an <sup>18</sup> F-labeled biomolecule (blue) using an <sup>18</sup> F-labeled prosthetic group (red). Nucleophilic aromatic substitution on a quaternary ammonium salt proceeds from the addition of <sup>18</sup> F <sup>-</sup> , followed by a deprotection step and then addition of the desired peptide sequence. ....	68
Scheme 4.3. Chart showing the production of [ <sup>18</sup> F]fluorine starting from cyclotron irradiation of <sup>18</sup> O water ( <sup>18</sup> O( <i>p,n</i> ) <sup>18</sup> F reaction). Following this is a flow chart on the steps taken to reach [ <sup>18</sup> F]fluorine with limited amounts of aqueous solution present (y is less than x). Adapted from Cai <i>et al</i> <sup>128</sup> .....	69
Scheme 4.4. Synthesis of ghrelin(1-18)-amide analogues with varying aromatic Dpr <sup>3</sup> side chains. ....	74
Scheme 4.5. The synthesis of low molecular weight [Tyr <sup>8</sup> ]ghrelin(1-7)-amide analogues with varying Dpr <sup>3</sup> side chains. ....	76
Scheme 4.6. A general S <sub>N</sub> Ar reaction involving the addition of fluorine to a protected benzoic acid to afford <sup>18</sup> F-fluorobenzoic acid.....	78

Scheme 4.7. Reductive amination of an ortho substituted amine. ....	80
Scheme 4.8. The synthesis of protecting carboxylic acid 23. ....	81
Scheme 4.9. Towards the synthesis of an ortho quaternary ammonium salt. ....	81
Scheme 4.10. The synthesis of a quaternary ammonium salt 4.38. ....	82
Scheme 4.11. Precursor synthesis of fluorine bearing prosthetic group. ....	83
Scheme 4.12. Synthesis of standard fluorinated naphthalene. ....	85
Scheme 4.13. Synthesis of an F-18 labeled novel prosthetic group. ....	88
Scheme 4.14. Towards the synthesis of 4-fluoro-1-naphthoic ethyl ester. ....	90
Scheme 4.15. An alternative approach to synthesizing 4-fluoro-2-naphthoic acid. ....	91

## List of Abbreviations and Symbols

$^{18}\text{F}$ -FDG	fluorodeoxyglucose
GLUT	glucose transporter
PET	positron emission tomography
SPECT	single-photon emission computed tomography
MRI	magnetic resonance imaging
CT	computed tomography
SPPS	solid phase peptide synthesis
BBB	blood brain barrier
Fmoc	9-fluorenylmethoxycarbonyl
HBTU	3-[bis(dimethylamino)methylumyl]-3 <i>H</i> -benzotriazol-1-oxide hexafluorophosphate
DMF	<i>N,N</i> -dimethylformamide
TIS	triisopropylsilane
TFA	trifluoroacetic acid
MS	mass spectrometry
HPLC	high-performance liquid chromatography
NMR	nuclear magnetic resonance
SBR	signal to background ratio
GHSR	growth hormone secretagogue receptors
PCa	prostate cancer
PSA	prostate specific antigen
TrUS	trans-rectal ultrasound
BPH	benign prostatic hyperplasia
GPCR	G-protein coupled receptors
GH	growth hormone
GOAT	ghrelin O-acyl transferase
EC <sub>50</sub>	half-maximal effective concentration
Ape	5-aminopentanoic acid
FITC	fluorescein isothiocyanate
Dpr	diaminopropanoic acid
MBHA	4-methylbenzylhydramine
DCM	dichloromethane
PIN	paraepithelial neoplasia
ESI	electrospray ionization
DIPEA	<i>N,N</i> -diisopropylethylamine
Alloc	allyloxycarbonyl
Boc	tert-Butyloxycarbonyl
Mtt	4-methyltrityl
DAPI	4',6-diamidino-2-phenylindole
EI	electron ionization
HRMS	high resolution mass spectrometry
IC <sub>50</sub>	half maximal inhibitory concentration
MeOH	methanol
TBME	tert-butylmethylether

tBu	tert-butyl
ACN	Acetonitrile
Tris-tbutyl-DOTA	1,4,7,10-tetraazacyclodecane-N,N',N'',N'''-tetraacetic acid
NET	neuroendocrine tumours
HATU	O-(7-Azabenzotriazol-1-yl)-N,N,N',N'-tetramethyluronium hexafluorophosphate
THF	tetrahydrofuran
DMSO	Dimethyl Sulfoxide
AcOH	acetic acid
HRMS	high resolution mass spectrometry
tBu	<i>tert</i> -butyl
EtOAc	ethyl Acetate
EWG	electron withdrawing group

## Introduction

### 1.1 Introduction to Molecular Imaging

Over the last 25 years, imaging techniques have enabled scientists to better understand and monitor disease processes<sup>1</sup>. In the early 1990s a new term, molecular imaging, became an extension of this thought process by allowing living subjects to be visualized in a more meaningful way<sup>1,2</sup>. Molecular imaging can be defined as “the visual representation, characterization, and quantification of biological processes occurring at the cellular or sub-cellular levels” (Massoud *et al*)<sup>3</sup>. Molecular imaging combines the basic sciences (cellular/molecular biology, chemistry, physics and pharmacology) with medical imaging to formulate a unique multidisciplinary field. Today, diagnostic imaging techniques either use contrast enhancing agents or structurally-based anatomical methods to visualize living subjects. In contrast to classical imaging techniques, molecular imaging enhances the spacial resolution, sensitivity, and specificity of an imaging agent. It provides a non-invasive approach in identifying early stages of disease(s), in contrast to the invasive method of a traditional surgical biopsy.

In order to image and identify malignant tumour cells, an imaging probe needs to be synthetically designed so that it can distinguish between abnormal and healthy tissues. When introduced to an *in vitro* or *in vivo* environment, imaging probes generally consist of two parts: (1) a *biomolecular vehicle* component to ensure successful delivery to the region of interest, and (2) a *signal source* to create contrast and be externally detected by the imaging modality of choice (Figure 1.1). Imaging probe design focuses on incorporating radionuclides or optical dyes as *signalling sources*. To limit interference

with the cellular binding regions a *linker* may be situated between the *signal source* and *biomolecular vehicle*.

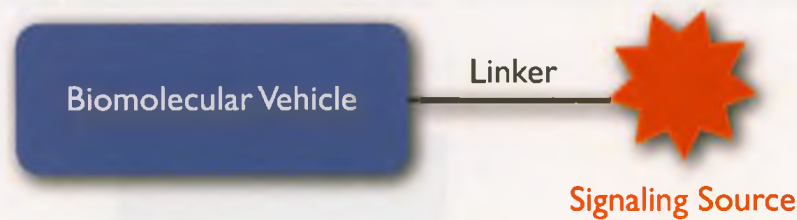


**Figure 1.1.** Schematic diagram of the design of molecular imaging probes.

In the past imaging techniques focused largely on identifying macroscopic physical, physiological, or metabolic changes within a subject, differentiating between diseased and normal tissue without the ability to identify specific molecular events. Molecular imaging is responsible for the shift from non-specific to specific imaging techniques. Its impact can be shown through our understanding of integrative biology, earlier detection methods, characterization of disease, and treatment approaches<sup>3</sup>. Fluorodeoxyglucose ( $^{18}\text{F}$ -FDG) is an example of a clinically approved molecular imaging probe which incorporates radioactive fluorine (*signal source*) into D-glucose (*biomolecular vehicle*) as a way of diagnosing disease in many tumour models including lymphoma, non small cell lung cancer, head and neck cancer, and colorectal cancer (Figure 1.2)<sup>4</sup>. In primary tumour cells, glucose metabolism is up-regulated by glucose transporter (GLUT) proteins and the expression of hexokinases. The ability of FDG to detect tumour cells with high specificity is because of this relationship between tumour growth and energy production by glucose metabolism (Warburg effect)<sup>5</sup>. FDG competes with glucose and is rapidly transported across the tumour cell membrane where

phosphorylation takes place. In healthy cells, glucose is phosphorylated by hexokinases to form glucose-6-phosphatases, which then undergo additional metabolism. Unlike glucose, FDG-6-phosphate cannot be further catabolized, which causes it to remain in the intracellular compartment of tumour cells, thus further improving the imaging potential.

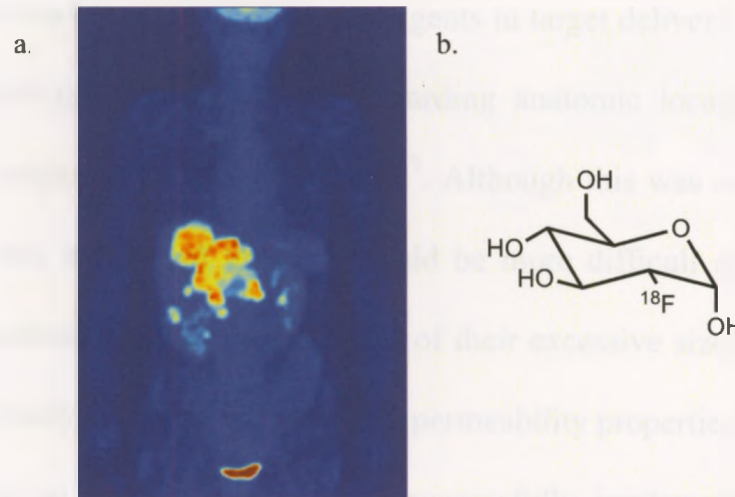


**Figure 1.2.** (a) Maximum intensity projection of whole body PET scan using the molecular imaging probe  $^{18}\text{F}$ -2-Deoxy-D-Glucose ( $^{18}\text{F}$ -FDG) <sup>6</sup> (b) Structure of  $^{18}\text{F}$ -FDG.

Modalities utilized in molecular imaging include: positron emission tomography (PET), single photon emission computed tomography (SPECT), optical fluorescence imaging, magnetic resonance imaging (MRI), computed tomography (CT), and ultrasound imaging. While each imaging modality is unique with its own strengths and limitations, the principal goals remain the same. The goal of molecular imaging is to: (a) develop a non-invasive technique to assist in clinical diagnosis by providing anatomical and macrofunctional images of high specificity and sensitivity and (b) improve earlier diagnosis of disease, leading to higher survival rates.



## 1.2 Designing Peptide Based Imaging Probes

The field of molecular imaging has developed several efforts to ensure earlier and more accurate diagnosis of disease. Initial efforts in developing novel probes utilized the placement of a radioisotope incorporated within a small molecule or macromolecule<sup>7</sup>. For example, the development of antibodies 25 years ago became a popular theme in cancer imaging. These antibodies acted as biological agents in target delivery for *in vivo* studies. Antibodies provided specific information regarding anatomic location of a particular disease, tissue of origin, and biologic potential<sup>7</sup>. Although this was a simple principle it became apparent this method of imaging would be more difficult in translating to the clinical setting. Antibodies are limited because of their excessive size (150 kDa), lack of clearance from the body and poor diffusion and permeability properties<sup>8,9</sup>.

In order for an imaging probe to be successfully implemented into a clinical setting, it should provide a sufficient target to background ratio to maximize the signal-to-noise contrast in the image. An ideal imaging candidate should bind with high affinity, show specific uptake and retention time, have high stability and above all be safe for human use<sup>8</sup>. Peptides represent a viable class of imaging probes that can fulfill the above-mentioned criteria<sup>10</sup>. These molecules consist of several amino acid sequences, linked together through peptide bonds. They are smaller than proteins, as they do not form well-defined three dimensional tertiary structures<sup>10</sup>. Generally, peptides play a limited role within their biological environments by targeting specific receptors within the brain, gastrointestinal tract, endocrine, vascular or lymphoid systems. Their functions are facilitated by high affinity, specific receptors, many of which belong to the G- protein-coupled family of receptors. These peptide receptors have demonstrated an overexpression in multiple cancer models, even though they play a physiological role



within the human body<sup>8,11,12,13</sup>. This overexpression is why peptide receptors have become popular and unique in diagnostic imaging applications (Figure 1.3).

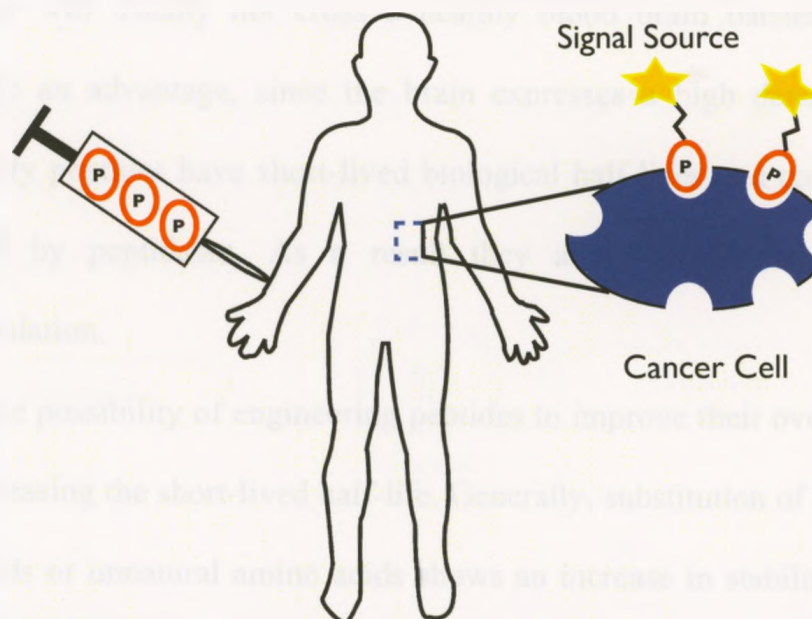


**Figure 1.3.** Principle behind targeting cancer-specific receptors. Signalling source would create a signal to detect the peptide binding to its overexpressed receptor.

Peptides offer several advantages over small molecules and macromolecules when being used as a biomolecular vehicle. Bioactive peptides and peptide-based hormones have a relatively low molecular weight, consisting of less than 50 amino acids. Lower molecular weight peptides have improved biodistribution because of their excellent tissue diffusion, specific target accessibility and rapid clearance from the blood<sup>9</sup>. While peptides play a limited role within their physiological environment they have limited immunogenicity as compared to other macromolecules<sup>8</sup>. Peptides can be readily synthesized by solid phase peptide synthesis (SPPS), and further manipulated to incorporate a radioisotope or optical dye<sup>14</sup>.

There are also some disadvantages associated with the use of peptide-based imaging probes. Peptides are limited to imaging tumours present within the peripheral organs. Less than 0.1% of the peptide will end up circulating within the brain, and consequently they will usually not cross a healthy blood brain barrier (BBB). This however could be an advantage, since the brain expresses a high density of peptide receptors<sup>15</sup>. Usually peptides have short-lived biological half-lives and consequently are rapidly degraded by peptidases. As a result they are excreted through renal or hepatobiliary circulation.

There is the possibility of engineering peptides to improve their overall metabolic stability, thus increasing the short-lived half-life. Generally, substitution of L-amino acids with D-amino acids or unnatural amino acids shows an increase in stability. Alternative methods in improving the peptides stability *in vivo* can occur through side chain modification, adding in hydrophilic or hydrophobic substituents, peptide cyclization, and acetylation or amidation of the peptide backbone<sup>16</sup>. Due to the small size of peptides, incorporating a signalling source such as a fluorescent dye or radionuclide, can disturb the binding affinity of the imaging probe towards the desired receptor target<sup>9</sup>.

Four different strategies exist when incorporating a radioisotope as the signalling source to form a peptide-based imaging agent. The first strategy incorporates the radioisotope directly through a pendent amino acid side chain in one step (Figure 1.4.a). This method significantly shortens the reaction time, requires low amounts of precursor and provides reasonable yields<sup>17</sup>. In a similar approach, a chelate can be incorporated through a pendent side chain to covalently bind the radioactive element (Figure 1.4.b)<sup>18</sup>. The location and size of the chelate is critical for preserving the peptides binding affinity to the targeted receptor. In a different approach, a prosthetic group can be readily

radiolabelled prior to being added into the backbone of the peptide (Figure 1.4.c). Methods for incorporating the radioisotope to form the prosthetic group, adding the group into the peptide and purification techniques along the way, need to be considered to ensure no loss in radioactivity. The last approach is an integrated design where the radioactive element is incorporated directly into the structure of the peptide (Figure 1.4.d). The following chapters will discuss the use of chelators and prosthetic groups for incorporating radioactive elements.

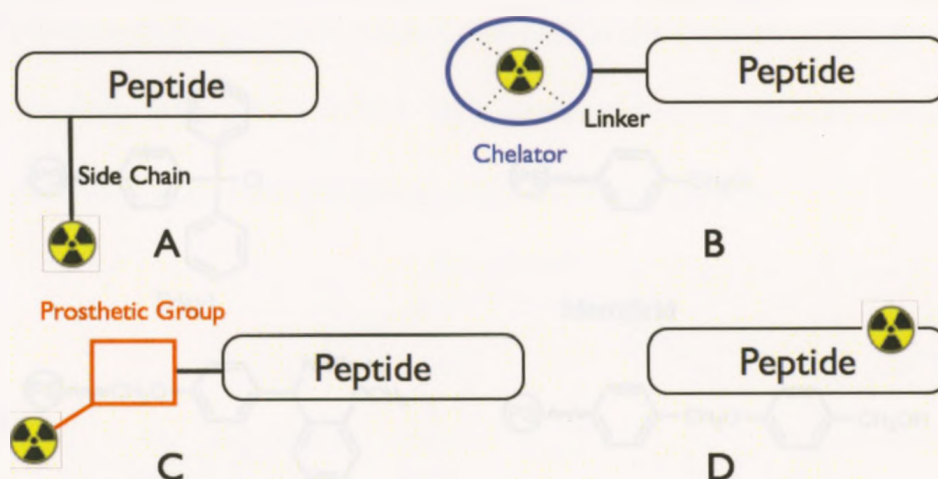


**Figure 1.4.** Various methods for incorporating radioisotopes for PET nuclear imaging: (a) Direct labeling pendent design (b) Pendent chelate design (c) Prosthetic group design (d) Integrated design.

### 1.3 Fmoc Solid Phase Peptide Synthesis

Merrifield first reported the synthesis of linear peptides on a solid support in 1963<sup>19</sup>. Prior to solid-phase peptide synthesis (SPPS), peptides were synthesized by classical solution phase techniques<sup>20</sup>. Solution-phase peptide synthesis is a time-consuming and arduous task requiring purification after each synthetic step. The intent of SPPS was to simplify the vigorous task of synthesizing a polypeptide by: creating an easier method to separate reagents from products, increasing the purity of the peptide by



having soluble byproducts, removing solvents in a timely efficient process by filtration and allowing excess reagents to drive reactions to completion. Since Merrifield's discovery, SPPS has developed into the most commonly used method for preparing peptides. Currently, SPPS uses a polystyrene based solid support (resin) with particle diameters in the range of 20-50  $\mu\text{m}$ <sup>21</sup>. Various cleavable linkers are utilized to attach the amino acid residues to the solid support, allowing for the release of the final linear peptide sequence (Figure 1.5)<sup>21</sup>.

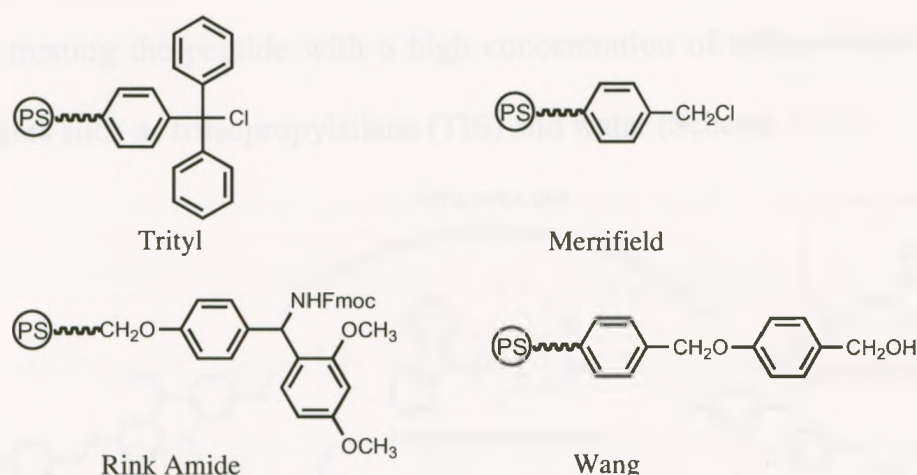
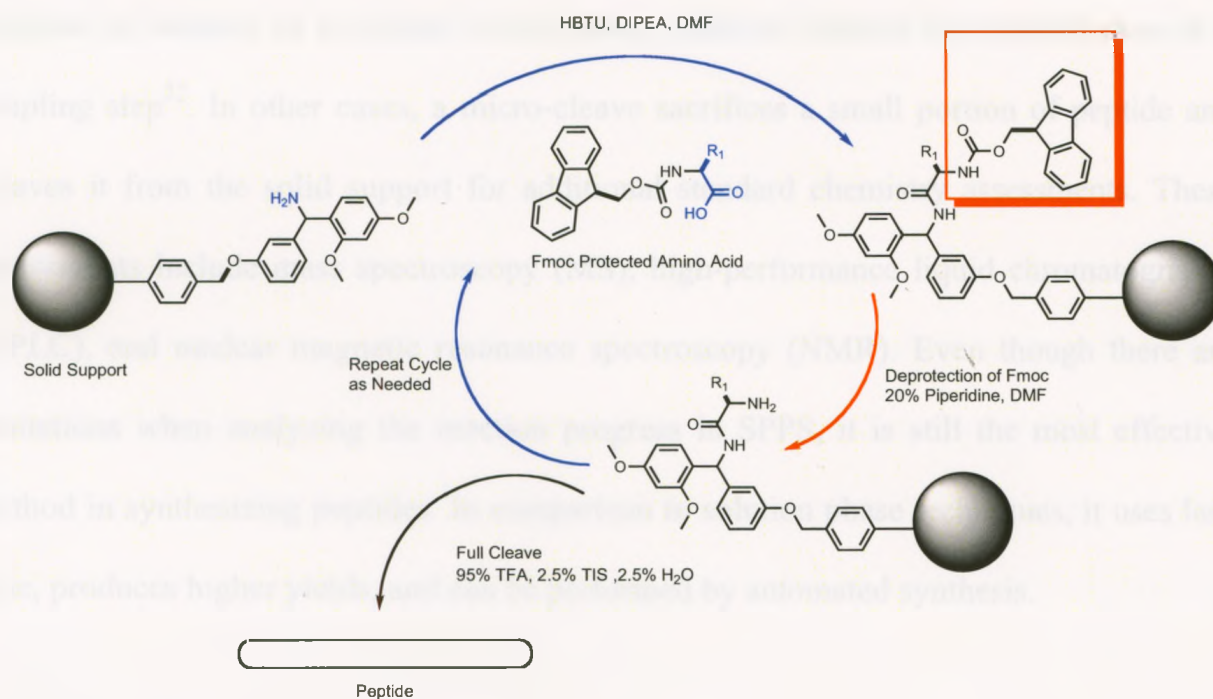


**Figure 1.5.** Structures of commonly used linkers in SPPS.

Fmoc SPPS is a technique where amino acid residues are added one by one to the insoluble solid support, in a C to N-terminal methodology. A base-labile Fmoc group protects the  $\alpha$ -amine while an acid-labile group protects the amino acid side chain functionality. The synthesis starts off by deprotecting the organic linker attached to the polystyrene resin. The first amino acid is attached to the free amine on the organic linker by the free carboxylic acid (Scheme 1.1). This occurs *in situ* where the acid forms an activated ester by reaction with a coupling reagent such as, 3-

[bis(dimethylamino)methyl]imidazolium hexafluorophosphate (HBTU)<sup>14</sup>. Afterwards, the Fmoc protecting the  $\alpha$ -amine (on the N-terminus) is removed under basic condition using 20% piperidine in dimethylformamide (DMF). This in turn produces the free amine, which can undergo a subsequent reaction with the C-terminus of another free carboxylic acid using standard coupling conditions. The cycle of removing the Fmoc protecting group on the amino acid linked to the insoluble support, followed by the addition of another amino acid is repeated until the anticipated sequence is made. After no further modifications are needed, the acid-labile protecting groups and resin are cleaved by treating the peptide with a high concentration of trifluoroacetic acid (TFA) and scavengers such as triisopropylsilane (TIS) and water (Scheme 1.1).



**Scheme 1.1.** General peptide synthesis using SPPS.

When further modifications to individual side chains are needed or to that of the resin, an additional orthogonal protecting group strategy is required. This allows for the selective removal of one protecting group in the presence of others having the same functionality. This can be done through the use of unique resins or protecting groups that

tolerate each other's deprotection strategies. There are a number of different methods that allow for the selective removal of protecting groups and resins. For example, hyper-acid sensitive and photo-labile resins are able to give a non-conventional C-terminus upon being cleaved. Other conventional methods include using weakly acidic protecting groups and palladium catalyzed protecting groups for further modification to the peptide.

Monitoring the reaction progress in SPPS is a difficult task and causes a degree of uncertainty during each reaction step. This error is a result of the peptide being linked to an insoluble solid support that cannot be analyzed using standard chromatographic techniques. As a result, a small portion of the resin is sacrificed in order to evaluate the reaction progress. For example, the Kaiser test is a qualitative test that can detect the presence or absence of a primary amine group, and can confirm the completeness of a coupling step<sup>22</sup>. In other cases, a micro-cleave sacrifices a small portion of peptide and cleaves it from the solid support for additional standard chemistry assessments. These assessments include mass spectroscopy (MS), high-performance liquid chromatography (HPLC), and nuclear magnetic resonance spectroscopy (NMR). Even though there are limitations when analyzing the reaction progress in SPPS, it is still the most effective method in synthesizing peptides. In comparison to solution phase techniques, it uses less time, produces higher yields, and can be performed by automated synthesis.

#### **1.4 Positron Emission Tomography**

*Positron emission tomography* (PET) is a sensitive modality used to create three-dimensional images based on the decay of positron emitting radioisotopes. PET images provide information about pathophysiological, physiological, and metabolic processes in comparison to imaging techniques that only display structure, such as CT and MRI



imaging. However, this technique has been shown to be expensive, uses ionizing radiation and has limited spacial resolution. Radioisotopes such as  $^{18}\text{F}$ ,  $^{11}\text{C}$ ,  $^{13}\text{N}$ , and  $^{15}\text{O}$  can all be produced via a cyclotron. When attached to a *biomolecular vehicle* and injected intravenously into a patient, the positron containing agent decays based on its' half-life. In the case of fluorine-18, the radionuclide emits a positron, which upon traveling a short distance, collides with an electron (Figure 1.6). This annihilation results in the emission of two gamma ray photons of 511 keV at a coincidence angle of 180 degrees. The image acquisition is based on the detection of a series of 180 degree coincidence gamma rays. The scintillation detectors are then able to convert the signal into three-dimensional images with computer software creating the PET image<sup>23</sup>. In addition to PET's increased sensitivity and accuracy, it is also available in tandem with other imaging modalities such as CT or MRI.

### 1.5 Radioisotopes used in PET Nuclear Imaging

Fluorine-18 has a short half-life of 110 minutes, high-bonding energy with carbon (481 kJ/mol in  $\text{CH}_3\text{-F}$ ), small atomic size (0.5 Å), and high electronegativity (3.98)<sup>24,25</sup>. "Physiological radionuclides"  $^{11}\text{C}$ ,  $^{13}\text{N}$  and  $^{15}\text{O}$  are preferred for labeling organic compounds, but due to their short half-lives of 20.4, 10.0, and 2.0 minutes respectively, these isotopes are limited in designing peptide-based probes labeled with a tracer<sup>26</sup>.  $^{18}\text{F}$  has an acceptable half-life leaving enough time for both chemical synthesis as well as imaging experiments, with moderate levels of radiation dose to the patient. Its use is valuable for PET imaging with 97% of the isotope decaying through positron emission<sup>26</sup>. Incorporating fluorine into an imaging probe has shown to affect the probe activity and stability. Its chemical and nuclear properties have been referred to as the "fluorine effect"

because depending on the biological system, fluorine can have a positive or negative effect<sup>27</sup>. Fluorine can also change the lipophilicity of a peptide, which in turn could increase or decrease binding affinity to receptors. Although fluorine is closely related to hydrogen in size, when replacing hydrogen with fluorine it affects the peptide's electrostatic interactions as well as electron densities<sup>27</sup>.

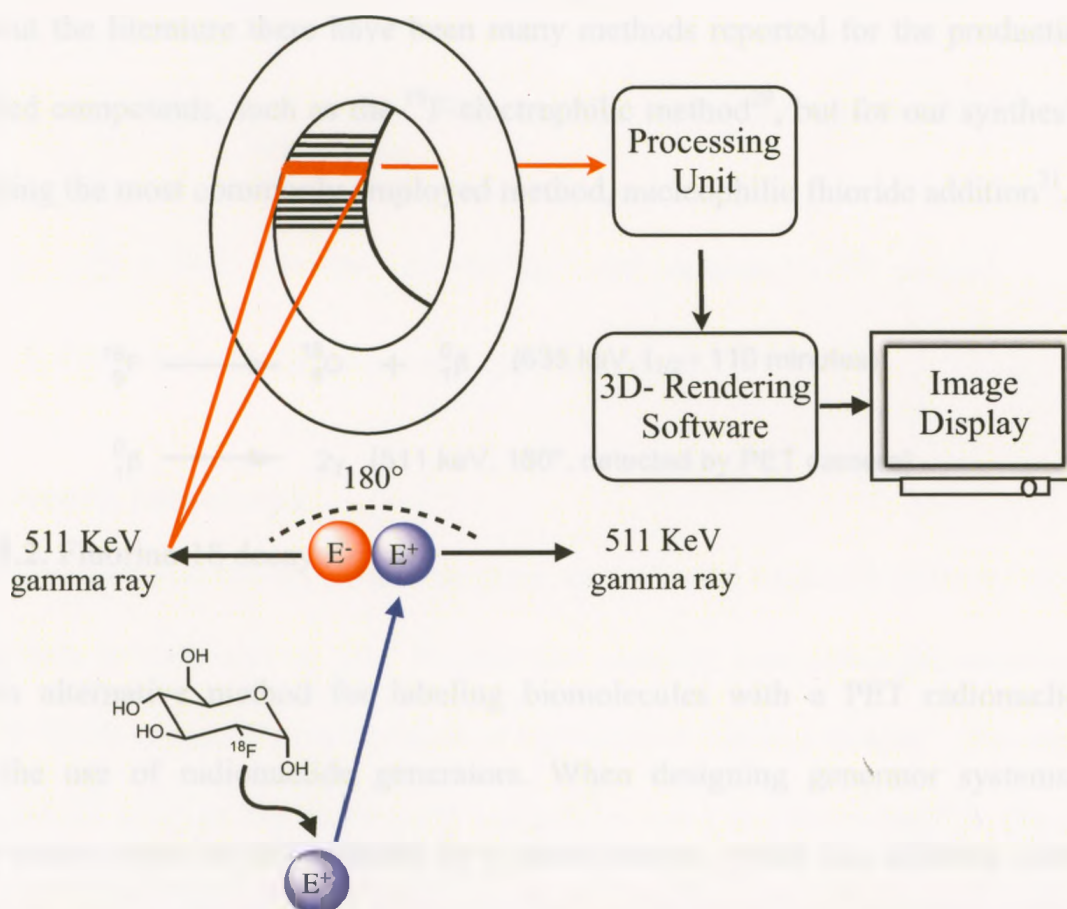
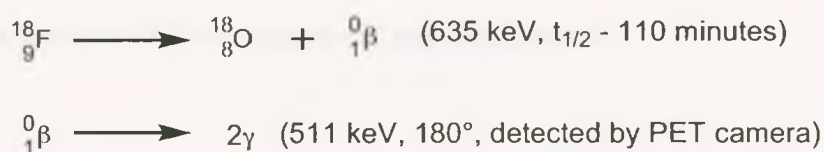


**Figure 1.6.** The interaction of a positron ( $E^+$ ) emitted from a radioactive source ( $^{18}\text{F}$ -FDG) with an electron ( $E^-$ ). This annihilation event produces two gamma rays at 180 degrees apart. Both gamma rays are detected by scintillation detectors in a PET instrument, and rendered to display an image.

$^{18}\text{F}$  is generally produced from a cyclotron or linear particle accelerator where proton irradiation of an  $^{18}\text{O}$  enriched water target gives the radioisotope. This method of production generates high specific activity of  $^{18}\text{F}$  (1710 Ci/micromol); however after irradiation, the radionuclide has to be isolated in order to become reactive<sup>26</sup>. Generally the



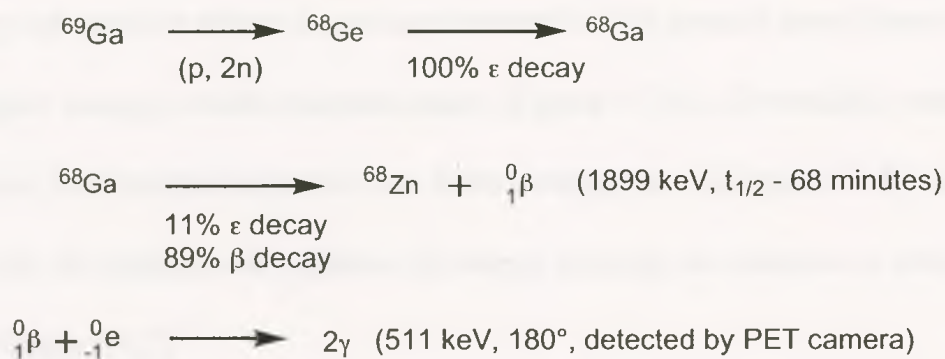
water is removed by the addition of an organic solvent, while heating under an inert atmosphere. Potassium carbonate is added to act as the cation source followed by the addition of kryptofix 222, which complexes to the potassium to enhance the nucleophilicity of fluoride<sup>28</sup>.  $^{18}\text{F}$  decays to  $^{18}\text{O}$  with a maximum decay energy of 635 keV, followed by gamma emission upon positron electron annihilation (Scheme 1.2)<sup>29,30</sup>. Throughout the literature there have been many methods reported for the production of  $^{18}\text{F}$ -labelled compounds, such as the  $^{18}\text{F}$ -electrophilic method<sup>29</sup>, but for our synthesis we will be using the most commonly employed method, nucleophilic fluoride addition<sup>31</sup>.



**Scheme 1.2.** Fluorine-18 decay

An alternative method for labeling biomolecules with a PET radionuclide is through the use of radionuclide generators. When designing generator systems, the radiation source must be accompanied by a parent source, which has different chemical properties, allowing for optimal separation. A long-lived parent isotope source gives the system an adequate lifetime for the synthesis of many tagged biomolecules. Although gallium generators have been well understood since the 1970's, their clinical application has not raised interest in the scientific community until a short time ago<sup>32</sup>. Within the Ge-68/ Ga-68 system, the long-lived source, Ge-68, is produced from the (p, 2n) reaction of Ga-69 (Scheme 1.3)<sup>33</sup>. This long-lived isotope decays with a half-life of 270 days to produce Ga-68 via 100% electron capture. As a result of its slower decay, these

generators can last up to two years<sup>32</sup>. Ga-68 can be eluted off the generator using various chromatographic techniques and integrated into peptides by using a chelator model. <sup>68</sup>Ga has a physical half-life of 68 minutes and decays 89% through positron emission at 1.92 MeV<sup>32</sup>.



**Scheme 1.3.** Production of Germanium-68 and Gallium-68.

## 1.6 Fluorescence Microscopy

Fluorescent microscopy is an emerging method used to detect different types of diseases. Both *in vitro* and *in vivo* fluorescence imaging uses low-light cameras and appropriate filters to quantify the emission of light present within a sample<sup>34</sup>. The samples that are used for imaging are whole-body animals (*in vivo*) or cells cultured in dishes (*in vitro*). Collectively, these imaging agents are more sensitive, safe, have longer shelf-lives and are easier to synthesize in comparison to radiopharmaceutical imaging agents. Yet, there are two reasons why it is technically challenging to develop a fluorescent probe for *in vivo* imaging. First, the penetration depth of a fluorescent probe is in the range of a few centimeters<sup>35</sup>. Secondly, tissues present within animals are able to absorb and scatter photons, which generates autofluorescence. This commonly leads to lower signal intensities and problems with quantifying fluorescence<sup>36</sup>. In addition to the autofluorescence revealed throughout normal tissue, the major decrease in signal to

background ratio (SBR) results from other photon absorbers such as water, lipids, oxyhemoglobin, and deoxyhemoglobin<sup>36</sup>.

When the fluorophore (signal source) absorbs light energy (photons), alterations in the molecules vibrational, electronic and rotational states occur. Sometimes the absorbed energy (photon) is able to move an electron from its ground state (lowest energy level) to a higher energy orbital (excited state) (Figure 1.7.A). Eventually, vibrational relaxation causes the electron to move to a lower energy state (Figure 1.7.B), which is then followed by the emission of a photon of energy causing the electron to return to its ground state (Figure 1.7.C)<sup>37</sup>.

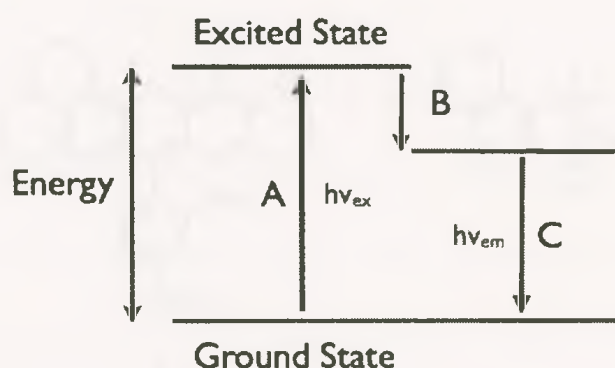


**Figure 1.7.** Fluorescence process: (A) Excitation, (B) Vibrational Relaxation, (C) Emission.

Although there are disadvantages in developing fluorescent imaging probes for *in vivo* use, cell-based fluorescence imaging is a widely accepted method. It is currently used for high-throughput screening of compounds for target validation and confirmation<sup>38</sup>. There are a number of different compounds that absorb in the visible region of the spectrum and as a result can be used to visualize and validate binding to potential molecular targets (Figure 1.8). Two types of fluorescent imaging probes exist: (a) non-targeting imaging probes, and (b) targeting probes. Targeting probes can be

divided into activatable or active agents. In this thesis, active targeting probes will be described to image the overexpression of receptors present within tumour cell models. Generally, compounds that exhibit this rapid transition from excited to relaxed states, display conjugated double bonds, aromatic motifs with pi bonds that can distribute valence electrons over wide areas. The more conjugated double bonds a fluorophore's structure contains, the lower the excited energy requirement, and the longer wavelengths the excitation light can be. This results in the emitted light being shifted in the same direction.

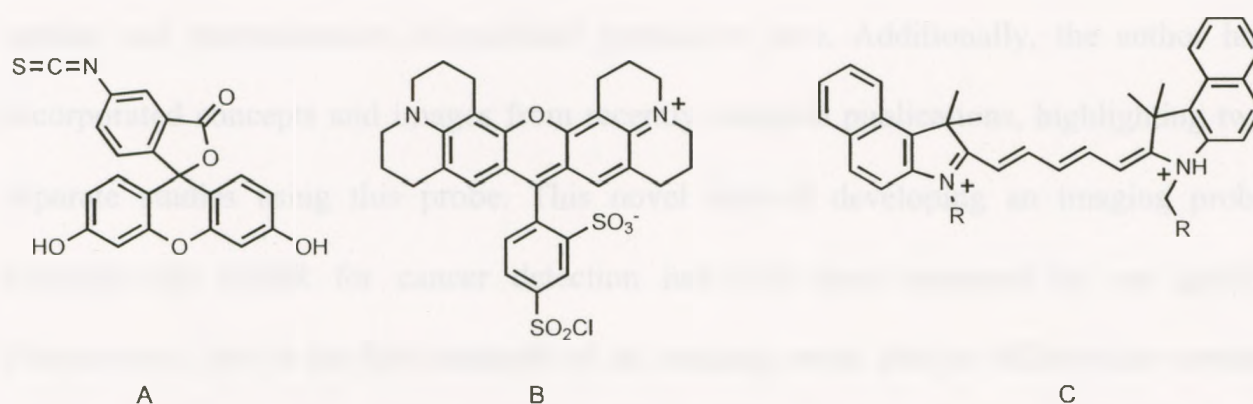


**Figure 1.8.** Commonly used fluorophores: (a) FITC,  $\lambda_{EX} \approx 494$  nm,  $\lambda_{EM} \approx 521$  nm (b) Texas Red,  $\lambda_{EX} \approx 589$  nm,  $\lambda_{EM} \approx 615$  nm (c) Cy-5.5,  $\lambda_{EX} \approx 494$  nm,  $\lambda_{EM} \approx 521$  nm.

## 1.7 Scope of Thesis

In this thesis, the concept of molecular imaging is used in parallel with the design of novel peptide based imaging probes that target cell-surface receptors. These receptors have a common feature, as they are overexpressed in abnormal cells and tissues. Each chapter will focus on the design, synthesis and application of peptide-based imaging probes. Additionally, each chapter represents a new approach to imaging disease whether



by incorporating fluorescent probes, gallium-68 or designing small prosthetic groups for fluorine-18 chemistry.

The second chapter of this thesis introduces the growth hormone secretagogue receptor (GHSR-1a) and its attractiveness as an imaging target. Ghrelin is a 28 amino acid peptide hormone and is the endogenous ligand for the GHSR-1a. Evidence from the literature suggests the GHSR is overexpressed in a number of tumour models and diseases. As an initial study, the objective was to design a novel fluorescent imaging probe using ghrelin, to target the GHSR. The reported design and synthesis of the imaging agent is highlighted within this chapter. The underlying goal was to validate the uptake and internalization of modified ghrelin *in vitro*. Additionally, the author has incorporated concepts and images from recently accepted publications, highlighting two separate studies using this probe. This novel idea of developing an imaging probe targeting the GHSR for cancer detection has only been proposed by our group. Furthermore, this is the first example of an imaging probe able to differentiate certain tissues present within *ex vivo* human prostate tissue. This project was in collaboration with Dr. Savita Dhanvantari and Dr. John Lewis, both assistant professors in Medical Biophysics from the University of Western Ontario.

The long-term goal of this project was to develop a radioactive imaging probe for PET nuclear imaging. Chapter's three and four look at two different approaches in designing radioactive peptide-based imaging probes using either gallium-68 (chapter three) or fluorine-18 (chapter four). Before developing radiolabeling strategies, both chapters report the design and synthesis of non-radioactive analogs. The binding affinities of these analogs were evaluated in a biological assay.

Chapter three of this thesis discusses the design and synthesis of incorporating a metal chelate into the peptide backbone of ghrelin. This chapter also reports the first radiolabelled ghrelin analogue for use in molecular imaging. The method of incorporating radioactive gallium will be discussed in great detail along with future objectives for this probe.

Chapter four of this thesis discusses methods for incorporating fluorine-18 into a peptide. Previously, we have published a paper discussing non-radioactive fluorine bearing ghrelin analogs for imaging the GHSR<sup>39</sup>. The site of fluorination was within ghrelin's unique lipophilic octanoylated side chain. The objective of this study was initially to improve the binding affinities of the fluorine labelled analogs. This was accomplished by designing second-generation fluorine bearing ghrelin analogs. Because of the improved binding affinities towards the GHSR a prosthetic group strategy for incorporating fluorine-18 is discussed. A number of attempts and synthetic routes are shown for the synthesis of three novel prosthetic groups. One of the prosthetic groups was radiolabelled with fluorine-18, and following this initial design and synthesis attempts were taken to form a fluorine-18 labelled ghrelin analogue.

## Chapter Two: The Design, Synthesis, and Application of a Fluorescein Labeled Ghrelin Analogue

### 2.1 Methods in Diagnosing Early Stage Prostate Cancer

Prostate cancer (PCa) is the leading malignancy in North American men. In 2010, it was estimated that 217,730 new cases developed and 32,050 deaths resulted from PCa in the United States<sup>40</sup>. In the last 20 years there has been great progress in our understanding of how to diagnose PCa effectively<sup>41</sup>. Currently, the standard method used to diagnose PCa is the analysis of a patient's prostate specific antigen (PSA) level<sup>42</sup>. Generally, healthy individuals have a PSA level below 4.0 nanograms per millilitre of blood (ng/mL)<sup>42</sup>. However, in one study 15.2% of patients living with PCa reported a PSA level below that of the healthy individual<sup>43</sup>. In addition to these results, 2.3% of the overall population had confirmed high-grade PCa with PSA values in the healthy range<sup>43</sup>. In another study, 65-75% of individuals who had PSA levels elevated above 4 ng/mL did not have PCa<sup>44</sup>. The rather large discrepancies observed in these studies display the inaccuracy associated with the PSA test and its inability to accurately differentiate between normal prostate and cancerous tissues. This problem in correctly diagnosing patients has led to numerous instances of false positives and negatives<sup>45,46</sup>.

Current imaging techniques used to detect early and advanced stages of PCa focus on the visualization and biophysical characterization of prostate carcinomas. For example, morphological T2 weighted MRI shows the gross anatomy of the prostate gland with high resolution and can serve as a method to help detect abnormal peripheral tissue (Figure 2.1.a)<sup>47</sup>. Trans-rectal ultrasound (TrUS) uses high frequency sound waves to detect changes within the prostate gland, distinguishing normal tissue from abnormal masses and tumours (Figure 2.1.b)<sup>47</sup>. Another technique utilized in detecting PCa is that of a



radioisotope for PET nuclear imaging. With the exception of  $^{18}\text{F}$ -FDG, the use of PET-radioisotopes within the clinical setting for diagnosing prostate disease has been limited<sup>47</sup>.  $^{18}\text{F}$ -FDG displays low accumulation in primary prostate cancer cells and is unable to detect local recurrence in patients who have undergone radical prostatectomy<sup>48,49</sup>. Although this agent has shown its ability in detecting later stages of PCa (Figure 2.1.c), often times when using it to image earlier stages, you observe surrounding interference and overlap in adjacent organs<sup>47</sup>.

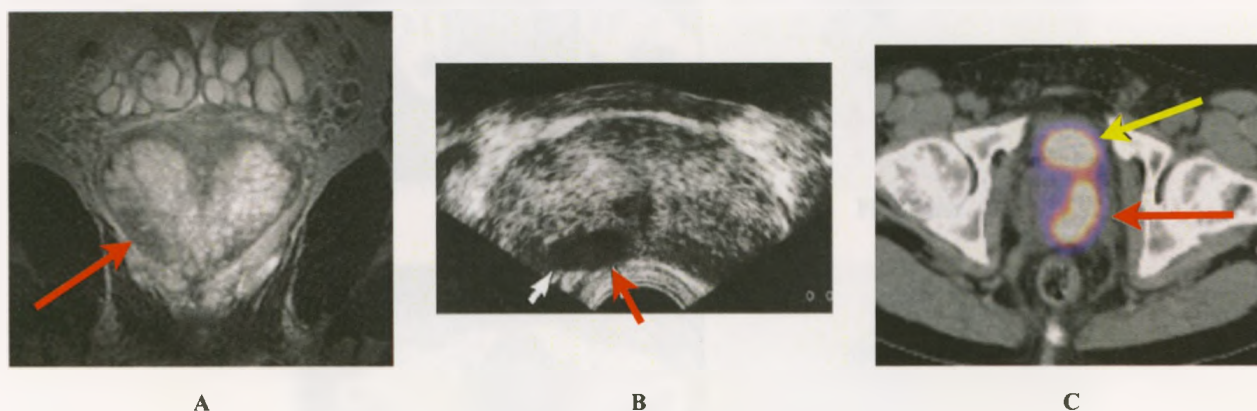


**Figure 2.1.** (a) T2 weighted MRI of advanced PCa (red arrow) on the periphery of the prostate gland. (b) Trans-rectal ultrasound of advanced PCa (red arrow). (c)  $^{18}\text{F}$ -FDG PET-CT overlay image showing advanced prostate cancer (red arrow) and surrounding bladder uptake (yellow arrow) (Fig c)<sup>47</sup>.

In a recent example the level of  $^{18}\text{F}$ -FDG accumulation within the prostate was shown to overlap between normal prostate tissue, benign prostatic hyperplasia (BPH), prostatitis and prostate cancer tissue<sup>50,51</sup>. This study demonstrated the difficulty in designing and optimizing imaging probes to differentiate between early staged PCa and benign prostate hyperplasia (BPH) (Figure 2.2)<sup>51</sup>. The level of FDG accumulates in both tissues, making it difficult to distinguish between malignant and benign conditions. In



addition to the overlap observed in Figure 2.2, both patients had similar PSA levels, which confirmed the inaccuracy of diagnosing early PCa using an alternative approach.

From this, it has become clear that balancing between early diagnosis and the potential for overtreatment of prostate cancer has resulted in a clinically relevant problem<sup>52,53</sup>. Non-invasive molecular imaging agents targeting cancer-specific receptors, may offer new insight into solving this dilemma, and could lead to improvements in distinguishing between aggressive and indolent disease.

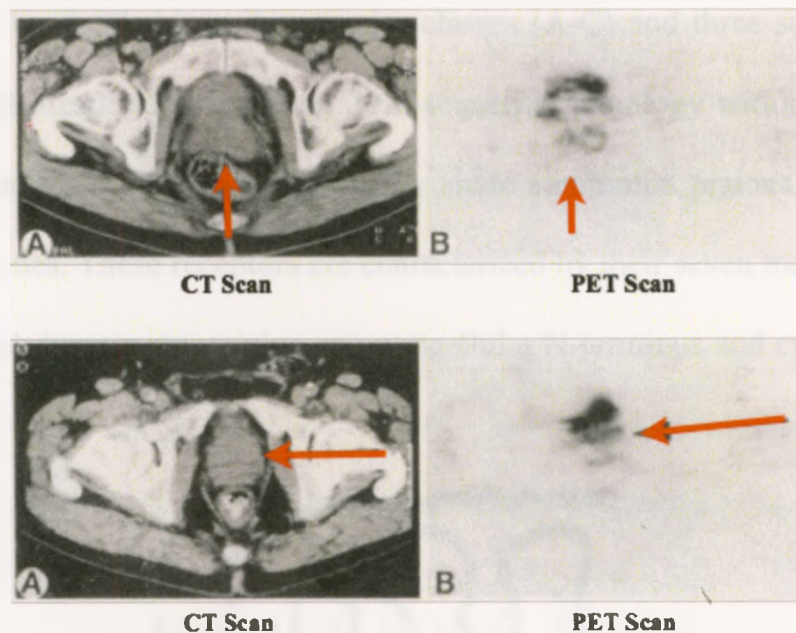


**Figure 2.2.** *Top* figure represents a patient with early stage PCa. *Bottom* figure represents a patient with BPH. In both figures, Red arrows show the anatomic location of the tumour (CT scan) and accumulation of  $^{18}\text{F}$ -FDG (PET scan). Each patient's condition was confirmed by post-surgical biopsies<sup>51</sup>.

## 2.2 Introduction to Imaging G-Protein Coupled Receptors

Cell-surface G-protein coupled receptors (GPCRs) are well-known targeting entities that are responsible for modulating almost all physiological processes<sup>54</sup>. GPCRs are considered the most diverse class of protein families within the human genome. Of the 35,000 human genes isolated from the human genome, approximately 720 encode for

GPCRs and 400 of these are expected to be potential drug targets<sup>55,56</sup>. Their popularity has risen over the past decade in behaving as *in vivo* targets because of their location lying largely within the plasma membrane of cells. This location has proven a crucial role in target accessibility, making GPCRs readily available to pharmaceutical agents. Yet, there has been limited interest in investigating this broad family of receptors for tumour imaging, even though targeting GPCRs statistically accounts for half of our current marketed drugs<sup>57</sup>.

GPCRs can be divided into three major classes (A-C) and three smaller classes (D-F). These classes are divided based on 20% sequence homology within the receptor domains<sup>58</sup>. Structurally, GPCRs as a superfamily share a common regional composition within their membranes. These receptors are characterized by their seven trans-membrane (7-TM) alpha helical domain, containing an extracellular N-terminus and cytoplasmic C-terminus.

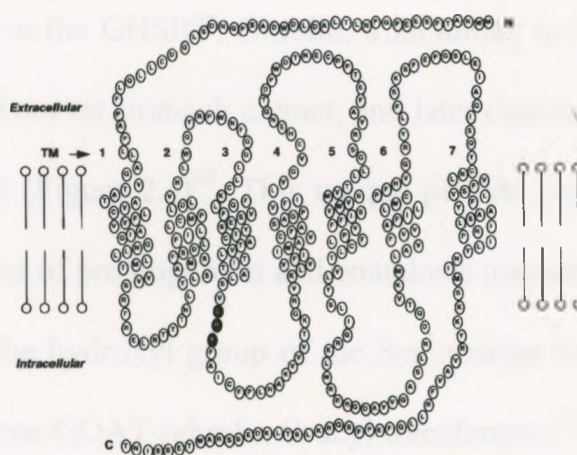


**Figure 2.3.** Growth hormone secretagogue receptor indicating the seven trans-membrane domain.<sup>59</sup>

### 2.3 Imaging the Growth Hormone Secretagogue Receptor-1a (GHSR-1a)

In 1996, Smith *et al* identified a sub-class of the GPCR family termed the growth hormone secretagogue receptor (GHSR)<sup>59</sup>. As is typical, this receptor contains the 7-TM

characteristic domain with alternating intracellular and extracellular loops (Figure 2.3)<sup>59</sup>. The GHSR consists of a 366 amino acid sequence and is involved in the regulation of growth hormone (GH) secretion<sup>60</sup>. GHSRs have been further subdivided into receptors containing an Asp-Arg-Tyr motif on the intracellular portion of loop III (GHSR-1), secretin family receptors (GHSR-2), and glutamate receptors (GHSR-3). In healthy individuals, the GHSR-1 has shown to be expressed within endocrine and reproductive organs, various regions of the brain (hypothalamus, and pituitary gland), bone marrow and the pancreas<sup>60,61,62,63</sup>. More importantly, a differential expression of the GHSR is observed in normal human tissue versus that of various types of tumours including breast carcinomas, prostate cancer cells, ovarian tumours, testicular tumours, pancreatic endocrine tumour, and intestinal carcinoids<sup>11,12,13,64,65,66,67</sup>. This evidence points towards the ability to use the GHSR as a cancer-specific target for molecular imaging.

In 1999, Kojima *et al.* reported the purification and identification of the first endogenous ligand specific to the GHSR<sup>68</sup>. Ghrelin, a 28 amino acid orexigenic peptide hormone was first isolated from rat stomach extract, and later determined to be expressed throughout the human body (Figure 2.4)<sup>68</sup>. This unique peptide originates from a post-translational cleavage product of preproghrelin and contains a unique hydrophobic moiety off of residue 3 (Ser<sup>3</sup>)<sup>69</sup>. The hydroxyl group of the Ser<sup>3</sup> residue is octanoylated in the cell's cytosome by the enzyme GOAT (ghrelin O-acyl transferase)<sup>70,71</sup>. Des-octanoylated (ghrelin with the absence of Ser<sup>3</sup> side chain) ghrelin does exist in excess throughout the body, which is regulated by esterase enzymes via ester hydrolysis<sup>69</sup>.



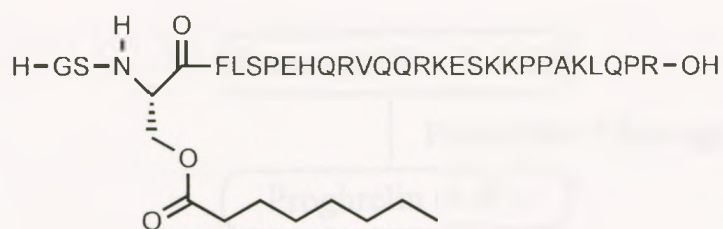


**Figure 2.4.** Structure of Human Ghrelin.

Ghrelin binds to the growth hormone secretagogue receptor-1 (GHSR-1) with high affinity and selectivity to form an internalized GHSR-ghrelin complex<sup>68</sup>. Two transcripts within the GHSR-1 complex have been identified; GHSR-1a is the biologically active form of the receptor which ghrelin is able to bind to, while GHSR-1b is a truncated version lacking domains 6 and 7<sup>72</sup>. The goal of this project was to synthesize molecular imaging probes containing a ghrelin peptide sequence to target tissues which show a high GHSR-1a expression. Our objective was to delineate cancerous tissues present within the prostate from that of benign tissues using a modified ghrelin analogue.

Numerous half-maximal effective concentration ( $EC_{50}$ ) and half-maximal inhibitory concentration ( $IC_{50}$ ) values have been reported throughout the literature pertaining to ghrelin's binding affinity to the GHSR-1a<sup>73,74,75,76</sup>. In one study, alanine scans, where an alanine amino acid was substituted in place of each amino acid in the peptide sequence, were performed on truncated versions of ghrelin<sup>75</sup>. In ghrelin(1-14), no significant change in binding affinity was observed when substituting the majority of the

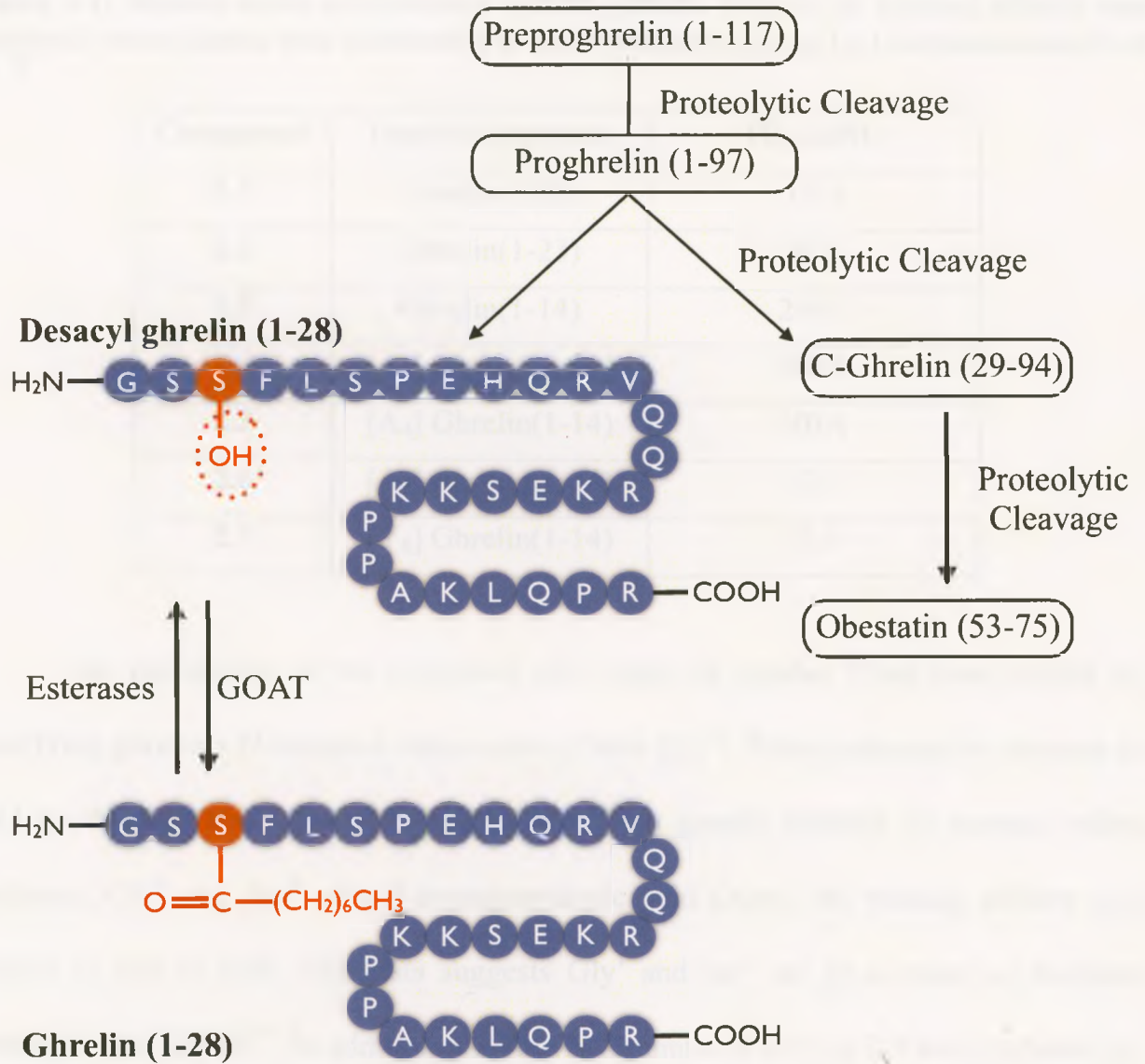


**Figure 2.5.** Origins of human ghrelin.<sup>69</sup>

amino acids with alanine. However, when replacing the octanoylated Ser<sup>3</sup>, and Phe<sup>4</sup> residues a significant decrease in binding affinity was observed (Table 2.1). Modifying position eight with either tyrosine or alanine leads to an increased receptor recognition and activation to ghrelin fragments<sup>73,75</sup>. These results demonstrate that several residues in ghrelin's sequence could be modified while having little to no loss in the peptides binding affinity.

**Table 2.1.** Alanine scans on truncated human ghrelin. NBA is no binding affinity was observed when alanine was substituted in these positions. Study by Cancraenenbroeck *et al.*<sup>75</sup>

Compound	Peptide Sequence	IC <sub>50</sub> (nM)
2.1	Ghrelin(1-28)	10.5
2.2	Ghrelin(1-23)	36.1
2.3	Ghrelin(1-14)	219.1
2.4	[A <sub>3</sub> ] Ghrelin(1-14)	NBA
2.5	[A <sub>4</sub> ] Ghrelin(1-14)	NBA
2.6	[A <sub>8</sub> ] Ghrelin(1-14)	33.9
2.7	[Y <sub>8</sub> ] Ghrelin(1-14)	21.8

The positioning of the acetylated side chain off residue 3 has been studied by modifying ghrelin's N-terminal amino acids (Table 2.2)<sup>74</sup>. When reducing the distance in **2.13** by deleting Ser<sup>2</sup>, ghrelin's binding affinity is greatly reduced. In contrast, when replacing Gly<sup>1</sup> and Ser<sup>2</sup> with 5-aminopentanoic acid (Ape), the binding affinity was similar to that of **2.10**. This data suggests Gly<sup>1</sup> and Ser<sup>2</sup> act as a spacer to facilitate binding to the GHSR<sup>74</sup>. In addition, the free N-terminus of Gly<sup>1</sup> in **2.9** was evaluated by comparing it to acetylated **2.15**. Acetylated **2.15** was 20-fold less potent than **2.9**, suggesting a positively charged N-terminus improves ghrelin's binding affinity<sup>75</sup>. In addition to modifying the N-terminus of ghrelin, the C-terminus has been altered by changing the native carboxylic acid to an amide moiety. Amide **2.12** displayed enhanced binding affinity over acid **2.11**<sup>74</sup>. From this it was concluded a truncated ghrelin(1-5) (**2.12**) was the shortest peptide chain responsible for eliciting a biological response to the GHSR<sup>75</sup>.

**Table 2.2.** The Importance of Gly<sup>1</sup> and Ser<sup>2</sup> in ghrelin analogs. Study by Matsumoto *et al.*<sup>73,74</sup>

Compound	Peptide Sequence	EC <sub>50</sub> (nM)
2.8	Human Ghrelin(1-28)	1.3
2.9	Ghrelin(1-14)	19
2.10	Ghrelin(1-7)-amide	2.6
2.11	Ghrelin(1-5)	68
2.12	Ghrelin(1-5)-amide	6.2
2.13	Desacyl-Ser <sup>2</sup> -Ghrelin(1-7)-amide	380
2.14	[N <sup>α</sup> -Ape] Ghrelin(3-7)-amide	3.4
2.15	[N <sup>α</sup> -acetyl] ghrelin(1-14)	>10,000

Ghrelin is the first natural peptide observed to contain an acylated side chain, with most of the existing research focused on exploring the role of this unique functionality<sup>77</sup>. Recently, spectroscopic studies have shown that the octanoylated side chain and the Phe<sup>4</sup> residue to be required for receptor binding<sup>70</sup>. Placing the acylated side chain on other serine residues (Ser<sup>2</sup>, Ser<sup>6</sup>, Ser<sup>18</sup>) in human ghrelin proved to be detrimental to the binding affinity (Figure 2.6.a,b,c,d)<sup>76</sup>. In the absence of the acylated side chain, desacyl-ghrelin displayed a complete loss in of affinity for the GHSR, which inherently confirms the importance of the lipophilic chain (Figure 2.6.e)<sup>70</sup>. Additional D- or L-amino acids have been substituted in place of the Ser<sup>3</sup> residue. However, the unnatural amino acid 2,3-diaminopropionic acid (Dpr) is the only viable option which has not been detrimental to binding affinity (Figure 2.6.f)<sup>73</sup>.



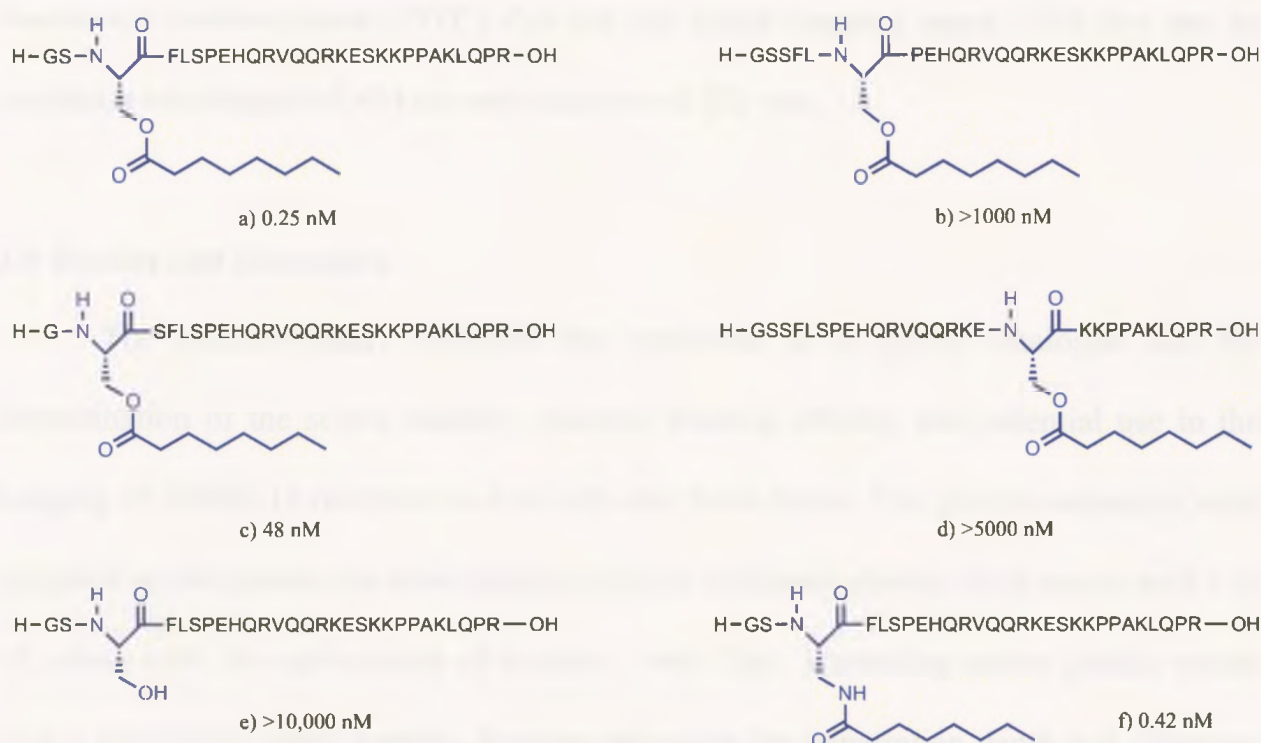


**Figure 2.6.**  $IC_{50}$  values reported for modified ghrelin(1-28) analogs. Results show the importance of the acylated side chain to the GHSR binding affinity. Positioning the acylated side chain towards the N-terminus (b) shows a loss in binding affinity. A substantial decrease in binding affinity is observed in analogs where the side chain is positioned towards the C-terminus (c and d). In the absence of the acylated side chain (e) binding is reduced. Replacing serine with 2,3-diaminopropionic acid (Dpr) (f) shows a relatively small change in binding affinity to the GHSR.

### 2.3.1 Incorporating an Optical Imaging Agent into a Modified Ghrelin Peptide

Optical imaging agents are used to evaluate the performance of an imaging probe *in vitro* before proceeding with radiolabelling methodologies. Using an optical dye in initial studies can assess the potential of the imaging agent for targeting a specific receptor. These moieties offer safer and easier methods for synthesizing imaging probes and have longer shelf-lives than radioactive materials. However, fluorescent probes are limited in value due to their low penetration depths of only a few centimeters through tissue and thus are not suitable for *in vivo* imaging. For our purposes we used a

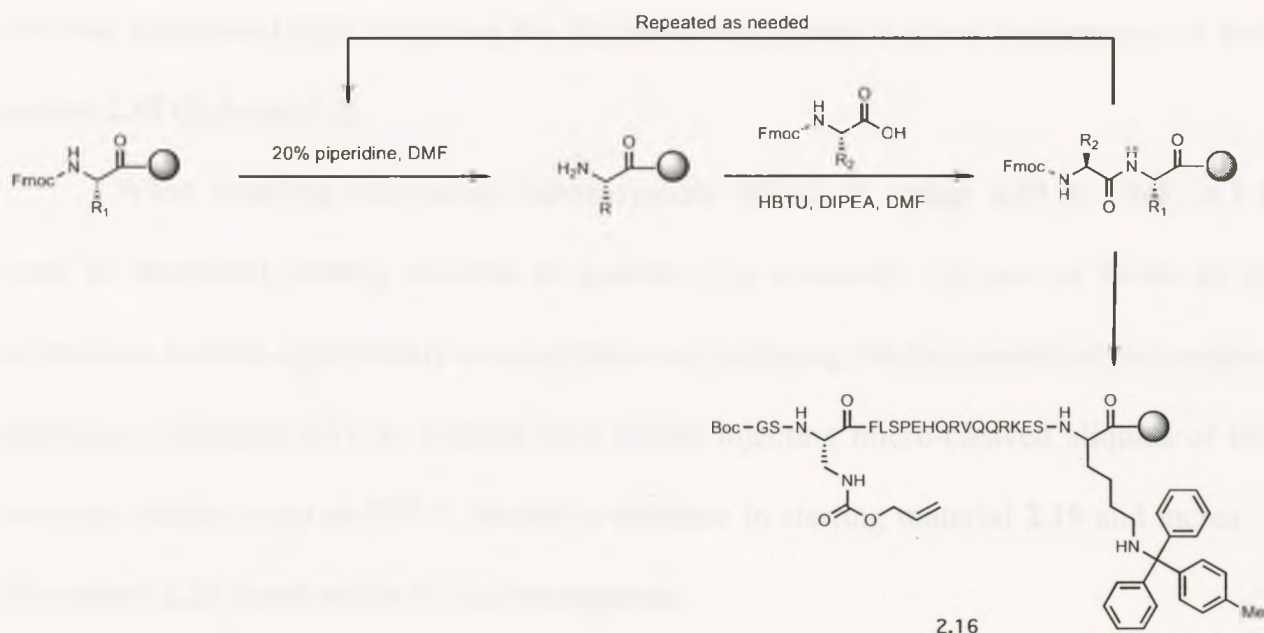


fluorescein isothiocyanate (FITC) dye for our initial imaging agent. This dye has an excitation wavelength of 494 nm and emission of 521 nm.

## 2.4 Results and Discussion

The present study, discusses the synthesis of a ghrelin analogue and the determination of the serum stability, receptor binding affinity, and potential use in the imaging of GHSR-1a receptors in live cells and fixed tissue. The ghrelin analogues were designed to incorporate the most critical residues of human ghrelin, from amino acid 1 to 18, along with the replacement of residue 3 with Dpr. Truncating native ghrelin would give a moderately small peptide, thereby enhancing the penetration depth and clearance properties of the peptide. In addition, replacing Ser<sup>3</sup> with the unnatural amino acid Dpr<sup>3</sup> had previously been proposed to enhance the peptides stability by limiting *in vivo* ester hydrolysis<sup>78</sup>. It was also decided to change the C-terminal carboxylic acid with an amide functionality by using a rink amide 4-methylbenzylhydramine (MBHA) resin. This addition was to further improve the stability towards cellular exopeptidases, slowing the metabolism of ghrelin *in vivo*.

The synthesis of [Dpr(octanoyl)<sup>3</sup>,Lys(fluorescein)<sup>19</sup>]ghrelin(1-19)-amide **2.21** was carried out in three steps. The 19 amino acid peptide sequence was synthesized manually according to standard Fmoc-SPPS techniques (Scheme 2.1). The incorporation of Lys<sup>19</sup> at the C-terminus of the peptide provides a site of attachment for the fluorescein isothiocyanate dye. Placing the optical dye near the C-terminus would greatly reduce the interference with the N-terminal binding region of each ghrelin analogue, thereby maintaining the binding affinity (Scheme 2.1).

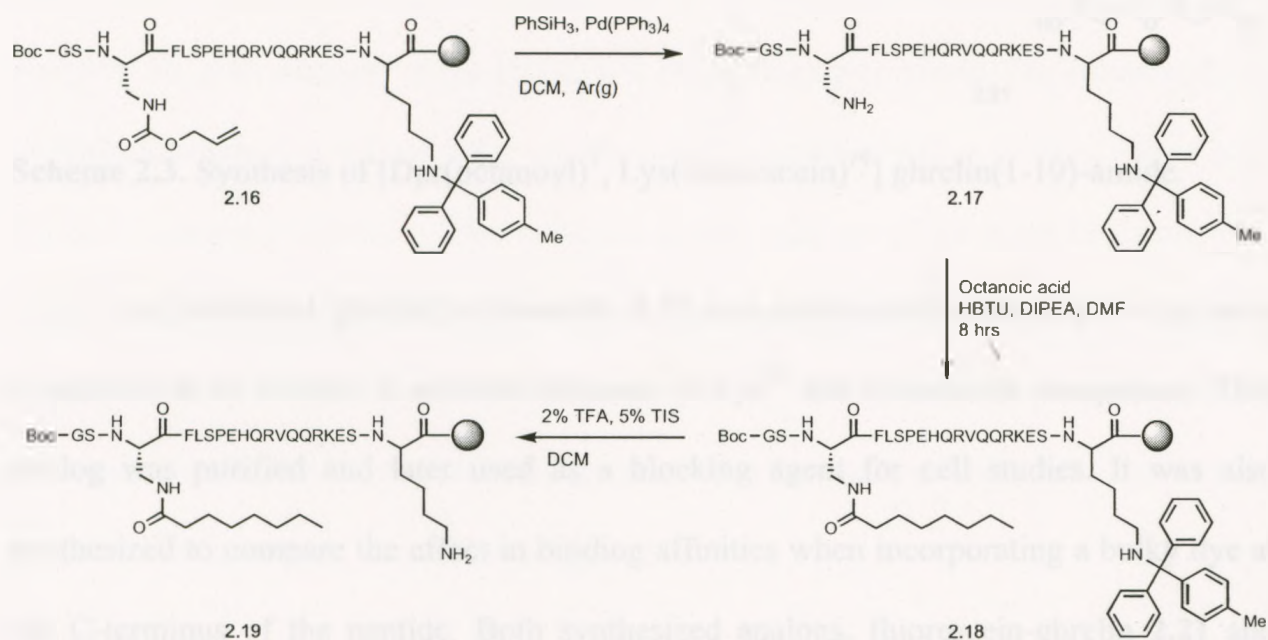


**Scheme 2.1.** Design of ghrelin(1-18)-amide peptides.

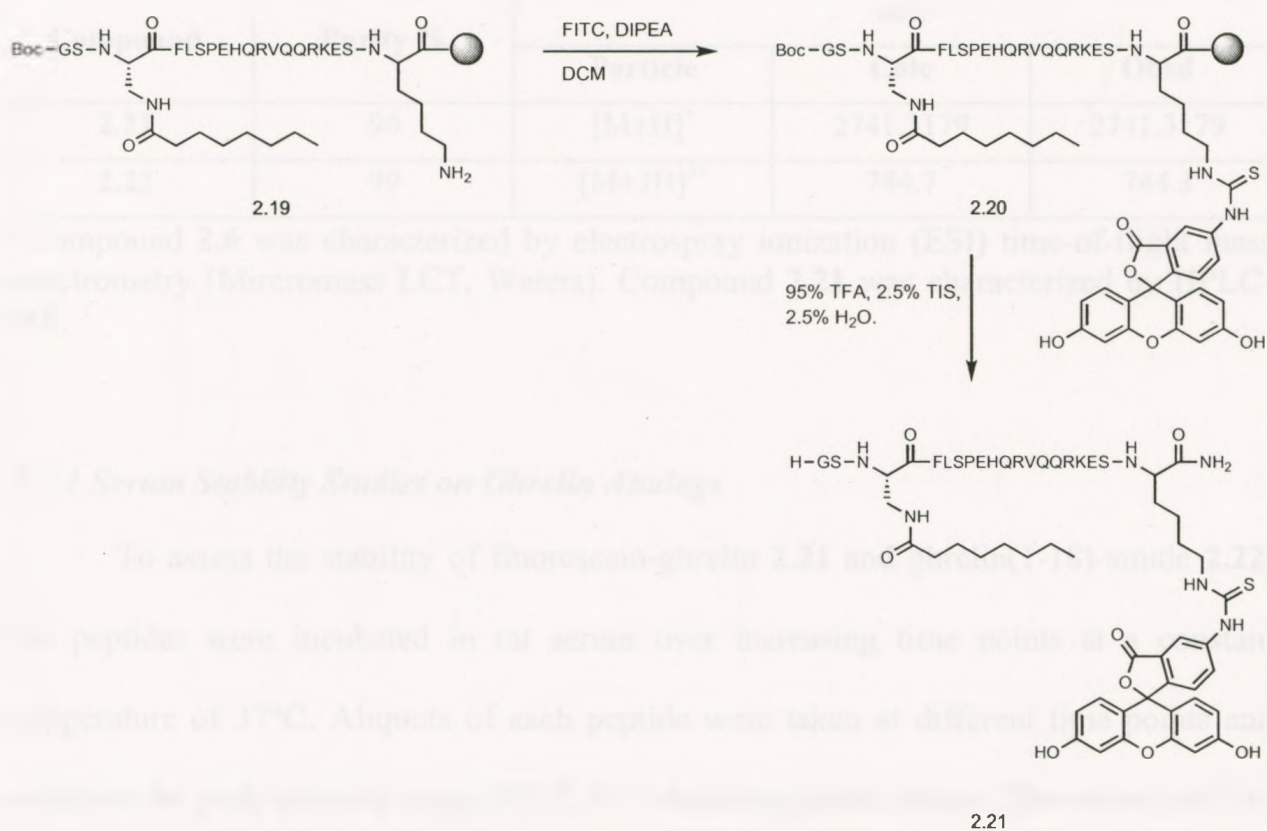
An orthogonal protecting group strategy was designed to allow for the selective removal of Dpr<sup>3</sup> and Lys<sup>19</sup> side chain protecting groups for additional modifications to the peptide (Scheme 2.2). For that reason, Dpr<sup>3</sup> and Lys<sup>19</sup> were protected with allyloxycarbonyl (alloc) and 4-methyltrityl (Mtt) respectively (Scheme 2.1). All other amino acids were protected using standard Fmoc orthogonal protecting groups that could only be removed with greater than 50% trifluoroacetic acid. While still on resin, selective removal of Dpr (alloc) was accomplished by using phenylsilane and a tetrakis(triphenylphosphine)palladium(0) catalyst. The addition of octanoic acid to free amine **2.17** afforded **2.18**, which was characterized by HPLC-MS. Following this, the addition of weak acid selectively deprotected the protected Lys<sup>19</sup> side chain. Deprotection of 4-methyltrityl (mtt) proved to be challenging and required multiple treatments of dilute trifluoroacetic acid (2.5% TFA) solution in dichloromethane (DCM). A qualitative Kaiser

test was performed after removing the Mtt protecting group to show the presence of free amine **2.19** (Scheme 2.2).

When coupling fluorescein isothiocyanate (FITC) to amine **2.19** in DMF, a 1:1 ratio of unreacted starting material to product was observed. The use of DCM as an alternative solvent significantly reduced this ratio, allowing for the reaction to occur more efficiently (Scheme 2.3). At various time points, injecting micro-cleaved aliquots of the reaction mixture onto an HPLC showed a decrease in starting material **2.19** and increase in product **2.21** based on the UV-chromatogram.



**Scheme 2.2.** Orthogonal Protecting group strategy for the synthesis of [Dpr(octanoyl)<sup>3</sup>, Lys(flourescein)<sup>19</sup>] ghrelin(1-19)-amide.



**Scheme 2.3.** Synthesis of [Dpr(octanoyl)<sup>3</sup>, Lys(fluorescein)<sup>10</sup>] ghrelin(1-19)-amide.

An additional ghrelin(1-18)-amide **2.22** was synthesized according to the same conditions as in scheme 2 with the absence of Lys<sup>19</sup> and fluorescein component. This analog was purified and later used as a blocking agent for cell studies. It was also synthesized to compare the effect in binding affinities when incorporating a bulky dye at the C-terminus of the peptide. Both synthesized analogs, fluorescein-ghrelin **2.21** and ghrelin(1-18)-amide **2.22** were purified by HPLC-MS and isolated with yields of 15% and 13% respectively (Table 2.3).



**Table 2.3.** Ghrelin analogs with their purity, calculated, and observed mass.

Compound	Purity %	m/z		
		Particle	Calc	Obsd
2.21	96	[M+H] <sup>+</sup>	2741.3179	2741.3179
2.22	99	[M+3H] <sup>3+</sup>	744.7	744.3

\*Compound **2.6** was characterized by electrospray ionization (ESI) time-of-flight mass spectrometry (Micromass LCT, Waters). Compound **2.21** was characterized by HPLC-MS.

#### 2.4.1 Serum Stability Studies on Ghrelin Analogs

To assess the stability of fluorescein-ghrelin **2.21** and ghrelin(1-18)-amide **2.22**, the peptides were incubated in rat serum over increasing time points at a constant temperature of 37°C. Aliquots of each peptide were taken at different time points and analyzed for peak intensity using HPLC UV chromatographic traces. The serum stability of fluorescein-ghrelin did not differ significantly from that of native ghrelin, with a half-life of 27 minutes (Table 2.4). This validated the potential use of the probe in later *ex vivo* imaging studies. Ghrelin(1-18)-amide **2.22** displayed a far better half-life of 83 minutes in comparison to fluorescein-ghrelin **2.21** (Table 2.4). The shorter half-life of analogue **2.21**, is proposed to be due to enzymes initially degrading the pendent lysine side chain which connects the fluorescein component (Figure 2.7).

#### 2.4.2 Binding Assays

A receptor-binding assay using membranes overexpressing human GHSR-1a was developed by our collaborator Dr. Savita Dhanvnatari, in order to investigate the receptor binding affinities of the fluorescein-ghrelin and ghrelin(1-18)-amide (Table 2.4). The

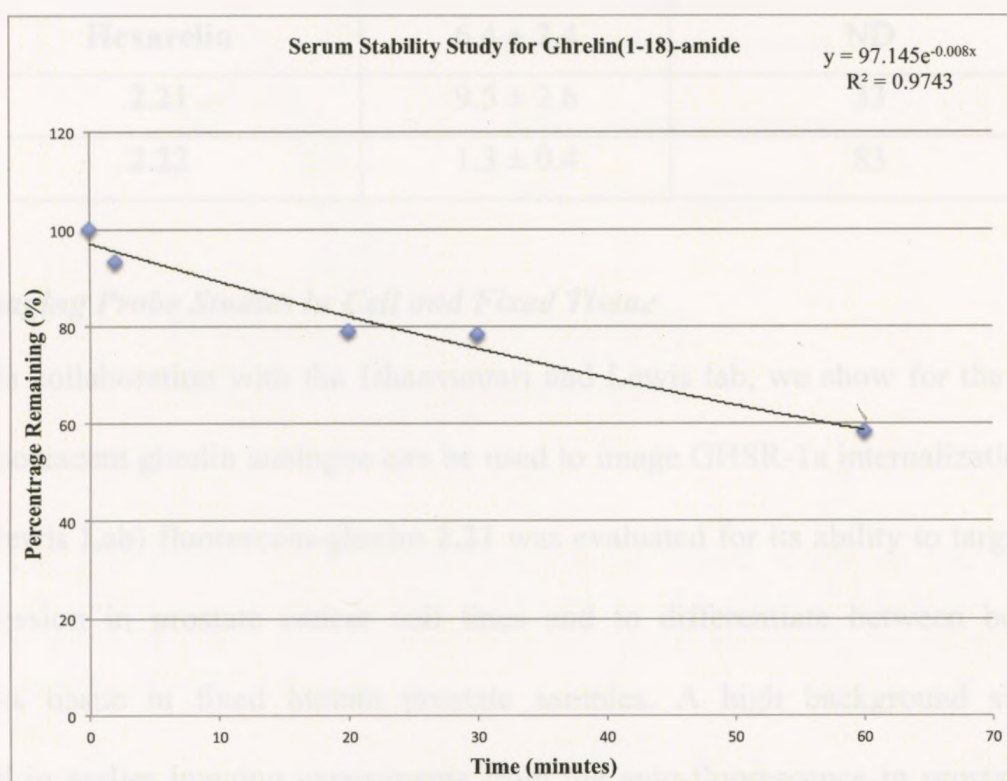
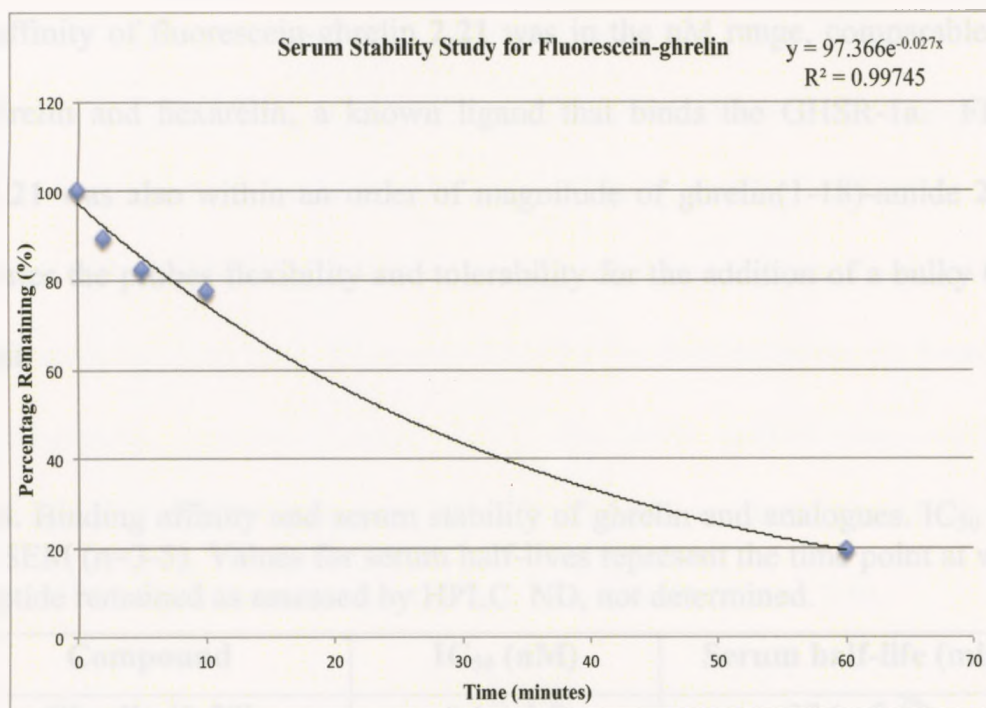


**Figure 2.7.** Serum stability studies for fluorescein-ghrelin **2.21** (top) and ghrelin(1-18)-amide **2.22**. Half-lives were extrapolated and calculated at 50% (based on line of best fit).



binding affinity of fluorescein-ghrelin **2.21** was in the nM range, comparable to that of native ghrelin and hexarelin, a known ligand that binds the GHSR-1a. Fluorescein-ghrelin **2.21** was also within an order of magnitude of ghrelin(1-18)-amide **2.22** which demonstrates the probes flexibility and tolerability for the addition of a bulky C-terminal substituent.

**Table 2.4.** Binding affinity and serum stability of ghrelin and analogues. IC<sub>50</sub> values are means  $\pm$  SEM (n=3-5). Values for serum half-lives represent the time point at which 50% of the peptide remained as assessed by HPLC. ND, not determined.

Compound	IC <sub>50</sub> (nM)	Serum half-life (min)
Ghrelin [1-28]	8.1 $\pm$ 1.0	27 (ref. <sup>79</sup> )
Hexarelin	6.4 $\pm$ 2.4	ND
<b>2.21</b>	9.5 $\pm$ 2.6	33
<b>2.22</b>	1.3 $\pm$ 0.4	83

#### 2.4.3 Imaging Probe Studies in Cell and Fixed Tissue

In collaboration with the Dhanvantari and Lewis lab, we show for the first time that a fluorescent ghrelin analogue can be used to image GHSR-1a internalization. In one study (Lewis Lab) fluorescein-ghrelin **2.21** was evaluated for its ability to target GHSR-1a expression in prostate cancer cell lines and to differentiate between benign and cancerous tissue in fixed human prostate samples. A high background signal was observed in earlier imaging experiments from the auto-fluorescence in prostate tissues, making it difficult to confirm the specificity of the probe. To solve this problem the hapten amplification technique was used to both amplify the signal and shift the detection of the probe to the near infrared spectral window (Figure 2.8)<sup>80</sup>.

Two GHSR-expressing human prostate cancer cell lines, PC3 and LNCaP were chosen to validate the affinity of the fluorescent probe. Binding of fluorescein-ghrelin probe **2.21** was observed for both cell lines at the membrane and in the endosomal compartment (Figure 2.9). The fluorescent probe was further blocked by the competitive binding of unlabelled ghrelin(1-18)-amide **2.22**, further demonstrating the formation of an internalized-ghrelin complex (Figure 2.10). The cells studies also confirmed our fluorescein-ghrelin's specificity towards the GHSR-1a as no uptake was observed in non-expressing GHSR benign prostate hyperplasia (BPH) cells (Figure 2.9).

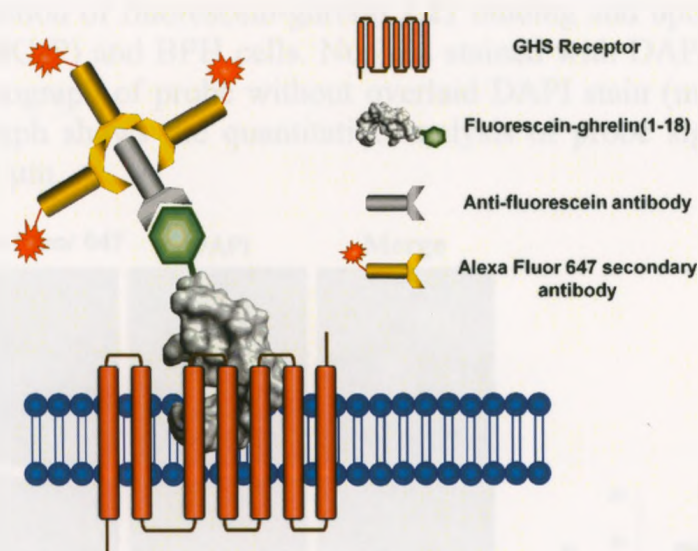


**Figure 2.8.** The hapten amplification technique is shown where an anti-fluorescein antibody is incubated with the probe, followed by the addition of Alexa Fluor 647 secondary antibody. This approach amplifies the signal and shifts the detection of the probe to the near infrared spectrum.

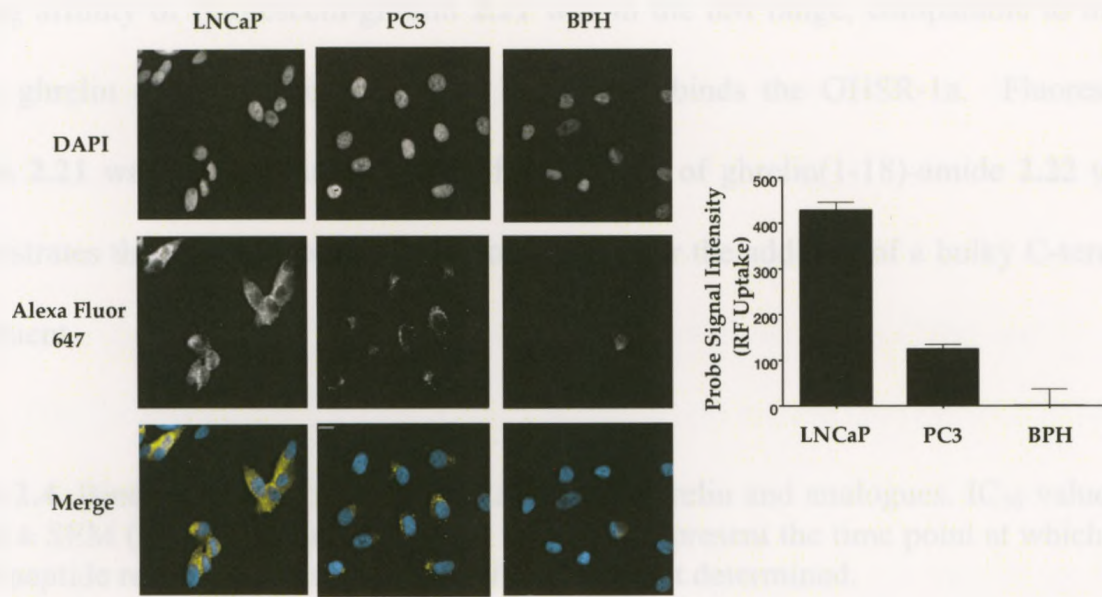


**Figure 2.9.** Evaluation of fluorescein-ghrelin 2.21 binding and uptake in prostate cancer cells (PC3 and LNCaP) and BPH cells. Nucleus stained with DAPI blue (upper panels). Fluorescence micrograph of probe without overlaid DAPI stain (middle panel) and with (lower panel). Graph shows the quantitative analysis of probe signal intensity in cells lines. Scale bar 10  $\mu$ m.

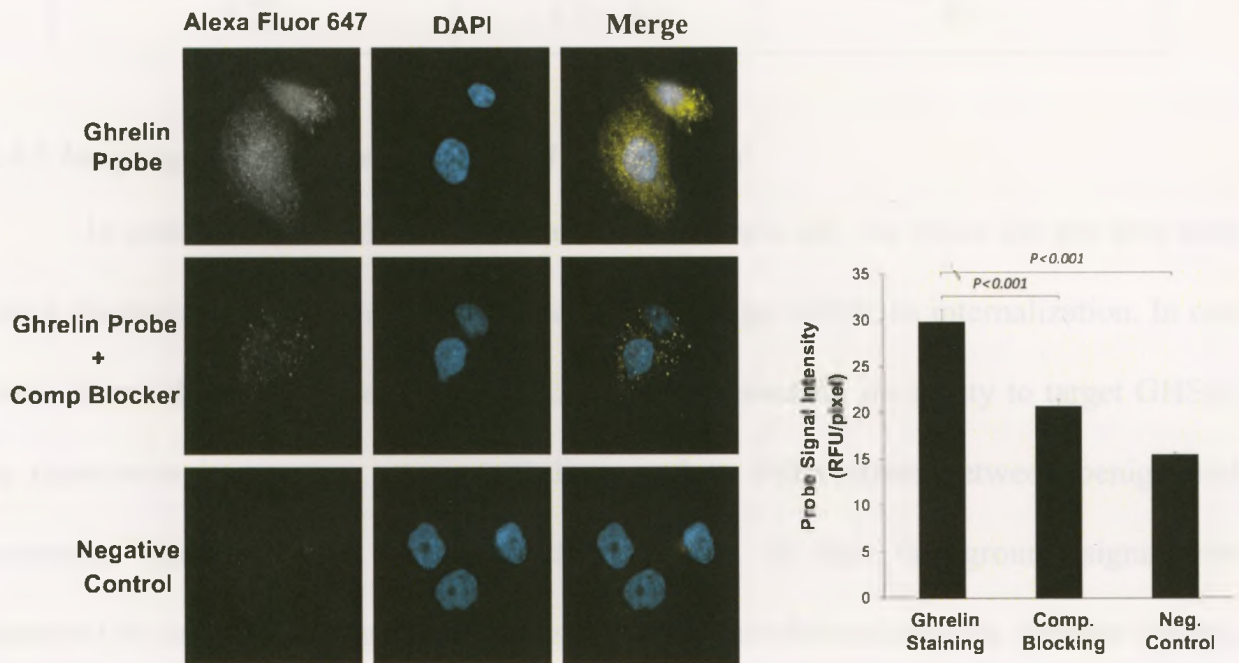


**Figure 2.10.** Evaluation of fluorescein-ghrelin 2.21 and uptake in PC3 cells. Fluorescence micrograph of PC3 cells incubated with fluorescein-ghrelin 2.21 in the presence (middle and panels) and absence (upper panels) of excess ghrelin(1-18)-amide 2.22. Negative control (lower panels) contained no fluorescent probe. Graph shows the quantitative analysis of probe signal intensity with and without the presence of unlabelled ghrelin(1-18)-amide 2.22. Scale bar 5  $\mu$ m.



binding affinity of fluorescein-ghrelin **2.21** was in the nM range, comparable to that of native ghrelin and hexarelin, a known ligand that binds the GHSR-1a. Fluorescein-ghrelin **2.21** was also within an order of magnitude of ghrelin(1-18)-amide **2.22** which demonstrates the probes flexibility and tolerability for the addition of a bulky C-terminal substituent.

**Table 2.4.** Binding affinity and serum stability of ghrelin and analogues. IC<sub>50</sub> values are means ± SEM (n=3-5). Values for serum half-lives represent the time point at which 50% of the peptide remained as assessed by HPLC. ND, not determined.

Compound	IC <sub>50</sub> (nM)	Serum half-life (min)
Ghrelin [1-28]	8.1 ± 1.0	27 (ref. <sup>79</sup> )
Hexarelin	6.4 ± 2.4	ND
<b>2.21</b>	9.5 ± 2.6	33
<b>2.22</b>	1.3 ± 0.4	83

#### 2.4.3 Imaging Probe Studies in Cell and Fixed Tissue

In collaboration with the Dhanvantari and Lewis lab, we show for the first time that a fluorescent ghrelin analogue can be used to image GHSR-1a internalization. In one study (Lewis Lab) fluorescein-ghrelin **2.21** was evaluated for its ability to target GHSR-1a expression in prostate cancer cell lines and to differentiate between benign and cancerous tissue in fixed human prostate samples. A high background signal was observed in earlier imaging experiments from the auto-fluorescence in prostate tissues, making it difficult to confirm the specificity of the probe. To solve this problem the hapten amplification technique was used to both amplify the signal and shift the detection of the probe to the near infrared spectral window (Figure 2.8)<sup>80</sup>.

To test the selectivity of our fluorescein-ghrelin probe for imaging prostate cancer over benign prostate tissue, standard prostate samples were gathered from patients undergoing radical prostatectomies in the Department of Urology at the London Regional Health Science Centre. *Ex vivo* prostate tissue was confirmed by pathological reports and divided into three categories: (a) PCa, (b) paraepithelial neoplasia (PIN) and (c) BPH tissue. The fluorescein-ghrelin 2.21 probe was able to distinguish between PCa tissue and normal adjacent tissue (Figure 2.11). The selectivity of our probe was additionally observed by its ability to differentiate between PCa and BPH. To our knowledge this is the first example where prostate cancer tissue has been selectively differentiated from benign tissues through the use of a receptor targeted imaging agent.

A subsequent study in collaboration with the Dhanvantari lab looked at GHSR-1a expression within a murine model. This study was based on a recent finding showing an increase in GHSR-1a expression within the myocardium of patients suffering congestive heart failure<sup>81</sup>. Western blot analysis revealed the strongest expression of GHSR-1a to be within the heart and brain. More importantly, GHSR-1a expression was not evident within organs such as the liver, stomach, kidney, pancreas, intestine and spleen<sup>63,82</sup>. Our initial results presented a new possibility of using our modified ghrelin probe for imaging cardiac pathology. This was tested by incubating fluorescein-ghrelin alone in murine heart tissue, or with excess unlabelled ghrelin(1-28) or hexarelin added. Interestingly, heart tissue incubated with fluorescein-ghrelin alone was brightly fluorescent, where as lower fluorescence was observed when adding excess ghrelin(1-28) or hexarelin. The blocking of fluorescence with ghrelin(1-28) or hexarelin indicated the specific binding of our probe to GHSR-1a in the heart.



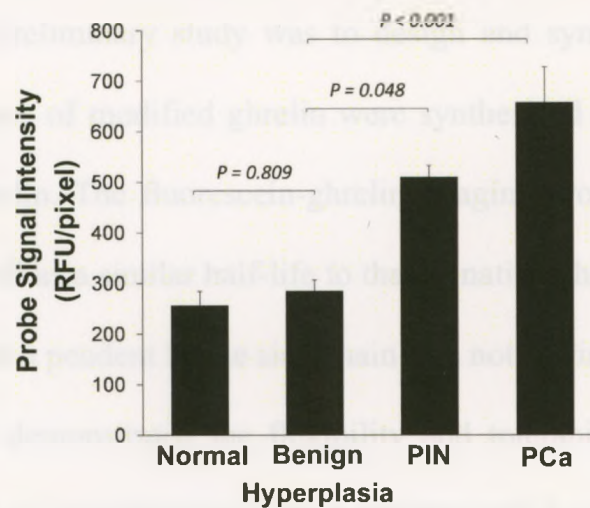
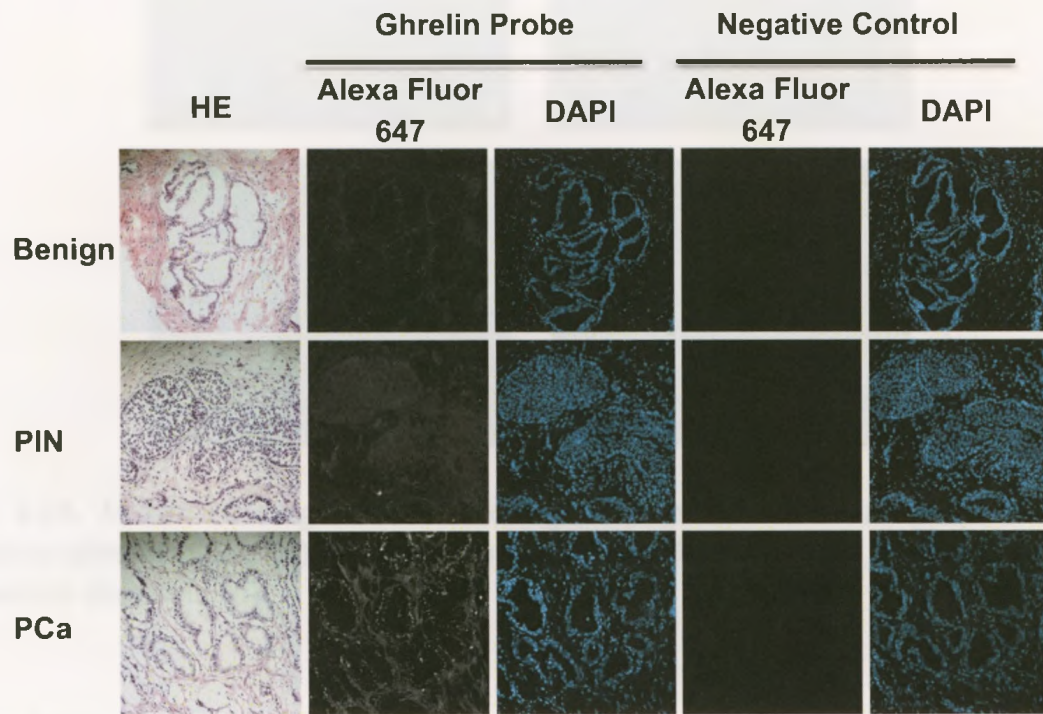


**Figure 2.11.** Evaluation of fluorescein-ghrelin 2.21 probe in *ex vivo* human prostate biopsy tissue. Preferential uptake was found in PIN and PCa, as compared to normal prostate and BPH. Scale bar 10  $\mu$ m.

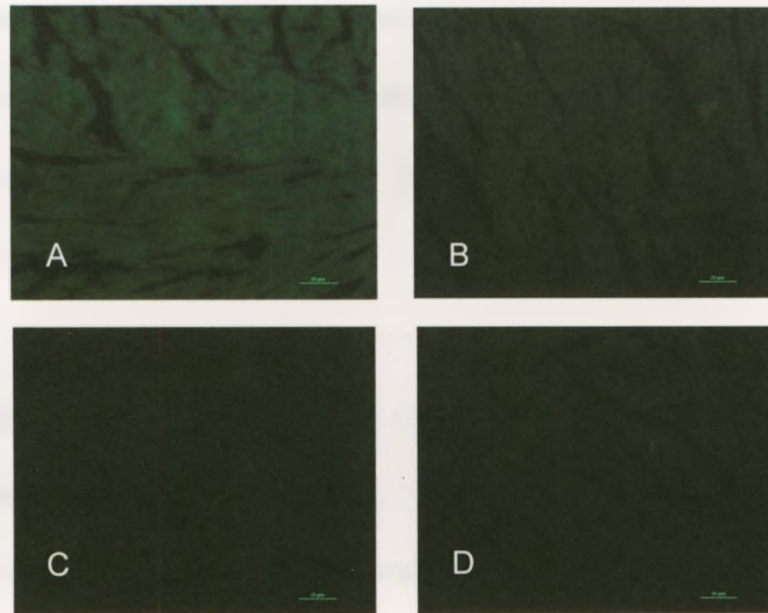


**Figure 2.12.** *In situ* binding of fluorescein-ghrelin in murine heart tissue. Binding of fluorescein-ghrelin alone (a), or in the presence of ghrelin (b) or hexarelin (c). Autofluorescence shown in (d).

## 2.5 Conclusions

The objective of this preliminary study was to design and synthesize an optical imaging probe. Two analogues of modified ghrelin were synthesized to incorporate the most critical residues of ghrelin. The fluorescein-ghrelin imaging probe **2.21** showed a 9.5 nM binding affinity as well as a similar half-life to that of native ghrelin. The addition of a fluorescent probe through a pendent lysine side chain was not detrimental to ghrelin's binding affinity and further demonstrated the flexibility and tolerability of our probe. Internalization of the probe was visualized using two different cell lines that were known to express the GHSR-1a. *Ex vivo* human prostate tissue treated with the fluorescein-ghrelin probe **2.21** demonstrated high selectivity in differentiating prostate cancer from indolent disease. In addition to this study, the probe demonstrated binding to normal murine heart tissue. This initial result raises the possibility of using this probe for monitoring heart disease in patients with cardiomyopathy.

These results have set the stage by validating our probe for use in *in vitro* and *ex vivo* imaging. More importantly, the present study allows for future modifications to ghrelin(1-18)-amide **2.22** by incorporating other dyes or chelators for a new use in positron emission tomography (PET).

## 2.6 Experimental

### 2.6.1 Materials and Equipment

All chemicals and solvents were purchased from Sigma-Aldrich Chemical Co., Peptides International, VWR or Fisher Scientific and were used without further purification unless noted. High-resolution mass spectra were obtained on a Finnigan MAT 8400 Mass Spectrometer (EI), Micromass LCT Mass Spectrometer (ESI). Low-resolution mass spectra were obtained on a Micromass Quattro Micro API (MS-ESI and LC-MS-ESI). Anhydrous DCM was prepared by distillation from CaH under argon. Oven-dried or flame dried glassware was used in water sensitive reactions with the flow of argon. Analytical HPLC was performed using a Grace Vydac Protein/Peptide RP-C18 column 4.6 x 250 mm, 5  $\mu\text{m}$  or a Sunfire RP-C18 column 4.6 x 250 mm, 5  $\mu\text{m}$ . Preparative HPLC was performed using a Grace Vydac Peptide/Protein SP-C18 column 22.0 x 250 mm, 10  $\mu\text{m}$  or a Sunfire SP-C18 column 22.0 x 250 mm, 10  $\mu\text{m}$ . A gradient system was used: water + 0.1% TFA (solvent A) and  $\text{CH}_3\text{CN}$  + 0.1% TFA (Solvent B). The absorbance was detected in the 200 nm to 500 nm wavelength range.

### 2.6.2 General Procedure for Peptide Assembly

Fully protected resin bound peptides were synthesized manually according to general procedures in Fmoc solid phase peptide synthesis<sup>14</sup>. Fmoc protected rink amide MBHA



resin (loading 0.56 and 0.47 meq/ g) was used as the solid support. N-Fmoc amino acids with strong acid labile protecting groups for side chain functional groups, were used in general, and N-Boc amino acids were used for the N-terminus. Fmoc-Dpr<sup>3</sup>, with the  $\beta$ -amine protected with allyloxycarbonyl (alloc), was used for residue-3. Fmoc-lysine (Lys), with the  $\beta$ -amine protected with 4-methyltrityl (Mtt), was used for residue-19. Fmoc removal was achieved by adding 20% piperidine in DMF for 5 and 15 minutes, followed by successive washes with DMF and DCM after each treatment. For each amino acid coupling, resin was treated twice with 3 eq. of Fmoc or Boc amino acids, 3 eq. of 3-[bis(dimethylamino)methyl]-3H-benzotriazol-1-oxide hexafluorophosphate (HBTU) and 6 eq. of N,N-diisopropylethylamine (DIPEA) in 2 mL of DMF for 30 minutes to 2 hours. Couplings were followed by multiple washes with DMF, and DCM. Using this general procedure, peptides were prepared on resin.

### ***2.6.3 General Procedure for Selective Deprotection's and Resin Cleavage***

Selective deprotections were carried out using an orthogonal deprotection strategy for residues 3 and 19. The  $\beta$ -amine protected with allyloxycarbonyl (alloc) was selectively removed by shaking the resin with 0.35 eq. of tetrakis(triphenylphosphine)palladium ( $\text{Pd}(\text{PPh}_3)_4$ ), and 20 eq. of phenylsilane ( $\text{PhSiH}_3$ ) in 2 mL of dry DCM. This treatment was repeated twice, followed by successive washes with DMF, and DCM. The  $\beta$ -amine protected with 4-methyltrityl (mtt) was selectively removed by shaking the resin with 2% trifluoroacetic acid (TFA), and 5% triisopropylsilane (TIS) in DCM for 2 minutes. This treatment was carried out 8 times, followed by multiple washes with DMF, and DCM. The Kaiser test was used to monitor the presence or absence of a free amine. After modifications towards the peptides were

completed, the peptide was deprotected and cleaved from the resin using 95% TFA, 2.5% TIS, and 2.5% water for 3-6 hours. The resin was filtered and rinsed with a small amount of TFA. Cold tert-butyl methyl ether (TBME) was added to the filtrate to form a precipitate. Following the addition of TBME, the slurry was centrifuged and decanted. The peptide was rinsed with TBME and collected again. The solid was dissolved in water with the addition of acetonitrile (ACN) when needed, froze and lyophilized to obtain a crude peptide as a powder. Purification was carried out using preparative HPLC, and the purity of the isolated product was determined by analytical HPLC.

#### 2.6.4 [Dpr<sup>3</sup>(Octanoic acid)][Lys<sup>19</sup>(Fluorescein)]ghrelin(1-19)-amide (2.21)

[Dpr<sup>3</sup>(alloc)][Lys<sup>19</sup>(Mtt)]ghrelin(1-18) **2.1** was manually synthesized according to the general procedure for peptide assembly. Selective alloc deprotection was performed on residue-3 of **2.1** according to the general procedure to obtain a free amine **2.2**. Octanoic acid was coupled to the peptide to obtain **2.3** according to the general procedure for peptide assembly. Selective Mtt deprotection was performed on residue-19 to give the free amine, according to general procedures. Fluorescein isothiocyanate (FITC) (0.2 mmol, 0.078 g) was coupled to the peptide with the addition of 3 eq. DIPEA in 2 mL of DMF. Following this, a final cleavage and deprotection was conducted according to the general procedure to obtain the crude peptide. Purification was performed by HPLC (gradient 30-60% solvent A in B) to obtain **2.6** with a 15% yield as a yellow powder (ESI-MS and purity reported in Table 2.3).



### 2.6.5 [Dpr<sup>3</sup>(Octanoic acid)] ghrelin(1-18)-amide (2.22)

[Dpr<sup>3</sup>(alloc)] ghrelin(1-18) **2.1** was manually synthesized according to the general procedure for peptide assembly. Selective alloc deprotection was performed on residue-3 according to the general procedure to obtain a free amine. Octanoic acid was coupled to the peptide according to the general procedure for peptide assembly. Following this, a final cleavage and deprotection was conducted according to the general procedure to obtain the crude peptide. Purification was performed by HPLC (gradient 30-60% solvent A in B) to obtain **2.7** with a 15% yield as a yellow powder (ESI-MS and purity reported in Table 2.3).

### 2.6.6 Receptor Binding Assays<sup>83</sup>

Binding assays were performed using cell membranes over-expressing recombinant human GHS-R-1a (Millipore). The binding reaction consisted of 5mg membrane, 30,000 cpm (0.037nmol/L) [<sup>125</sup>I]-ghrelin (Perkin Elmer), and a range of concentrations (10<sup>-6</sup> to 10<sup>-11</sup>M) of hexarelin (a synthetic ghrelin with similar binding properties as endogenous ghrelin), ghrelin(1-18) or fluorescein-ghrelin(1-18) in a total volume of 100  $\mu$ L binding buffer (50 mM Hepes, pH 7.4, 5mM MgCl<sub>2</sub>, 1 mM CaCl<sub>2</sub>, 0.2% BSA, passed through a 0.45  $\mu$ m filter). Total binding was determined by adding only [<sup>125</sup>I]-ghrelin and membrane preparations to binding buffer. Tubes were incubated at 37°C with shaking at 500 rpm for 1 h, centrifuged at 13,000 rpm for 20 min and the pellet was washed once in wash buffer (50 mM Hepes, pH 7.4, 500 mM NaCl, 0.1% BSA, passed through a 0.45  $\mu$ m filter) to remove any unbound radioactivity. The radioactivity in membrane pellets was determined in a gamma counter, and binding curves (dose-response sigmoidal fit) were generated in Graph Pad Prism 5. IC<sub>50</sub> values for hexarelin, ghrelin(1-18)-amide **2.22** and

fluorescein-ghrelin(1-18) **2.21** were determined as previously described<sup>84</sup>. Each sample was analyzed in triplicate and assays were repeated five times for all peptides.

### **2.6.7 Serum Stability Study<sup>83</sup>**

To assess the stability of **2.21** and **2.22** in serum, peptides (1 mg/ml peptide in acetate buffer pH 6.2) was incubated in rat serum (final sample volume 0.5 ml; final peptide concentration 20 mM) over increasing time points at 37°C. The incubation period ended with the addition of 20 mL aqueous 10% TFA. Samples were then applied to C18 reverse-phase cartridges (Light C18 Sep-Pak, Waters), washed with 4 ml aqueous 0.1% trifluoroacetic acid (TFA), and eluted with 3 ml 70% acetonitrile in aqueous 0.1% TFA. After lyophilization, samples were analyzed using analytical RP-HPLC, as previously described<sup>84</sup>. Half-lives of the peptides were calculated using Microsoft Excel.

### **2.6.8 Tissue Expression of GHSR-1a<sup>83</sup>**

All mice were treated in accordance with the guidelines set by the Animal Use Subcommittee of the Canadian Council on Animal Care at the University of Western Ontario. To determine the levels of GHS-R1a expression in various tissues, adult (8-10 weeks) female C57BL/6 mice were sacrificed using CO<sub>2</sub> and heart, brain, liver, stomach, kidney, pancreas, islets, intestine, and spleen were immediately removed. Protein was extracted as described previously<sup>85</sup>. Fifty mg of protein from each tissue were used for Western blot analysis as described above, using rabbit anti-GHS-R (1:500, Santa Cruz Biotechnology).

### ***2.6.9 Binding of Fluorescein-ghrelin to heart tissue in situ***<sup>83</sup>

Adult (8-10 weeks) female C57BL/6 mice were sacrificed using CO<sub>2</sub> and the hearts were immediately removed and fixed in 4% paraformaldehyde (in PBS) overnight. Whole hearts were then equilibrated in 30% sucrose in PBS, snap-frozen in Tissue-Tek OCT using dry-ice cooled ethanol, and subsequently cryosectioned at 10  $\mu$ m. Sections were thawed in PBS and incubated for 1h at room temperature in the following: 1 mM fluorescein-ghrelin(1-18) alone; 1 mM of **2.21** with 100 mM ghrelin (Bachem); 1 mM of **2.21** with 100 mM hexarelin; or PBS alone to assess autofluorescence. Slides were then rinsed 3X5 min in 9 PBS and viewed under a fluorescent microscope using the fluorescein filter. Ten random fields of view were captured for each of 3 slides per tissue per mouse.

### ***2.6.10 Evaluation of Fluorescein-ghrelin in PC3, LNCaP, and BPH cell lines***<sup>86</sup>

PC-3 (CRL-1435, ATCC) cells were grown in F-12K medium (30-2004, ATCC) supplemented with 10% fetal calf serum (FCS) and streptomycin (15 mg/ml). LNCaP (CRL-1740, ATCC) were grown in RPMI (Invitrogen) with 10% FCS, streptomycin (15 mg/ml) and 1x sodium pyruvate. BPH (generous gift from Dr. Michael Cox, VGH) were grown in DMEM (Invitrogen) with 5% FBS and streptomycin (15 mg/ml). Cells were grown on glass coverslips and frozen sections from prostate tissue samples were collected onto poly-L-lysine-coated slides. Slides were fixed using 4% formaldehyde for 10 minutes at room temperature, and incubated with a 1/500 dilution of fluorescein-ghrelin **2.21** (1 mM/L) for 2 h at room temperature. The binding of fluorescein-ghrelin **2.21** was amplified with an anti-fluorescein antibody (anti-fluorescein/Oregon Green mouse monoclonal IgG antibody, A-6421, Invitrogen) and a secondary antibody (Alexa Fluor 647-R-phycoerythrin goat anti-mouse IgG, A-20990, Invitrogen). After incubation with



the fluorescein-ghrelin **2.21**, slides were incubated with a 1/500 dilution of the anti fluorescein antibody (1 mg/mL) for 2 h at room temperature, and then incubated with a 1/2500 dilution of the secondary antibody (1 mg/mL) for 1 h at room temperature. The nuclei in PC-3 cells and prostate tissue were counterstained with DAPI (D1306, Invitrogen). The ghrelin probe and antibodies were diluted in PBS with 10% goat serum and 1% bovine serum albumin to block the non-specific binding. For the assessment of specific binding between fluorescein-ghrelin **2.21** and its receptor, a competitive blocking study was performed in the presence of 10 times concentration of unlabeled ghrelin(1-18)-amide **2.22**. For negative control of ghrelin probe staining, the series slides with same areas were incubated without fluorescein-ghrelin **2.21**, but with the anti fluorescein antibody and the secondary antibody.

#### ***2.6.11 Evaluation of Fluorescein-ghrelin in ex vivo prostate samples***<sup>86</sup>

To assess the selectivity of the fluorescein-ghrelin **2.21** for prostate cancer (PCa) over prostate intraepithelial neoplasia (PIN) or benign tissue, standard prostate sextant biopsy samples were collected from fresh surgery specimens of 13 patients undergoing radical prostatectomy in the Department of Urology at the London Health Sciences Centre. The prostate core biopsy samples were embedded in OCT immediately after collection and stored at -80°C, until processed for serial frozen sections. For each block, one serial frozen section slide underwent hematoxylin and eosin (H&E) staining and was subjected to pathological analysis (Department of Pathology, UWO), and another serial section was used for ghrelin probe staining. Prostate tissue was categorized into PCa, PIN or benign tissue based on the pathological changes in H&E staining. Ghrelin probe staining in the equivalent area on the adjacent serial section was quantitatively analyzed as described below. This study obtained approval from an independent local Ethics Committee (UWO REB #16840E), and obtained the informed consent from all patients for the research use of their tissues.



### ***2.6.12 Quantitative Analysis for ghrelin analogue binding<sup>86</sup>***

Fluorescein-ghrelin(1-18) staining was captured by fluorescence confocal microscopy and quantified by image analysis (Volocity 5.0, PerkinElmer). The signal intensity in a selected region of interest (ROI) was calculated in relative fluorescence units (RFU) per pixel. For the cancer cell staining, 20 images were captured for each experimental group for quantitative analysis. The region of interest was established using bright field images, and the mean signal intensity of each group was calculated. Negative controls were incubated with no ghrelin probe but otherwise treated equivalently. For tissue staining, the signal intensity of fluorescein-ghrelin **2.21** was normalized by the signal intensity in the series negative control slides with the same area (normalized signal intensity = signal intensity ghrelin - signal intensity negative control). For tissue slides, regions of interest were selected manually consisting only of prostatic epithelium. Three fields were captured from each slide, and up to 3 ROIs were selected per field for quantitative analysis. A total of 167 images from 76 human prostate tissue slides were analyzed quantitatively. The mean signal intensity for each histological feature was first calculated on a per-patient basis, and these values were then averaged to determine the mean signal intensity of each group.

## Chapter Three: The Design and Synthesis of a Gallium-68 Labelled Ghrelin Analogue for PET Nuclear Imaging

### 3.1 Introduction

There has been growing interest in designing radiolabelled peptides to significantly improve the detection of disease, through the targeting of peptide receptors<sup>87,88,89,90,91</sup>. A number of peptides labelled with varying radionuclides such as  $^{68}\text{Ga}$ ,  $^{66}\text{Ga}$ ,  $^{18}\text{F}$ ,  $^{86}\text{Y}$ ,  $^{111}\text{In}$  and  $^{64}\text{Cu}$  have been investigated<sup>92,93,94,95,96</sup>.  $^{18}\text{F}$ -FDG, being the front-runner of PET radiopharmaceuticals, has gained popularity in diagnosing a wide-range of malignant diseases within the clinic<sup>97</sup>. It's use in staging and re-staging of malignant disease(s) is due to its high specificity and simplicity in production syntheses. However,  $^{18}\text{F}$ -FDG does have its limitations when (a) imaging tumours with high differentiation and low growth rates such as prostate carcinomas, (b) evaluating tissues located within or adjacent to high metabolic activity or physiological accumulation (bladder), and (c) distinguishing malignant tissue from inflammatory diseases<sup>97</sup>. Furthermore, the intricate chemistry of incorporating radioactive fluorine-18 into a biomolecule is rather challenging and limited when not having access to onsite cyclotron facilities<sup>98</sup>. To overcome these limitations, much of the existing research has focused on developing new radiopharmaceuticals for the detection of cancer. An alternative approach, when not having access to a cyclotron facility, is the use of an in-house generator system. Generator systems are a cost-effective approach to storing radionuclides such as  $^{68}\text{Ga}$ ,  $^{82}\text{Rb}$ , and  $^{62}\text{Cu}$ <sup>99</sup>. Although, the  $^{68}\text{Germanium}/^{68}\text{Gallium}$  ( $^{68}\text{Ge}/^{68}\text{Ga}$ ) generator has been around since the 1970s, the use of gallium-68 for positron emissions tomography (PET) nuclear imaging has only recently been investigated<sup>100,101,102,103,104</sup>. The generator functions by storing a long-lived parent isotope, which decays to a short-lived daughter isotope. In  $^{68}\text{Ge}/^{68}\text{Ga}$  generators,  $^{68}\text{Ge}$  is

produced from a cyclotron by the  $(p, 2n)$  reaction on a  $^{69}\text{Ga}$  target<sup>32</sup>. Germanium-68 acts as the parent isotope source with a half-life of 270 days, giving the system an adequate lifetime for the synthesis of many labelled molecules (Figure 3.1). Furthermore, a purification strategy based on the different chemical properties of the isotopes is used to elute off  $^{68}\text{Ga}$  in the presence of  $^{68}\text{Ge}$ . This separation technique of removing  $^{68}\text{Ge}$  from  $^{68}\text{Ga}$  is critical to avoid the breakthrough of unwanted  $^{68}\text{Ge}$  in the imaging agent. In most cases, an acidic solution of hydrochloric acid is used to elute off the  $^{68}\text{Ga}^{3+}$ <sup>99</sup>.

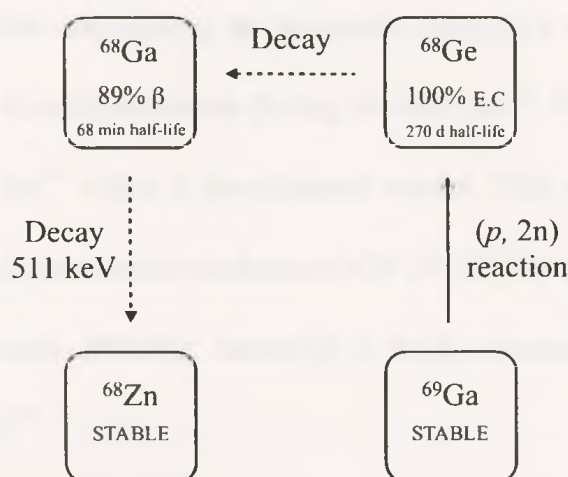


**Figure 3.1.** The production of  $^{68}\text{Ga}$  through the  $(p, 2n)$  reaction with  $^{69}\text{Ga}$ .

Gallium-68 is a positron-emitting radioisotope that decays by 89% positron emission and 11% electron capture. Among its 30 isotopes, two non-radioactive isotopes of gallium exist; gallium-69 and gallium-70, with natural abundances of 60.11% and 39.89% respectively<sup>32</sup>. Importantly, gallium-68 has a positron emission energy of 1899 keV, which is higher than that of fluorine-18. This higher positron energy can potentially lead to a lower spatial resolution for a PET image<sup>32</sup>. In comparison to other radioisotopes, the 68 minute half-life makes it compatible with the pharmacokinetics of most



radiopharmaceuticals including peptides and oligonucleotides<sup>105</sup>. Furthermore, a labelling kit procedure for incorporating gallium-68 into biomolecules has been investigated allowing for wide availability<sup>106</sup>.

In solution,  $\text{Ga}^{3+}$  ions act as a hard Lewis acid, forming thermodynamically stable complexes with ligands that are hard Lewis bases. Hard Lewis bases include ligands containing nitrogen and oxygen, such as carboxylates and amines. Thus, in order to incorporate  $\text{Ga}^{3+}$  into the backbone of a biomolecule, a chelator system must be used to coordinate the gallium. In addition to its ligand binding properties, the type of chelator becomes imperative when attempting to maintain gallium's thermodynamic stability towards hydrolysis and kinetic inertness during *in vivo* use<sup>99</sup>. Generally, most chelators designed to coordinate  $\text{Ga}^{3+}$  adopt a hexadentate model. This can be seen through the crystal structure of 1,4,7,10-tetraazacyclododecane-*N,N',N'',N'''*-tetraacetic acid (tris-tbutyl-DOTA); a commonly used chelator; adopting a  $\text{N}_4\text{O}_2$  encapsulated pseudo-octahedral gallium-DOTA complex<sup>107</sup>.

$^{68}\text{Ga}$ -DOTA-TOC, an octreotide peptide, has recently shown a number of promising properties when labelled with gallium<sup>94,108</sup>. In one study,  $^{68}\text{Ga}$ -DOTA-TOC was compared with  $^{18}\text{F}$ -FDG in patients who had confirmed neuroendocrine tumours (NET)<sup>108</sup>. Based on qualitative analysis,  $^{68}\text{Ga}$ -DOTA-TOC displayed tumour uptake in 57/63 lesions, whereas  $^{18}\text{F}$ -FDG only displayed uptake in the 43/63 lesions. In an additional study, higher tumour uptake as well as lower kidney uptake was observed when compared with other radiolabelled pharmaceuticals<sup>94</sup>.



### 3.1.1 The Design and Synthesis of a Gallium Ghrelin Analogue

Based on the design and synthesis of truncated peptides that bind well to the GHSR, we investigated the design and synthesis of a gallium labelled ghrelin analogue used for PET nuclear imaging<sup>39,83,86</sup>. In our preliminary study described in chapter two, the fluorescein-ghrelin analogue demonstrated a strong binding affinity to the GHSR when positioning the fluorescein dye within the C-terminus of modified ghrelin. It became clear that in order to maintain ghrelin's high binding affinity when designing modified analogues, placement of the bulky substituent had to be within sufficient distance of the N-terminal amino acid binding region of ghrelin. Additionally, ghrelin's unique octanoylated side chain off residue three was required for its' strong binding affinity to the GHSR.

Recently, Matsumoto *et al.*<sup>74</sup> reported a low nM binding affinity for a truncated ghrelin(1-5)-amide analogue, however in a preliminary study we demonstrated that upon functionalization, these analogues display poor binding affinities of greater than 2000 nM<sup>39</sup>. In order to maintain potent receptor recognition, this study suggested that larger peptide sequences were required when derivatizing ghrelin analogues. Thus, as in the synthesis of fluorescein-ghrelin **2.21**, an 18-mer amino acid sequence was designed to incorporate the most critical amino acids for receptor recognition.

The addition of Lys<sup>19</sup> on the C-terminus of ghrelin provided a site of attachment for the metal chelation system. Placing the metal chelator on the C-terminus would limit the interference between the N-terminal binding region of the peptide, thereby maintaining potent binding affinity with the GHSR. As in previous syntheses, replacing Ser<sup>3</sup> with Dpr<sup>3</sup> demonstrated a larger serum stability half-life of 83 minutes in ghrelin(1-18) **2.22** in comparison to native ghrelin's 27 minutes. Furthermore the C-terminus was

also converted to amide functionality by using a rink amide 4-methylbenzylhydramine (MBHA) resin. As in both fluorescein-ghrelin **2.21** and ghrelin(1-18) **2.22**, this addition was further improved the stability towards cellular exopepsidase, slowing the probes metabolism *in vivo*.

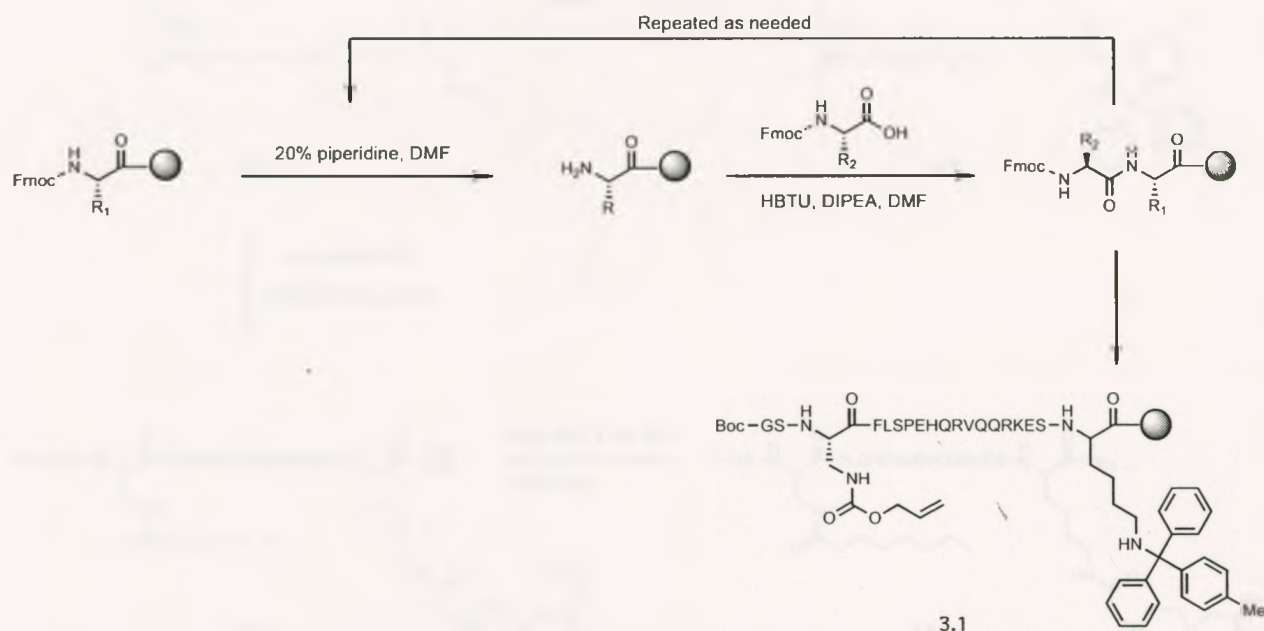
### 3.2 Results and Discussion

The synthesis of [Dpr(octanoyl)<sup>3</sup>, Lys(DOTA)<sup>19</sup>]ghrelin(1-19)-amide **3.6** was carried out in five steps. The 19 amino acid peptide sequence was synthesized manually according to standard Fmoc-SPPS techniques (Scheme 3.1). As in the synthesis of fluorescein-ghrelin **2.21**, an orthogonal protecting group strategy allowed for further modification to modified ghrelin. For this reason, Dpr<sup>3</sup> and Lys<sup>19</sup> were protected with allyloxycarbonyl (alloc) and 4-methyltrityl (Mtt) respectively. All other amino acids were protected using standard Fmoc orthogonal protecting groups.

While on resin, selective removal of the alloc protecting group proceeded in one step using phenylsilane and a palladium catalyst to provide amine **3.2**. Using standard coupling condition, octanoic acid was added to free amine **3.2** to afford **3.3**, which was characterized by HPLC-MS (Scheme 3.2). The sequential deprotection of Mtt was carried out by multiple washes using a weakly acidic solution of trifluoroacetic acid in dichloromethane (DCM). A qualitative Kaiser test was performed to observe the presence of free amine **3.4** off the Lys<sup>19</sup> amino acid side chain (Scheme 3.2).

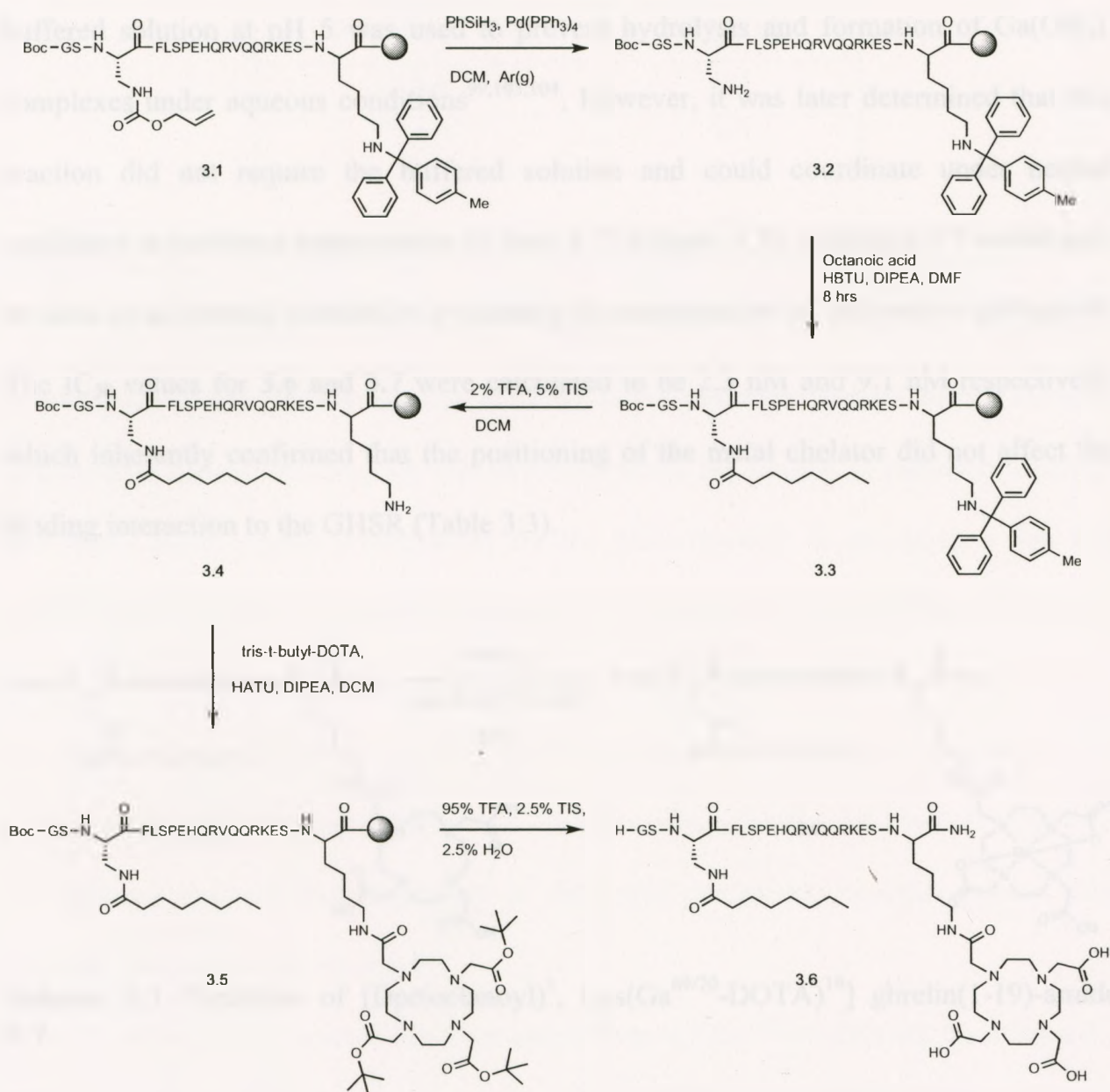
When coupling in tris-*t*-butyl-DOTA to analogue **3.4**, an incomplete reaction was observed when using the standard coupling reagent HBTU, based on HPLC-MS. As a result, an alternative peptide-coupling reagent was used to carry out the addition of tris-*t*-butyl-DOTA to analogue **3.4**. O-(7-Azabenzotriazol-1-yl)-N,N,N',N'-tetramethyluronium

hexafluorophosphate (HATU) is similar in structure to HBTU, however has shown to react faster with less epimerization during coupling and was found to give better yields than when using HBTU<sup>109,110,111</sup>. Based on HPLC-MS, the addition of DOTA to analogue **3.4** using HATU, drove the reaction to completion to provide **3.5** (Scheme 3.2). The final step in this synthesis, was the addition of concentrated acid to cleave the analogue from the solid support to afford peptide **3.6** in a 7.7% yield (Table 3.1).



**Scheme 3.1.** Fmoc-SPPS synthesis of on resin [Dpr(alloc)<sup>3</sup>, Lys(Mtt)<sup>19</sup>]ghrelin(1-19)-amide **3.1**. All other amino acids were protected using standard Fmoc chemistry protecting groups.





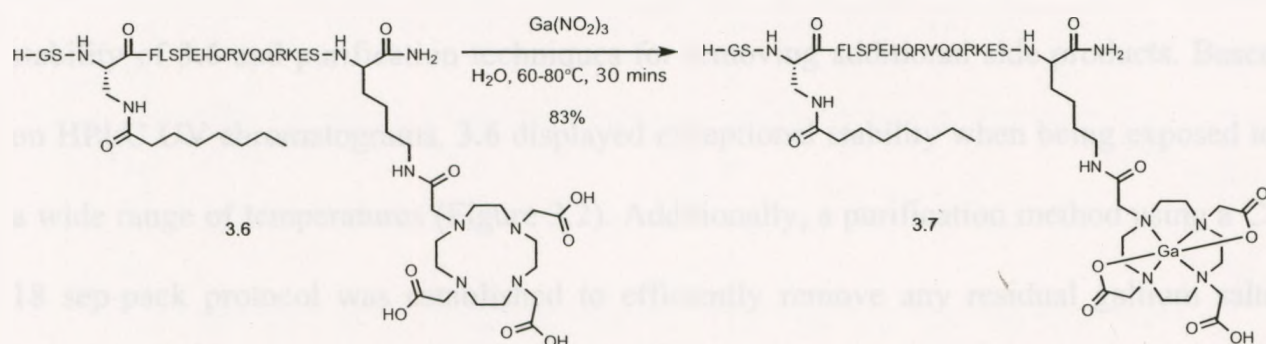
**Scheme 3.2.** Synthesis of [Dpr(octanoyl)<sup>3</sup>, Lys(DOTA)<sup>19</sup>] ghrelin(1-19)-amide **3.6**.

**Table 3.1.** [Dpr(octanoyl)<sup>3</sup>, Lys(DOTA)<sup>19</sup>] ghrelin(1-19)-amide **3.6** calculated and observed exact mass, and purity determined after HPLC purification.

Compound	Purity %	m/z		
		Particle	Calc	Obsd
3.6	97.4	[M+4H] <sup>4+</sup>	687.65	687.63



The DOTA conjugated peptide **3.6** underwent coordination with nonradioactive gallium nitrate hydrate in an aqueous buffered solution. Initially a reaction in a sodium buffered solution at pH 5 was used to prevent hydrolysis and formation of  $\text{Ga}(\text{OH})_4^-$  complexes under aqueous conditions<sup>99,103,104</sup>. However, it was later determined that this reaction did not require the buffered solution and could coordinate under neutral conditions at moderate temperatures to form **3.7** (Scheme 3.3). Analogue **3.7** would later be used as an internal standard in evaluating the incorporation of radioactive gallium-68. The  $\text{IC}_{50}$  values for **3.6** and **3.7** were calculated to be 2.3 nM and 9.1 nM respectively, which inherently confirmed that the positioning of the metal chelator did not affect the binding interaction to the GHSR (Table 3.3).



**Scheme 3.3.** Synthesis of  $[\text{Dpr}(\text{octanoyl})^3, \text{Lys}(\text{Ga}^{69/70}\text{-DOTA})^{19}]$  ghrelin(1-19)-amide **3.7**.

**Table 3.2.**  $[\text{Dpr}(\text{octanoyl})^3, \text{Lys}(\text{Ga}^{69/70}\text{-DOTA})^{19}]$  ghrelin(1-19)-amide **3.6** calculated and observed exact mass, and purity determined after HPLC purification.

Compound	Purity %	m/z		
		Particle	Calc	Obsd
<b>3.7</b>	95.0	$[\text{M}+3\text{H}]^{3+}$	937.10	937.64

**Table 3.3.** Comparing the binding affinities of synthesized ghrelin analogs to native ghrelin.

Compound	IC <sub>50</sub> (nM)
Ghrelin [1-28]	8.1 ± 1.0
<b>3.6</b>	2.3
<b>3.7</b>	9.1

### 3.2.1 The Design and Synthesis of a Gallium-68 Radiolabelled Ghrelin Analogue

When designing peptide-based imaging probes for PET nuclear imaging, a number of reaction parameters are required to be optimized before incorporating a radionuclide source. In doing so, this technique limits the amount of radiation exposure and thus creates a safer environment for the radio-chemist. In designing a fast and efficient synthesis for incorporating gallium-68 into **3.6**, we investigated the temperature stability of **3.6** and purification techniques for removing additional side products. Based on HPLC UV chromatograms, **3.6** displayed exceptional stability when being exposed to a wide range of temperatures (Figure 3.2). Additionally, a purification method using a C-18 sep-pack protocol was established to efficiently remove any residual gallium salts from the reaction when forming **3.7**.

Gallium-68 was eluted off of an ionic positron <sup>68</sup>Ge/<sup>68</sup>Ga generator by using a 0.1 molar solution of hydrochloric acid, leaving behind the germanium-68 isotope. A 1 mg sample of **3.6** was weighed out and dissolved in 1 mL of water. From this solution 100 µL was taken and placed inside a lead shielded automated gallium synthesis box, run by Modular-Lab software. <sup>68</sup>Ga<sup>3+</sup> in HCl was added to the aqueous solution of **3.6** while stirring at a temperature of 80 °C (Scheme 3.4). After 20 minutes of stirring, analogue **3.8** was injected onto a C-18 Sep-Pak<sup>®</sup> and eluted off with a 50% solution of acetonitrile and

water. The completeness of the reaction was confirmed by lining up the UV HPLC trace of standard **3.7** with the gamma trace of **3.8** (Figure 3.3). A 75% decay corrected radiochemical yield was achieved for **3.8**, based on the principle of first order decay<sup>112</sup>.

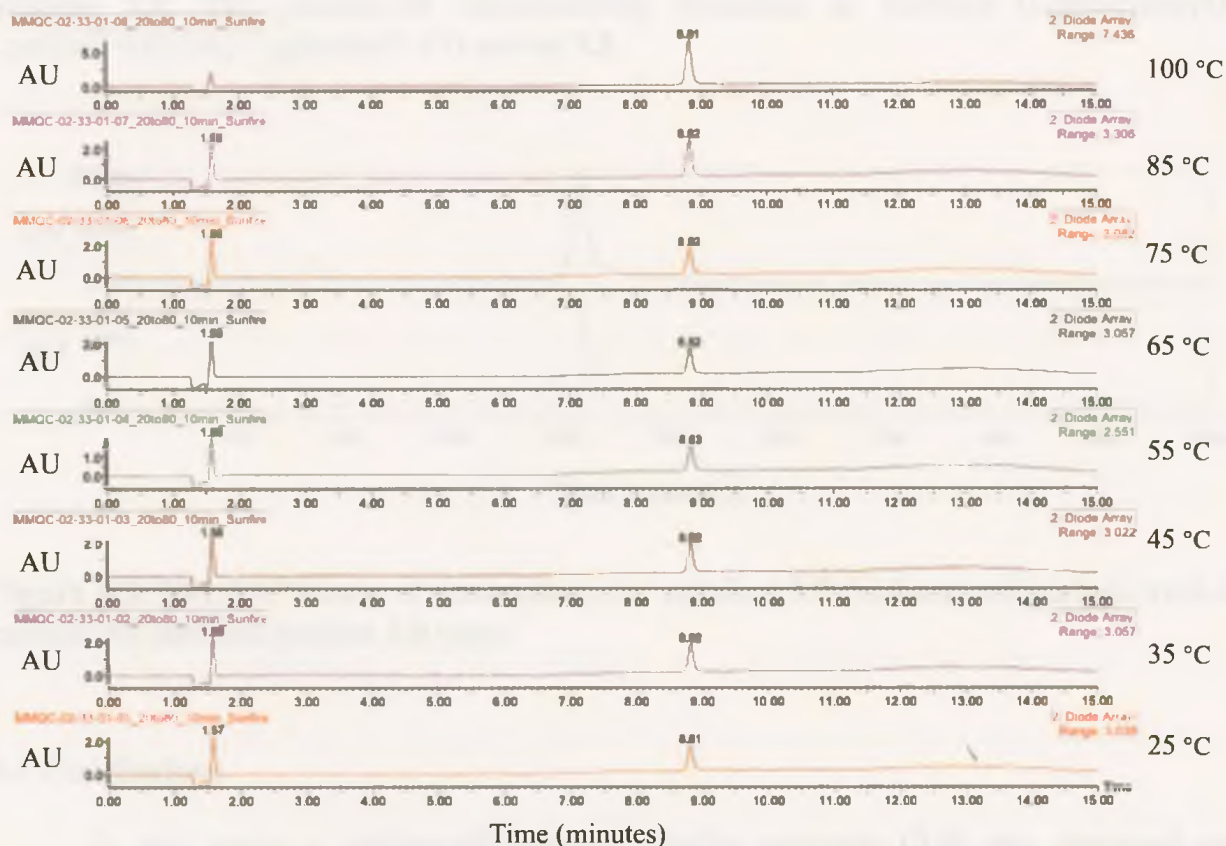
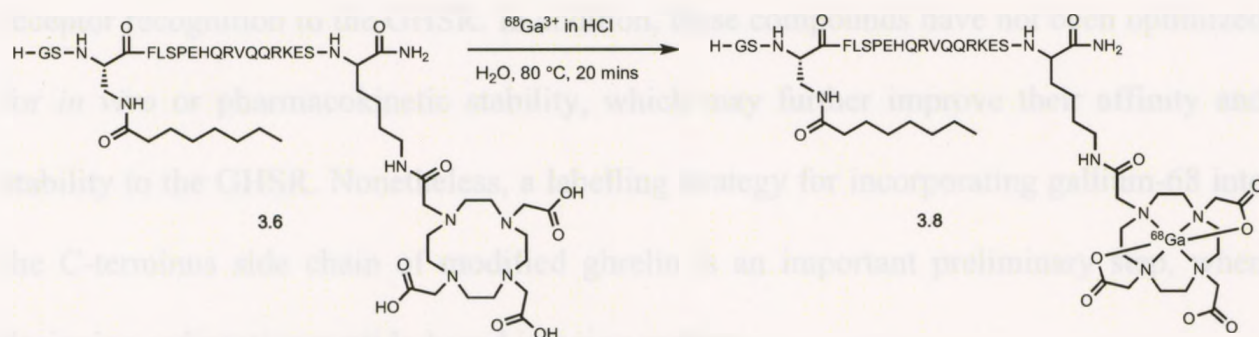


**Figure 3.2.** Temperature stability study of  $[\text{Dpr}(\text{octanoyl})^3, \text{Lys}(\text{DOTA})^{19}] \text{ghrelin}(1-19)\text{-amide}$  **3.6**. Analogue **3.6** was dissolved in an aqueous solution at room temperature. At ten-minute time intervals, aliquots of **3.6** were taken from the solution and injected onto the HPLC to assess the peptide's stability. UV chromatograms show no decomposition in analogue **3.6** when being exposed to various temperatures based on the peak retention times.





**Scheme 3.4.** The gallium-68 radiolabelling synthesis in forming [Dpr(octanoyl)<sup>3</sup>, Lys(Ga<sup>68</sup>-DOTA)<sup>19</sup>] ghrelin(1-19)-amide **3.8**.

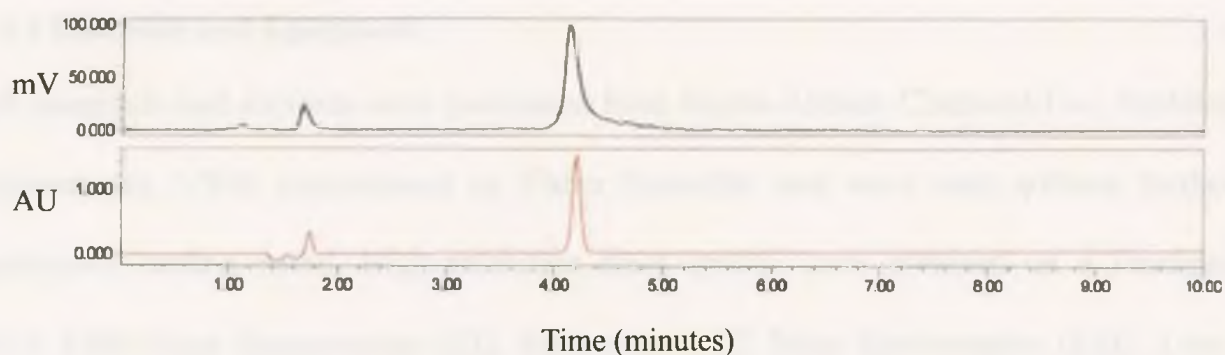


**Figure 3.3.** HPLC UV trace of non-radioactive standard **3.7** (bottom) and gamma trace of gallium-68 labelled product **3.8** (top).

### 3.3 Conclusions

In this study a gallium-68 labelled ghrelin analogue (**3.8**) was designed and synthesized. This is the first radiolabelled ghrelin analog synthesized for PET nuclear imaging. The high stability of **3.6** in a wide-range of temperatures and ease of purification, allowed for the radiolabelling process to be completed in a timely efficient process. In the future, this will help assist in the preparation of high specific activity product, a requirement for evaluating **3.8** in animal models. The 2.3 nM and 9.1 nM binding affinities calculated for both unlabelled **3.6** and gallium labelled **3.7** respectively, demonstrate the ability to incorporate a radio-metal chelator while maintaining potent



receptor recognition to the GHSR. In addition, these compounds have not been optimized for *in vivo* or pharmacokinetic stability, which may further improve their affinity and stability to the GHSR. Nonetheless, a labelling strategy for incorporating gallium-68 into the C-terminus side chain of modified ghrelin is an important preliminary step, when designing radioactive peptide-based imaging probes.

### 3.4 Experimental

#### 3.4.1 Materials and Equipment

All chemicals and solvents were purchased from Sigma-Aldrich Chemical Co., Peptides International, VWR international or Fisher Scientific and were used without further purification unless noted. High-resolution mass spectra were obtained on a Finnigan MAT 8400 Mass Spectrometer (EI), Micromass LCT Mass Spectrometer (ESI). Low-resolution mass spectra were obtained on a Micromass Quattro Micro API (MS-ESI and LC-MS-ESI). Anhydrous DCM was prepared by distillation from CaH under argon. Oven-dried or flame dried glassware was used in water sensitive reactions under argon. A Eckert and Ziegler  $^{68}\text{Ge}/^{68}\text{Ga}$  generator was used for the production of radioactive gallium. The radiolabelling synthesis was done on an automated synthesis unit using Modular Lab Software 4.0. A Waters symmetry, 4.6 x 150 mm, 5 Å, C-18 column was used and coupled to a gamma detector. This system employed a Waters 1525 Binary HPLC pump, Waters 2487 dual  $\lambda$  absorbance detector, Waters In-Line degasser and Breeze software (version 3.30). Analytical HPLC was performed using a Grace Vydac Protein/Peptide RP-C18 column 4.6 x 250 mm, 5  $\mu\text{m}$  or a Waters Sunfire RP-C18 column 4.6 x 250 mm, 5  $\mu\text{m}$ . Preparative HPLC was performed using a Grace Vydac Peptide/Protein SP-C18 column 22.0 x 250 mm, 10  $\mu\text{m}$  or a Waters Sunfire SP-C18

column 22.0 x 250 mm, 10  $\mu$ m. A gradient system was used: ACN + 0.1% TFA (solvent A) and H<sub>2</sub>O + 0.1% TFA (Solvent B). The absorbance was detected in the 200 nm to 600 nm wavelength range.

### ***3.4.2 General Procedure for Peptide Assembly***

Fully protected resin bound peptides were synthesized manually according to general procedures in Fmoc solid phase peptide synthesis<sup>14</sup>. Fmoc protected rink amide MBHA resin (loading 0.56 and 0.47 meq/ g) was used as the solid support. In general, N-Fmoc amino acids with strong acid labile side chain protecting groups were used, and N-Boc amino acids were used for the N-terminus. Fmoc- Dpr<sup>3</sup>, with the  $\beta$ -amine protected with allyloxycarbonyl (alloc), was used for residue-3. Fmoc-lysine (Lys), with the  $\beta$ -amine protected with 4-methyltrityl (Mtt), was used for residue-19. Fmoc removal was achieved by adding 20% piperidine in DMF for 5 and 15 minutes, followed by washes with DMF and DCM after each treatment. For each amino acid coupling, resin was treated twice with 3 eq. of Fmoc or Boc amino acids, 3 eq. of 3-[bis(dimethylamino)methylumyl]-3H-benzotriazol-1-oxide hexafluorophosphate (HBTU) and 6 eq. of N,N-diisopropylethylamine (DIPEA) in 2 mL of DMF for 30 minutes to 2 hours. Couplings were followed by multiple washes with DMF, and DCM. Using this general procedure, peptides were prepared on resin.

### ***3.4.3 General Procedure for Selective Deprotection and Resin Cleavage***

Selective deprotections were carried out using an orthogonal deprotection strategy for residues 3 and 19. The  $\beta$ -amine protected as the allyloxycarbonyl (alloc) was selectively removed by shaking the resin with 0.35 eq. of

tetrakis(triphenylphosphine)palladium ( $\text{Pd}(\text{PPh}_3)_4$ ), and 20 eq. of phenylsilane ( $\text{PhSiH}_3$ ) in 2 mL of dry DCM. This treatment was repeated twice, followed by successive washes with DMF, and DCM. The  $\beta$ -amine protected with 4-methyltrityl (Mtt) was selectively removed by shaking the resin with 2% trifluoroacetic acid (TFA), and 5% triisopropylsilane (TIS) in DCM for two minutes. This treatment was carried out 8 times, followed by multiple washes with DMF, and DCM. The Kaiser test was used to monitor the presence or absence of a free amine. After peptide modifications were completed, the peptide was deprotected and cleaved from the resin using 95% TFA, 2.5% TIS, and 2.5% water for 3-6 hours. The resin was filtered and rinsed with a small amount of TFA. Cold *tert*-butyl methyl ether (TBME) was added to the filtrate to form a precipitate. Following the addition of TBME, the slurry was centrifuged and decanted. The peptide was rinsed with TBME and collected again. The solid was dissolved in water, frozen and lyophilized to obtain a crude peptide as a powder. Purification was carried out using preparative HPLC, and the purity of the isolated product was determined by analytical HPLC.

#### 3.4.4 *Dpr*<sup>3</sup>(octanoic acid)[Lys<sup>19</sup>(DOTA)]ghrelin(1-19)-amide (3.6)

**3.1** was manually synthesized on resin according to the general procedure for peptide assembly. Selective alloc deprotection was performed on residue-3 of **3.1** according to the general procedure to obtain a free amine. Octanoic acid was coupled to the peptide to obtain **3.3** according to the general procedure for peptide assembly. Selective Mtt deprotection was performed on Lys-19 to give free amine **3.4**, according to the general procedures. Tris-*t*-butyl-DOTA was coupled to the peptide using 3 eq. of HATU and 6 eq. of DIPEA. Following this, a final cleavage and deprotection was conducted according to the general procedure to obtain the crude peptide. Purification was performed by HPLC



(gradient 20-80% solvent A in B) to obtain **3.6** with a yield of 7.7% (21 mg) as a white powder (ESI-MS and purity reported in Table 3.1).

#### 3.4.5 [*Dpr*<sup>3</sup>(octanoic acid)]/[*Lys*<sup>19</sup>(<sup>69/71</sup>Ga-Dota)]ghrelin(1-19)-amide (**3.7**)

In a 5 mL round bottom flask, 400  $\mu$ L of water was added to **3.6** (8.4 mg, 0.0030 mmol) while stirring. Heat was applied to the reaction flask until a constant temperature of 60 °C was reached. At this time, gallium nitrate ( $\text{Ga}(\text{NO}_3)_3$ ) (15.6 mg, 0.0613 mmol) was added to the reaction flask. The resulting clear solution was stirred between 60-80 °C for 20 minutes. Passing the reaction solution through a Sep-Pak<sup>®</sup> purified gallium labeled **3.7**. The purification was achieved by using a gradient starting from 100% water (2 mL) and then 70% Acetonitrile: 30% water (3x 1 mL fractions). The four samples were frozen and lyophilized to obtain a white powder. HPLC traces (gradient 20-80% solvent A in B) confirm **3.7** as a white powder (ESI-MS and purity reported in Table 3.2) in a 83% yield.

#### 3.4.6 [*Dpr*<sup>3</sup>(octanoic acid)]/[*Lys*<sup>19</sup>(<sup>68</sup>Ga-Dota)]ghrelin(1-19)-amide (**3.8**)

To an oven dried conical glass vial was added 100  $\mu$ L of precursor **3.6** (1 mg/mL dissolved in a neutral solution of water), to which <sup>68</sup>Ga<sup>3+</sup> was added. The reaction mixture was then heated to 80 °C for 20 minutes. Prior to purifying **3.8**, a C-18 Sep-Pak<sup>®</sup> cartridge was conditioned with 5 mL of ethanol and 5 mL of water. The crude reaction mixture was then passed through the Sep-Pak<sup>®</sup>, followed by an additional of H<sub>2</sub>O and EtOH solution. The volume of the solution was then reduced to roughly 1 mL, by placing on a speed rotaryevaporator. Product **3.8** was then analyzed using HPLC coupled to a gamma detector and compared to the UV trace of non-radioactive standard **3.7**. A 75% radiochemical yield was calculated for **3.8**, decay corrected.



## Chapter Four: The Design and Synthesis of Fluorine Labelled Ghrelin Analogues For use in Positron Emission Tomography

### 4.1 Introduction

#### 4.1.1 Fluorine-18 in Recent Drug Developments

The incorporation of fluorine-18 into active biomolecules has emerged as a useful technique for diagnosing cancer in positron emission tomography (PET)<sup>30</sup>. Its 97% positron decay and energy of 0.633 MeV, makes it a suitable candidate for PET imaging. Among the many PET radionuclides, fluorine-18 has gained its popularity due to its: (a) longer half-life in comparison to other PET isotopes (Table 4.1), (b) enhanced spatial resolution from its relatively low positron decay energy, and (c) size similarities to the hydrogen atom, allowing it to be more readily incorporated into a lead compound<sup>113</sup>. While an estimated 15% of all pharmaceuticals contain fluorine, incorporating the radioactive <sup>18</sup>F into a biomolecule for PET imaging is a daunting task when considering the hazardous nature of the radioisotope and production timeframe<sup>114,115</sup>. Radiochemists are continually studying new ways to effectively manage the clock by either limiting the overall synthetic steps in the production of a radiopharmaceutical or optimizing the lengthy purification procedures. Failure to optimize these radiolabeling techniques will result in a loss of specific activity for imaging a particular disease *in vivo*. Nevertheless, <sup>18</sup>[F]-labelled compounds have become ideal imaging agents for PET nuclear imaging based on their high specific activities and ability to incorporate into small molecules (Table 4.2).

**Table 4.1.** Commonly used positron emitting radionuclides<sup>114</sup>.

Isotope	Half-life (min)	Positron Energy (MeV)	Positron Range (nM)
<sup>82</sup> Rubidium	1.26	3.15	1.7
<sup>15</sup> Oxygen	2.03	1.70	1.5
<sup>13</sup> Nitrogen	9.97	1.19	1.4
<sup>11</sup> Carbon	20.3	0.96	1.1
<sup>18</sup> Fluorine	109.8	0.64	1.0
<sup>64</sup> Copper	768	0.66	n/a

**Table 4.2.** Selected fluorine-18 labelled radiopharmaceuticals in clinical use<sup>116,117,118,119,120,121,122,123</sup>.

Compound	Synthetic Pathways	Clinical Use
[ <sup>18</sup> F]Fluoroethyltyrosine	O-alkylation with [ <sup>18</sup> F]fluoroethyl tosylate	Tumour imaging
5-[ <sup>18</sup> F]Fluorouracil	Electrophilic fluorination	Tumour imaging
[ <sup>18</sup> F]Fluoro- $\alpha$ -methyltyrosine	Electrophilic fluorination	Tumour imaging
16 $\alpha$ -[ <sup>18</sup> F]Fluoroestradiol	Nucleophilic Displacement	Estrogen receptor positive tumours
6-[ <sup>18</sup> F]Altanserlin	Nucleophilic aromatic substitution	5HT <sub>2A</sub> receptors
(-)-6-[ <sup>18</sup> F]Fluoronorepinephrine	Nucleophilic aromatic substitution	Cardiac sympathetic innervation
[ <sup>18</sup> F]Fluorodeoxyglucose	Electrophilic fluorination	Tumour Imaging

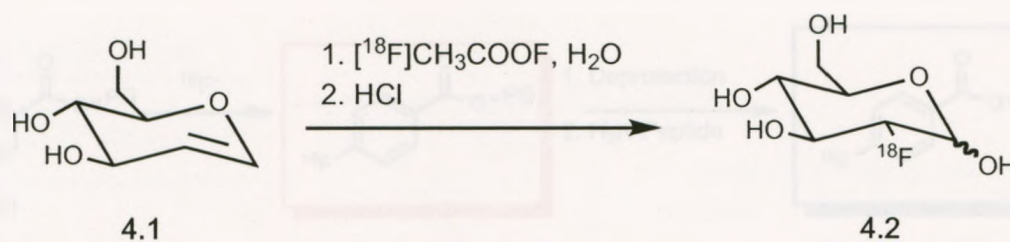
#### 4.1.2 Synthetic Approaches for Incorporating Fluorine-18 into Biomolecular Vehicles

Fluorination reactions are considered more difficult in comparison to other halogenation reactions, simply because most reagents containing fluorine are very toxic and too reactive<sup>124</sup>. Additionally, the chemistry utilized to make compounds containing fluorine-18 is different from that of non-radioactive fluorine-19. Fluorine-19 can be characterized using standard spectroscopic techniques such as proton NMR, carbon NMR, fluorine NMR and MS. In contrast, fluorine-18 is characterized by comparison with a non-radioactive standard using techniques such as radio-thin layer chromatography

(TLC) or HPLC. Additionally, radiochemical synthesis is subject to (a) small nano-molar reaction scales, (b) radiation protection and exposure and (c) fast chemistry techniques<sup>125</sup>. Reactions involving fluorine-18 are generally under non-equilibrium conditions and proceed in a pseudo-first-order pathway because of the high concentration of starting material present. Furthermore, selected radiolabeling procedures are under vigorous reaction conditions using high boiling point solvents. This allows for successful <sup>18</sup>F-fluorination of many precursor materials that would otherwise fail if using standard <sup>19</sup>F-fluorination methods. Lastly, yields in radiochemical synthesis are not always the subject of importance, as the overall concern is a safe and reliable method to produce at least one dose for PET nuclear imaging<sup>125</sup>.

Over the past decade, synthetic methods used to incorporate fluorine-18 into biologically active macromolecules such as peptides, proteins, sugars and oligonucleotides; have shown its usefulness for PET imaging of disease<sup>125</sup>. Chemically, fluorine can behave as either a nucleophile or electrophile when incorporating it into a lead compound. Today, electrophilic reactions are considered a classical way of incorporating fluorine into a compound. This reaction is considered unfavourable due to low specific activity (maximum radio chemical yield of 50% from [<sup>18</sup>F]F<sub>2</sub> production) and high reaction impurities. Though this method is less common, it did play a substantial role in the development of two well-known PET nuclear imaging agents: [<sup>18</sup>F]FDG (Scheme 4.1) and [<sup>18</sup>F]fluoro-L-Dopa<sup>125,126</sup>. In contrast to this classical method, nucleophilic fluorination reactions are commonly used today in developing radiopharmaceutical PET imaging agents. In this chapter, attention will be focused on nucleophilic fluorination, as the author used this synthetic reaction to form <sup>18</sup>F-labelled prosthetic groups.

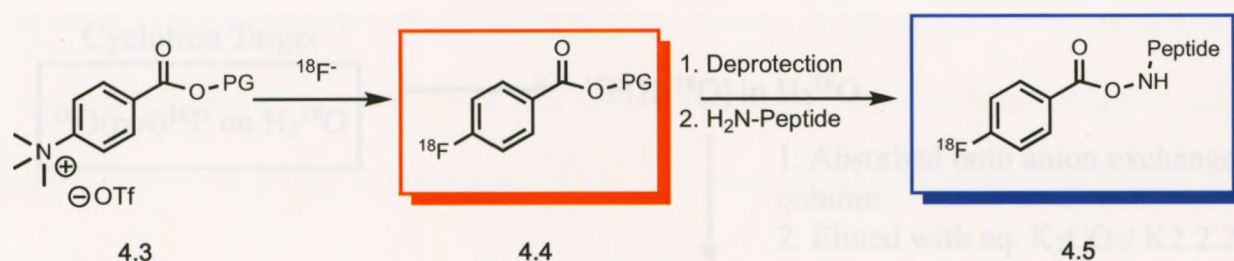




**Scheme 4.1.** An electrophilic fluorination reaction using [ $^{18}\text{F}$ ]acetyl-hypofluorite in the production of [ $^{18}\text{F}$ ]FDG<sup>127</sup>.

The chemistry of nucleophilic addition reactions can be divided into two different approaches; (a) direct fluorination and (b) indirect fluorination. Direct fluorination can be defined as the “direct” introduction of fluorine-18 into a target molecule in one-step. The latter method of  $^{18}\text{F}$  delivery is referred to as a prosthetic group approach (indirect), where a low molecular weight compound can be readily radiolabeled prior to being incorporated into a target. This strategy is generally used in a multistep synthetic approach when the complexity of a biological target can not tolerate direct labeling methods<sup>126</sup>. For example, fluorine-18 labelling of large peptides and electron rich arenes traditionally uses this indirect labeling method<sup>128</sup>. In these types of examples, the starting material undergoes a substitution type reaction with the fluorine source to form the prosthetic group. In order for the reaction to occur the starting material generally contains a halogen (Cl, Br, or I), sulfonate (mesylate, tosylate, triflate, or nosylate) or ammonium leaving group<sup>128</sup>. While the nucleophilic addition of fluorine occurs in one-step, a deprotection step must follow in order to give the biomolecule a site of attachment to the prosthetic group (Scheme 4.2). The advantages of this class of reaction are the quantitative radiochemical yields and high specific activities of the labeled biomolecules of interest.

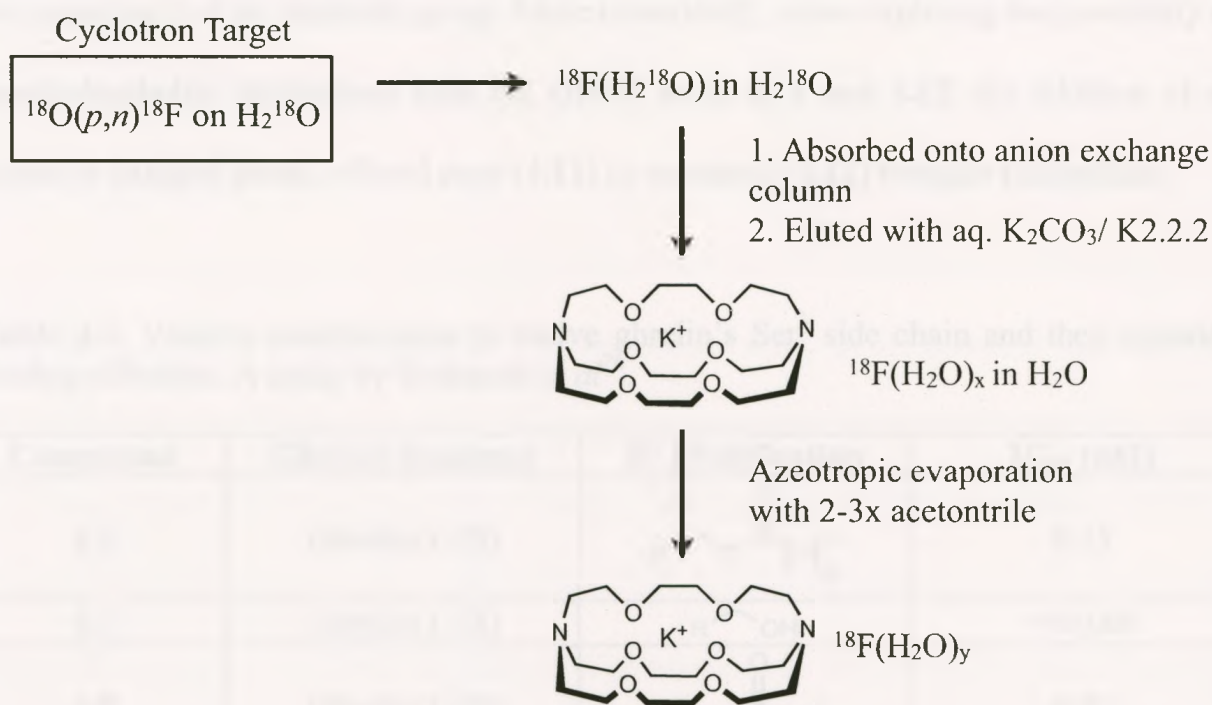




**Scheme 4.2.** Synthetic steps used to reach an  $^{18}\text{F}$ -labeled biomolecule (blue) using an  $^{18}\text{F}$ -labeled prosthetic group (red). Nucleophilic aromatic substitution on a quaternary ammonium salt proceeds from the addition of  $^{18}\text{F}^-$ , followed by a deprotection step and then addition of the desired peptide sequence.

#### 4.1.3 Production of Fluorine-18

Nucleophilic fluorine ( $[^{18}\text{F}]\text{F}^-$ ) is produced in high specific activity (185 GBq/ $\mu\text{mol}$ ) from a cyclotron, by proton irradiation of an  $^{18}\text{O}$  enriched water target (Scheme 4.3). All bulk amounts of  $[^{18}\text{O}]\text{water}$  are subsequently removed following the production, in order for the  $[^{18}\text{F}]\text{fluorine}$  to behave as a nucleophile. This process is accomplished by loading the radioactive aqueous media into an anion-exchange column followed by eluting off the  $[^{18}\text{F}]\text{fluorine}$  using a weak potassium carbonate base (Scheme 4.3)<sup>128</sup>. The residual water remaining from this process is further removed by azeotropic evaporation using acetonitrile. Generally, cations such as kryptofix [2.2.2] are added to enhance the nucleophilicity of the  $[^{18}\text{F}]\text{fluorine}$  and solubilize the nucleophile in polar aprotic media.



**Scheme 4.3.** Chart showing the production of [ $^{18}\text{F}$ ]fluorine starting from cyclotron irradiation of  $^{18}\text{O}$  water ( $^{18}\text{O}(p,n)^{18}\text{F}$  reaction). Following this is a flow chart on the steps taken to reach [ $^{18}\text{F}$ ]fluorine with limited amounts of aqueous solution present ( $y$  is less than  $x$ ). Adapted from Cai *et al.*<sup>128</sup>.

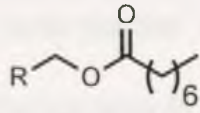
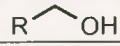
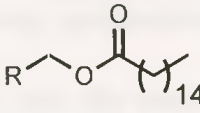
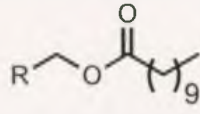
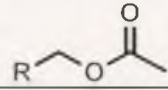
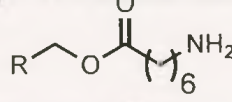
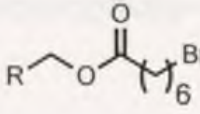
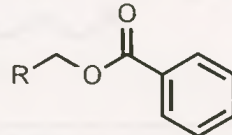
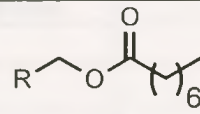
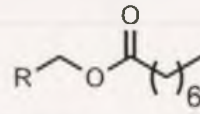
#### 4.1.4 Designing a Method for Incorporating Fluorine-18 into Ghrelin Analogues

As previously mentioned, ghrelin has a unique structure containing an octanoylated  $\text{Ser}^3$  ester residue, which is critical for binding to the GHSR<sup>39</sup>. Although the positioning of the acylated side chain cannot be altered, other bulky, flexible and rigid hydrophobic groups have been added as alternatives<sup>76</sup>. A study by Bednarek *et al.*<sup>76</sup> observed the relationship between the n-octanoyl group with its affinity to the GHSR-1a. Modified  $\text{Ser}^3$  side chains that resembled the size and shape of native **4.6** such as **4.8** and **4.9**, yielded similar potencies to that of ghrelin (Table 4.3)<sup>76</sup>.

When replacing the n-octanoyl group with acetyl **4.10**, a 20-fold decrease in receptor binding affinity to the GHSR was observed. Ghrelin in the absence of its side chain in **4.7** showed an even greater decrease in receptor binding affinity, demonstrating

the importance of the aliphatic group. More importantly, when exploring the possibility of non-hydrophobic interactions with the GHSR as in **4.11** and **4.12**, the addition of an amino or halogen group, offered poor (**4.11**) or enhanced (**4.12**) receptor recognition.

**Table 4.3.** Various modifications to native ghrelin's Ser<sup>3</sup> side chain and their reported binding affinities. A study by Badnarek *et al*<sup>76</sup>.

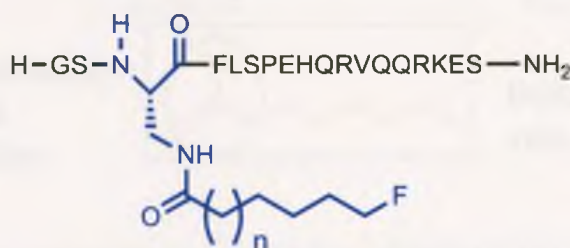
Compound	Ghrelin Sequence	R' Modification	IC <sub>50</sub> (nM)
4.6	Ghrelin(1-28)		0.25
4.7	Ghrelin(1-28)		>10,000
4.8	Ghrelin(1-28)		0.87
4.9	Ghrelin(1-28)		0.12
4.10	Ghrelin(1-28)		>2,000
4.11	Ghrelin(1-28)		>2,000
4.12	Ghrelin(1-28)		0.08
4.13	Ghrelin(1-28)		11
4.14	Ghrelin(1-5)-NH <sub>2</sub>		55
4.15	Ghrelin(1-14)		9.6



Furthermore, the tolerability and flexibility in modifying ghrelin's side chain was demonstrated by the addition of benzene **4.13**, showing similar binding affinity to that of native ghrelin.

Prior to the authors' involvement in this project, non-radioactive fluorine bearing ghrelin analogues were synthesized<sup>78</sup>. A preliminary study on the potential use of placing fluorine into the aliphatic side chain of ghrelin was evaluated. Modified ghrelin analogues were synthesized and optimized by replacing both the Ser<sup>3</sup> residue with Dpr<sup>3</sup> and the C-terminal carboxy acid with an amide moiety. Furthermore as Bednerak *et al.*<sup>76</sup> investigated varying aliphatic side chain lengths, our group synthesized three different fluorinated aliphatic side chains that were incorporated into the backbone of ghrelin(1-14)-amide (Table 4.4).

**Table 4.4.** Various fluorine bearing ghrelin(1-14)-amide analogs and their reported IC<sub>50</sub> values. N= 1, 4, 7. Study by Rosita *et al.*<sup>78</sup>



Compound	N Modification	IC <sub>50</sub> (nM)
<b>4.16</b>	1	147
<b>4.17</b>	4	39.6
<b>4.18</b>	7	27.9

This preliminary investigation displayed the use of ghrelin's aliphatic side chain as a potential site of fluorination. More importantly, the binding affinities of the analogues improved as the side chain length increased (Table 4.4). These results



demonstrated that fluorine bearing 14-mer ghrelin peptides had the potential to be developed into PET imaging agents for the GHSR<sup>78</sup>.

Chapters two and three of this thesis described both the design and synthesis of a fluorescein and radiolabelled ghrelin analog. In both of these cases, the location of the fluorescent probe and chelate (for gallium-68) was situated off a pendent lysine side chain towards the C-terminus of ghrelin. Instead of further modifying the C-terminus of ghrelin(1-18), we propose a new method for incorporating fluorine into modified ghrelin probes. Similar to the preliminary report by Rosita *et al.*<sup>78</sup> the design of novel aliphatic fluorine containing ghrelin peptides, the author of this thesis extends this approach by further developing unique fluorine labeled analogues (Figure 4.1).

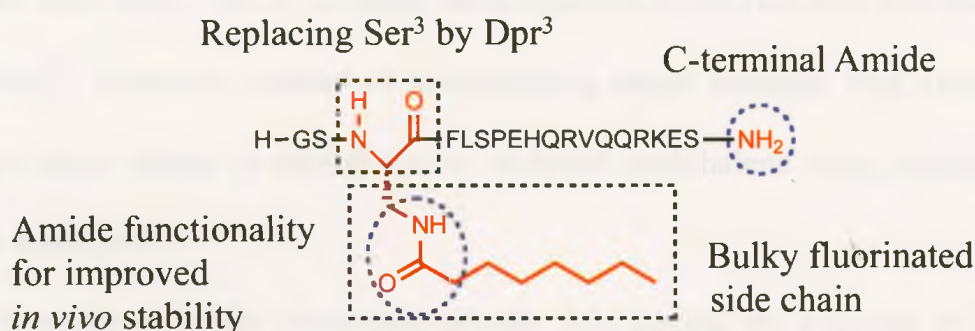


**Figure 4.1.** Our design approach in modifying ghrelin(1-18) for the incorporation of fluorine-18.

## 4.2 Results and Discussion

### 4.2.1 The Design of Non-radioactive Fluorine Bearing Ghrelin Analogues

The first parameter in developing PET-based imaging probes is the design and optimization of a variety of non-radioactive compounds. A lead candidate is then selected

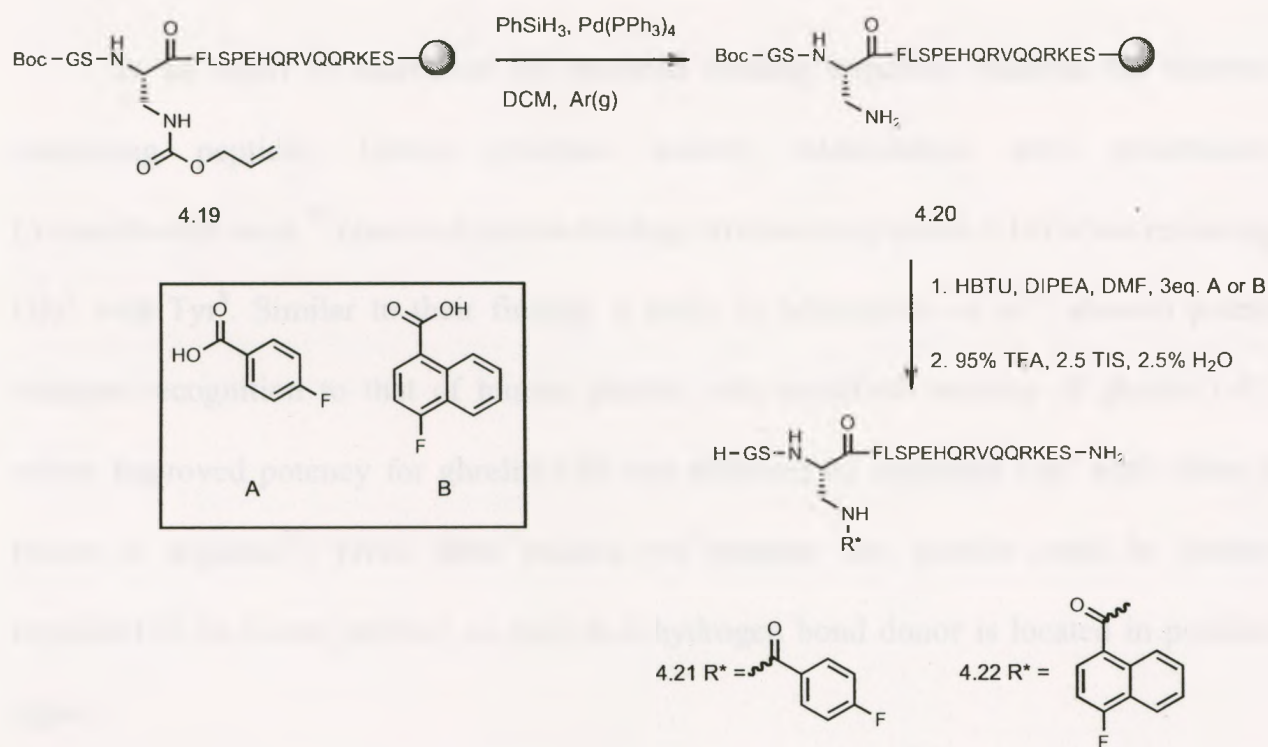
based on its binding affinity towards the receptor of interest. This evaluation process establishes the foundation in developing a successful PET imaging probe.

In order to maintain the highest binding affinity, the location of the radiotracer becomes significant when designing radioactive probes. The rationale behind our design focuses on the fluorination of unique side chains off residue-3 (Dpr<sup>3</sup>) (Figure 4.1). Our group has previously reported this design to have no significant effect on ghrelin's binding affinity<sup>78</sup>. Bednarek et al. further demonstrated this by comparing native ghrelin's 0.25 nM value to an improved 0.08 nM affinity when brominating the aliphatic side chain<sup>76</sup>. Instead of incorporating fluorine bearing octanoic acid analogs in residue-3 (Dpr<sup>3</sup>), we have converted ghrelin's natural aliphatic chain into an aromatic system. To our knowledge only one other group has incorporated benzene into the side chain off residue 3 (Dpr<sup>3</sup>). In their study, the IC<sub>50</sub> values were reported to be two-fold less than that of native ghrelin<sup>76</sup>. However, instead of incorporating single aromatic ring systems as in benzene, we have chosen to extend this to include naphthalene rings containing non-radioactive fluorine-19.

With evidence of the fluorescein-ghrelin **2.21** having the potential to become a novel optical imaging agent, non-radioactive fluorine analogues were synthesized manually according to our developed orthogonal protecting group strategy using SPPS (Scheme 4.4). The replacement of Ser<sup>3</sup> with the unnatural amino acid Dpr<sup>3</sup> and the C-terminal amide addition were to ensure maximum *in vivo* stability against cellular exopeptidases (Figure 4.1). Selective removal of the orthogonal Drp<sup>3</sup>-alloc protecting group was accomplished using phenylsilane and a palladium catalyst. Following this was the addition of commercially available fluorobenzoic acid or 4-fluoro-1-naphthoic acid to amine **4.20** using standard coupling conditions. Modified fluorine labeled ghrelin

analogues **4.21** and **4.22** were cleaved from the rink amide support and purified using HPLC-MS with yields of 8.5% and 7% respectively (Table 4.5)

$IC_{50}$  values for truncated peptides **4.21** and **4.22** were calculated by the Dhanvantari group (Table 4.6). The results confirmed that ghrelin(1-18)-amide peptides with fluorine-19 incorporated into the side chain of  $Dpr^3$  have slightly better binding affinities than that of human ghrelin. From our preliminary results, it appeared that the larger naphthyl ring in **4.22** provided enhanced receptor affinity as compared to that of phenyl ring **4.21**, further drawing our attention to developing more naphthyl labeled ghrelin analogs.



**Scheme 4.4.** Synthesis of ghrelin(1-18)-amide analogues with varying aromatic  $Dpr^3$  side chains.



**Table 4.5.** Fluorine bearing ghrelin analogues with their calculated and observed exact mass, as well as purity determination after HPLC purification.

Compound	Purity %	m/z		
		Particle	Calc	Obsd
4.21	99.0	$[M+3H]^{3+}$	742.04	742.84
4.22	96.5	$[M+3H]^{3+}$	759.52	759.71

**Table 4.6.** Comparing the binding affinities of synthesized fluorine bearing ghrelin(1-18)-amide analogs to native ghrelin and hexarelin (mean  $\pm$  s.d., n= 3)

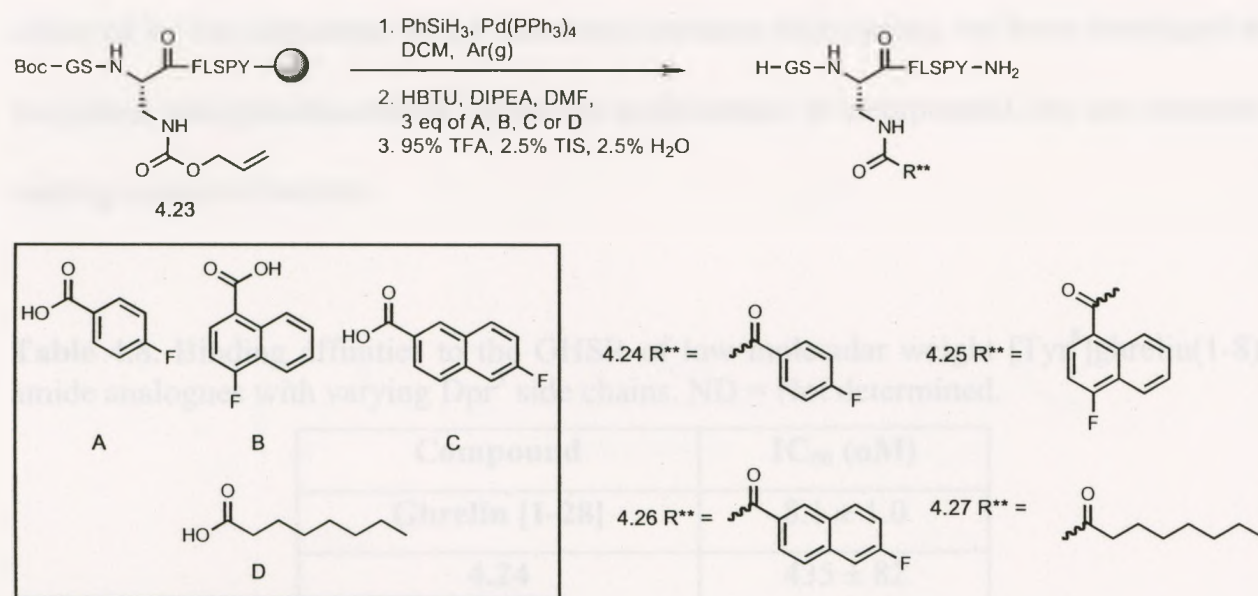
Compound	IC <sub>50</sub> (nM)
Ghrelin [1-28]	8.1 $\pm$ 1.0
Hexarelin	6.4 $\pm$ 2.4
4.21	7.2
4.22	2.9

In an effort to determine the minimal binding sequence required for fluorine containing peptides, further structure activity relationships were undertaken. Craenenbroeck *et al.*<sup>75</sup> observed similar binding affinities to ghrelin(1-14) when replacing Glu<sup>8</sup> with Tyr<sup>8</sup>. Similar to their finding, a study by Matsumoto *et al.*<sup>73</sup> showed potent receptor recognition to that of human ghrelin with modified versions of ghrelin(1-8), where improved potency for ghrelin(1-8) was achieved by replacing Glu<sup>8</sup> with either a lysine or arginine<sup>73</sup>. From these studies, we propose that ghrelin could be further truncated to an 8-mer peptide, as long as a hydrogen bond donor is located in position eight.

To limit the overall renal uptake for our probe during *in vivo* animal studies, it is suggested to avoid using lysine and arginine amino acids<sup>129</sup>. Instead tyrosine was incorporated into the low weight ghrelin peptides in accordance to scheme 4.4. Compounds 4.24, 4.25, 4.26 and 4.27 were synthesized manually using the orthogonal



SPPS methodology. Commercially available fluorobenzoic acid, 4-fluoro-1-naphthoic acid, 6-fluoro-2-naphthoic acid and octanoic acid were purchased and coupled into the Drp<sup>3</sup> side chain upon selective removal of the alloc protecting group. Upon cleaving, peptides **4.24**, **4.25**, **4.26** and **4.27** were purified and characterized by HPLC-MS with overall yields of 10%, 10%, 4% and 15% respectively (Table 4.7)



**Scheme 4.5.** The synthesis of low molecular weight [Tyr<sup>8</sup>]ghrelin(1-7)-amide analogues with varying Drp<sup>3</sup> side chains.

**Table 4.7.** Fluorine bearing ghrelin analogues with their calculated and observed exact mass, and purity determined after HPLC purification

Compound	Purity %	m/z		
		Particle	Calc	Obsd
<b>4.24</b>	99.1	[M+H] <sup>+</sup>	980.46	980.85
<b>4.25</b>	97.3	[M+H] <sup>+</sup>	1030.61	1030.05
<b>4.26</b>	94.4	[M+H] <sup>+</sup>	1030.61	1029.75
<b>4.27</b>	91.2	[M+H] <sup>+</sup>	984.06	983.99

Using a cellular binding assay, the affinities of the lower molecular weight [Tyr<sup>8</sup>]ghrelin(1-8)-amide analogues were determined (Table 4.8). Interestingly, modified ghrelin in the presence of a phenyl side chain as in **4.24**, was discovered to have a poor

receptor binding affinity to the GHSR. However, when increasing the bulkiness of the aromatic ring as in naphthyl **4.26**, the affinity to the GHSR dramatically increases. In comparison to ghrelin[1-28] and [Tyr<sup>8</sup>]ghrelin(1-8) with the octanoylated side chain **4.27**, our novel naphthyl side chains show a similar affinity towards the GHSR. The 18-mer and 8-mer novel peptide sequences have demonstrated the tolerability and flexibility of human ghrelin for use in PET imaging. In addition to the low nM binding affinities achieved by the placement of our unnatural aromatic side chains, we have developed an integrated radiopharmaceutical, where the radioisotope is incorporated into the receptor-binding region of interest.

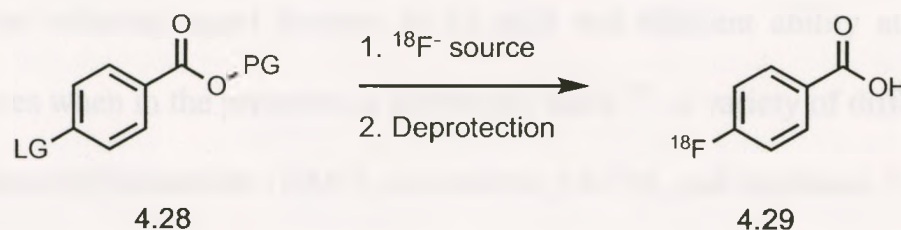
**Table 4.8.** Binding affinities to the GHSR of low molecular weight [Tyr<sup>8</sup>]ghrelin(1-8)-amide analogues with varying Dpr<sup>3</sup> side chains. ND = Not determined.

Compound	IC <sub>50</sub> (nM)
Ghrelin [1-28]	8.1 ± 1.0
<b>4.24</b>	435 ± 82
<b>4.25</b>	ND
<b>4.26</b>	9.9 ± 1.7
<b>4.27</b>	65 ± 22

#### **4.2.2 Designing an Integrated Radiopharmaceutical using Fluorine-18 prosthetic groups**

The development of a fluorine-18 labelled naphthalene prosthetic group was investigated, since the binding affinities for both 18-mer and 8-mer naphthyl containing peptides demonstrated potent binding affinity to the GHSR. To our knowledge, fluorine-18 labelled naphthyl rings used as prosthetic groups have not previously been reported. The synthesis of these novel prosthetic groups was investigated based on the results

obtained from Tables 4.6 and 4.8. These prosthetic groups would be used to establish a radiolabelling method for incorporating bulky side chains into the binding region of modified ghrelin analogues. Although the use of naphthalene compounds as prosthetic groups has not been studied, many successful radiochemical syntheses are reported for similar aromatic targets (Scheme 4.6)<sup>130</sup>. These well-established reactions have been applied to three different naphthalene compounds. Figure 4.2 displays the three targets we have investigated, with the goal of labeling a naphthalene group, which displayed low nM binding affinity in our modified ghrelin sequences. This would be the first example of a ghrelin analog radiolabeled with fluorine-18 for PET imaging.



**Scheme 4.6.** A general  $S_NAr$  reaction involving the addition of fluorine to a protected benzoic acid to afford  $^{18}F$ -fluorobenzoic acid<sup>130</sup>.

Incorporating fluorine-18 into an aromatic system requires a nucleophilic source of fluorine, an electron-withdrawing group (EWG) and a good leaving group (LG). Commonly used leaving groups for aromatic substitution reactions include:  $I < Br < Cl < F < NO_2$  and  $N^+Me_3$ <sup>128</sup>. In this chapter, we have chosen to use a quaternary ammonium salt as the leaving group in the nucleophilic aromatic substitution reactions ( $S_NAr$ ) (Scheme 4.6).



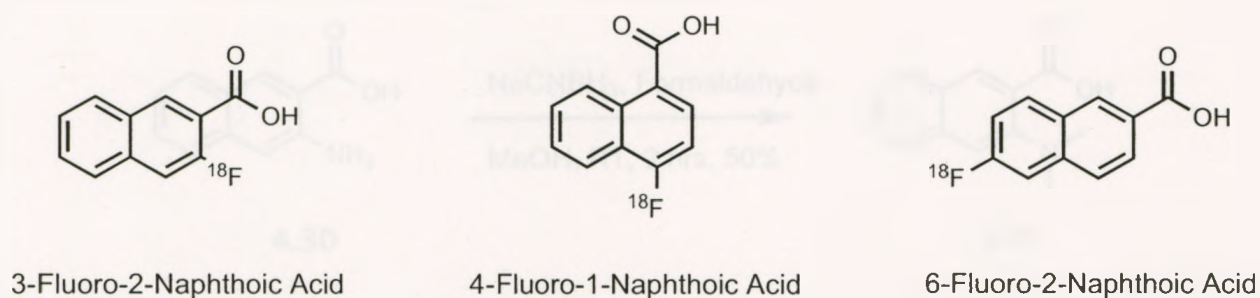
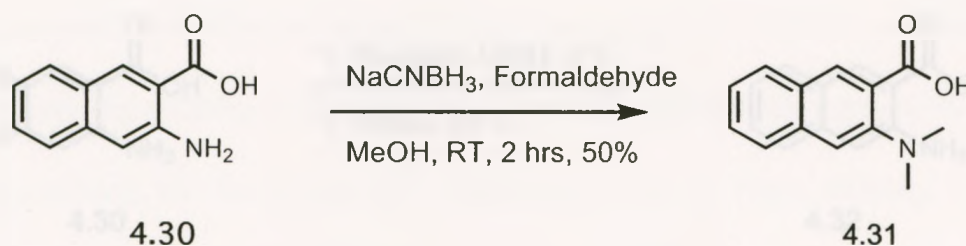


**Figure 4.2.** Novel Naphthalene prosthetic group targets.

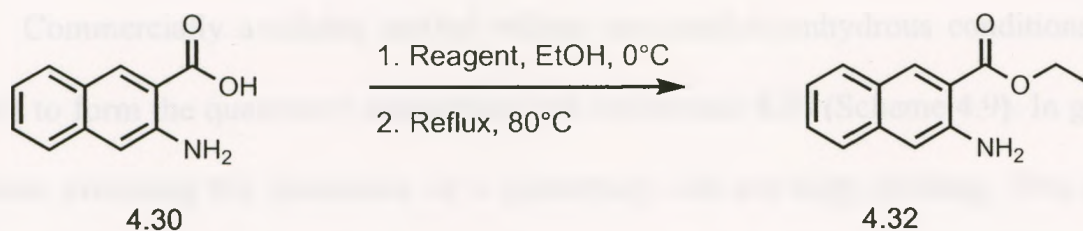
The synthetic approach used in developing a fluorine-18 labelled prosthetic group began with commercially available 3-amino-2-naphthoic acid. Amine **4.30** underwent a reductive amination with sodium cyanoborohydride and formaldehyde in methanol (MeOH) at room temperature to give **4.31** (Scheme 4.7). Sodium cyanoborohydride was chosen as the reducing agent because of its mild and efficient ability at synthesizing tertiary amines when in the presence of carboxylic acids<sup>131</sup>. A variety of different solvents including dimethylformamide (DMF), acetonitrile (ACN), and methanol (MeOH) were used in separate reactions all accounting for similar yields of 50% after purification. The lower yields achieved in this initial step can be accounted for due to the presence of the acid ortho to the amine. The electron withdrawing carboxylic acid could decrease the nucleophilicity of the aromatic amine as well as make it less accessible to the hydride source due to steric hindrance. Maintaining the pH at 3-5 through addition of acetic acid shortened the reaction time from 24 hours to 6 hours as indicated by thin layer chromatography (TLC). Other attempts were made to increase the yield by prolonging reaction times and adding excess of reagents. These attempts proved to be unsuccessful and resulted in 20% recovered starting material **4.30** and mono-substituted byproducts.





**Scheme 4.7.** Reductive amination of an ortho substituted amine.

Solubility issues limited **4.31** from undergoing a transformation to the ester. As a result **4.30** was first protected under acidic conditions to give ethyl ester **4.32** in a 80% yield (Scheme 4.8). Table 4.9 summarizes the three different approaches used to protect carboxylic acid **4.30**. Under reaction conditions **a**, a 42% yield was achieved through the formation of an acid chloride intermediate followed by the nucleophilic attack of ethanol. Monitoring this reaction by TLC showed the absence of starting material at 10 hours. Upon basic work-up conditions the ethyl ester **4.32** was isolated using flash chromatography. The low yield achieved under these conditions was caused by the hydrolysis of the ethyl ester when using sodium carbonate in the work-up. Based on proton NMR, addition of sodium carbonate to **4.32** showed a loss of peaks corresponding to the ethyl ester protons. Selecting a weaker base at lower concentrations (sodium bicarbonate) displayed a 10% improvement in isolating **4.32** (condition **b**) with a yield of 52% respectively. Instead of using  $\text{SO}_2\text{Cl}_2$  to produce the unstable acid chloride intermediate **4.30**, two alternative approaches using HCl and  $\text{H}_2\text{SO}_4$  were then used to protect **4.30**. When using additions of 10 molar hydrochloric acid and 12 molar sulphuric acid, the protection of the free acid increased from 55% to 80% respectively. Thus, sulphuric acid was chosen as the preferred reagent in forming **4.32**.

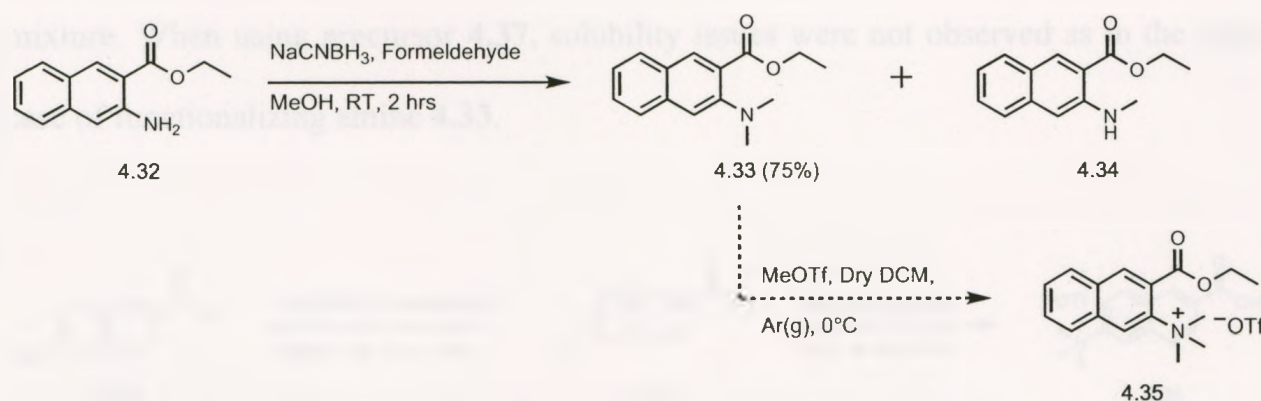


**Scheme 4.8.** The synthesis of protecting carboxylic acid **23**.

**Table 4.9.** Various reagents and conditions used for protecting 2-amino-3-naphthoic acid **4.30**.

Condition	Reagent	Eq.	Time (hrs)	Yield (%)
a	SO <sub>2</sub> Cl <sub>2</sub>	1.4	10	42
b	SO <sub>2</sub> Cl <sub>2</sub>	1.4	10	52
c	SO <sub>2</sub> Cl <sub>2</sub>	2.5	24	52
d	HCl	5.0	24	55
e	H <sub>2</sub> SO <sub>4</sub>	5.0	24	80

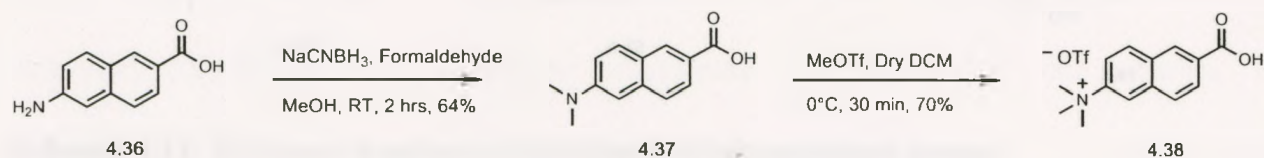
Reductive amination of the aromatic amine was carried out on **4.32** using the same method previously established in Scheme 4.7. Initially, reductive amination of **4.32** only formed the mono-substituted aromatic amine based on proton NMR. By constantly adjusting the pH (3-5) of the reacting solution using acetic acid, di-substituted **4.33** was isolated in a 75% yield (Scheme 4.9).



**Scheme 4.9.** Towards the synthesis of an ortho quaternary ammonium salt.

Commercially available methyl triflate was used in anhydrous conditions in an attempt to form the quaternary ammonium salt compound **4.35** (Scheme 4.9). In general, reactions involving the formation of a quaternary salt are high yielding. Yet, in this system, the electronics changed when placing an electron withdrawing group (EWG) ortho to the site of methylation. In addition, poor solubility starting material **4.33** was observed in a wide range of solvents including chloroform, DCM and tetrahydrofuran (THF). When attempting to drive the reaction forward, salt **4.35** was not formed even upon adding excessive amounts of methyl triflate.

With attempts at a synthetic route towards a radiolabeled precursor for 3-fluoro-2-naphthoic acid remaining unsuccessful, we elected to move ahead and focus on 6-fluoro-2-naphthoic acid. In this target compound the aromatic amine was assumed to be a better nucleophile due to its positioning on the opposing ring to the EWG. Scheme 4.10 shows the steps taken to form the quaternary ammonium salt using the same methods as reported in the attempt to synthesize 3-fluoro-2-naphthoic acid. Aromatic amine **4.36** underwent a reductive amination to give tertiary amine **4.37** with a 64% yield. The quaternary ammonium salt **4.38** was isolated in a 70% yield, upon being filtered from the reaction mixture. When using precursor **4.37**, solubility issues were not observed as in the latter case of functionalizing amine **4.33**.

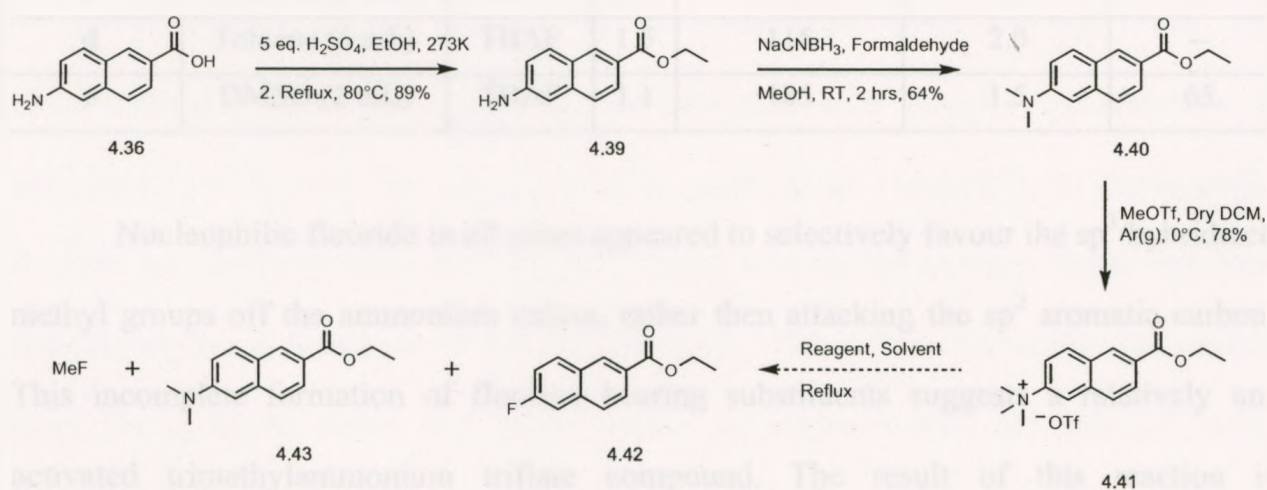


**Scheme 4.10.** The synthesis of a quaternary ammonium salt **4.38**.



This method of forming the quaternary ammonium ion was then re-applied to the initial protected acid using 6-amino-2-naphthoic acid (Scheme 4.11). The protection of **4.36** using the optimized sulfuric acid conditions gave the corresponding ethyl ester **4.39** in higher yields than previously observed with having the substituents ortho to one another. Amine **4.39** underwent a reductive amination to give the corresponding tertiary amine **4.40** in a 64% yield. Alkylation of **4.40** using methyl triflate gave the quaternary ammonium salt **4.41** in a 78% yield.

The remaining step in developing a radiolabeling method for 6-fluoro-2-naphthoic acid (**4.42**) was introducing a cold fluorine source and observing the displacement of the ammonium cation using NMR spectroscopy (Scheme 4.11). In general, an EWG is required to achieve a good substitution yield for a  $S_NAr$  reaction<sup>132</sup>. These substitution reactions are highly dependent on solvent choice, reaction temperatures, reaction times, amount of base and precursor concentrations<sup>28</sup>.



**Scheme 4.11.** Precursor synthesis of fluorine bearing prosthetic group.



An initial reaction reported by Seimbile *et al* was attempted at room temperature reaction using tetrabutylammonium fluoride (TBAF) in anhydrous acetonitrile<sup>133,134</sup>. Based on proton NMR, the outcome of this reaction formed 50% of demethylated **4.43** and recovered ammonium salt **4.41**. An additional reaction applying heat to 1.7 equivalents of TBAF *in situ* with starting material **4.41** resulted a 70% yield of **4.43**. It was anticipated that there would be formation of fluorinated **4.42** when applying more vigorous reaction conditions. However, in a number of different solvents including toluene, dimethyl sulfoxide, and dimethylformamide, a selective demethylation reaction occurred to give **4.43** (conditions **c-d**).

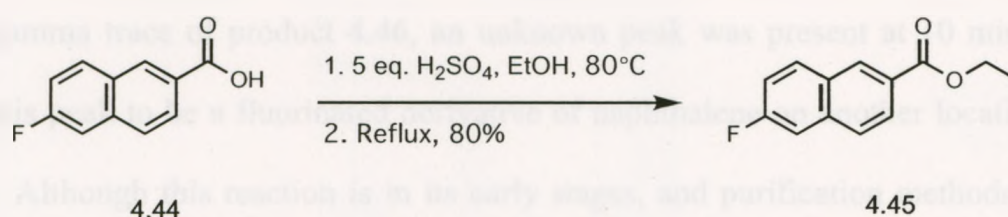
**Table 4.10.** Summary of fluorinating agents used to displace the quaternary ammonium salt **4.41**.

Condition	Solvent (mL)	Reagent	Eq.	Temp. (°C)	Time (hrs.)	Yield (%)
<b>a</b>	ACN (2 mL)	TBAF	1.0	RT	1.0	50
<b>b</b>	THF (2 mL)	TBAF	2.0	RT	1.0	0
<b>c</b>	Toluene (2 mL)	TBAF	1.7	115	2.0	70
<b>d</b>	Toluene (6 mL)	TBAF	1.5	115	2.0	--
<b>e</b>	DMSO (2 mL)	TBAF	1.1	185	1.5	65

Nucleophilic fluoride in all cases appeared to selectively favour the  $sp^3$  hybridized methyl groups off the ammonium cation, rather than attacking the  $sp^2$  aromatic carbon. This incomplete formation of fluorine bearing substituents suggests a relatively unactivated trimethylammonium triflate compound. The result of this reaction is summarized by the competing  $S_N2$  reverse Menshutkin reaction<sup>134</sup>. Furthermore, literature suggests these types of fluorination reactions are highly dependant on the environment of the aryl ring(s) substituents<sup>135</sup>. In one study, the authors comment that the

methyl groups on a quaternary ammonium cation are quite labile in the presence of anhydrous fluoride<sup>135</sup>.

In order to access the standard fluorinated naphthalene prosthetic group, commercially available 6-fluoro-2-naphthoic acid was protected using the same conditions as in Scheme 4.8. Non-radioactive **4.45** would later be used as a standard for comparison during the synthesis of the corresponding prosthetic group HPLC.



**Scheme 4.12.** Synthesis of standard fluorinated naphthalene.

#### 4.2.3 Incorporating Fluorine-18

As previously mentioned, the chemistry of fluorine-18 can differ greatly from that of non-radioactive fluorine because of its pseudo-first order kinetics. Thus, the radiochemical synthesis using salt **4.41** was attempted, even though the introduction of non-radioactive fluorine was unsuccessful in synthesizing standard **4.42**. Nucleophilic fluorine was produced from the  $^{18}\text{O}(p,n)^{18}\text{F}$  reaction using the Lawson Health Research Institute cyclotron facility at St. Joseph's Hospital. The radioactive media was washed from the cyclotron target and placed inside an enclosed lead hot cell for safety precautions. The media was then passed through an anion exchange column and eluted with a solution consisting of weak base and krytofix 2.2.2. The fluorine-18 solution was then placed inside a Tracer-Lab FX F-E automated synthesis unit made by General

Electric (Figure 4.3). This synthesizer allowed for the automated synthesis of compound **4.46** using Tracer Lab software, to limit the user from exposure to radiation.

To ensure limited amounts of water remained, acetonitrile was used to azeotrope the sample. Following this was the addition of **4.41** dissolved in dimethyl sulfoxide (DMSO) to the fluorine-18 media. A nucleophilic aromatic substitution reaction occurred with salt **4.41** to give product **4.46** (Scheme 4.13). This was confirmed from the HPLC UV trace of the standard **4.45** lining up with the gamma trace of **4.46** (Figure 4.4). Based on the gamma trace of product **4.46**, an unknown peak was present at 10 minutes. We reason this peak to be a fluorinated derivative of naphthalene on another location within the ring. Although this reaction is in its early stages, and purification methods have not been developed, we have shown that fluorination can occur when the EWG is on the opposing ring of naphthalene. Additionally, there was a large difference in retention times based on HPLC traces of precursor **4.41** and product **4.46** (Figure 4.5). This will lead to an easy purification method using an automated sep-pack procedure.

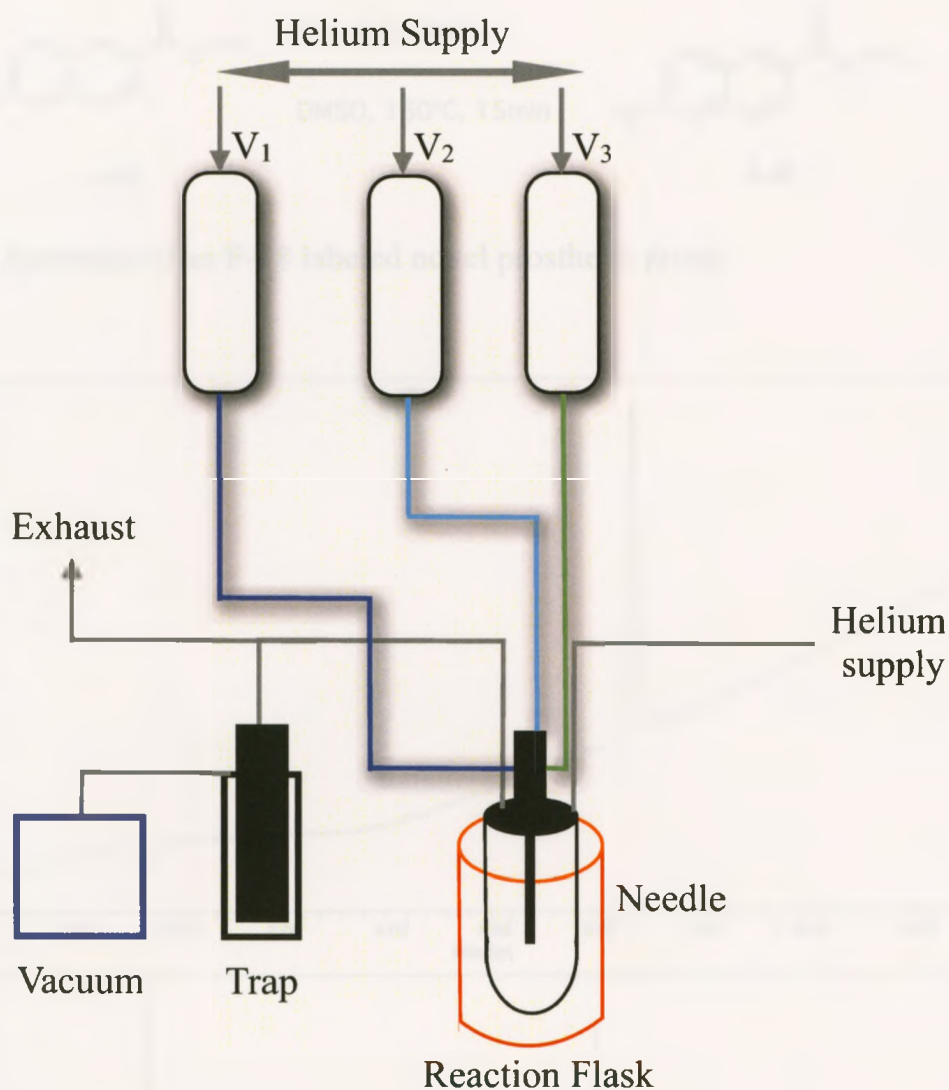
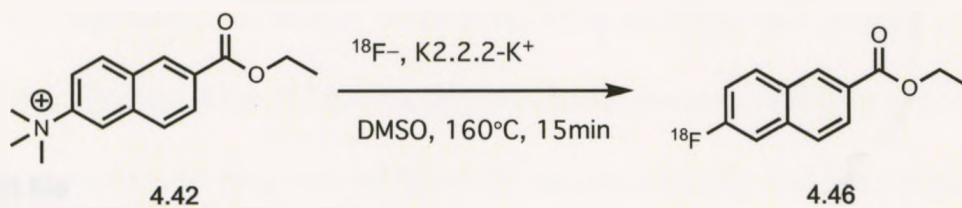


**Figure 4.3.** Schematic diagram of the Tracer Lab FX F-E system. Vials contained: Vial 1 (V<sub>1</sub>) a 2mL solution of Kryptofix 2.2.2 and <sup>18</sup>F<sup>-</sup>, Vial 2 (V<sub>2</sub>) a 2ml solution of anhydrous acetonitrile and Vial 3 (V<sub>3</sub>) a solution of Starting Material dissolved in 1mL anhydrous DMSO. Synthesis began by transferring vial 1 contents to the reaction flask. Azeotropic removal of residual water occurred by heating the reaction flask (under vacuum) with acetonitrile from vial 2. Vial 3 was then be added (under helium) to the reaction flask, starting the reaction.





**Scheme 4.13.** Synthesis of an F-18 labeled novel prosthetic group.

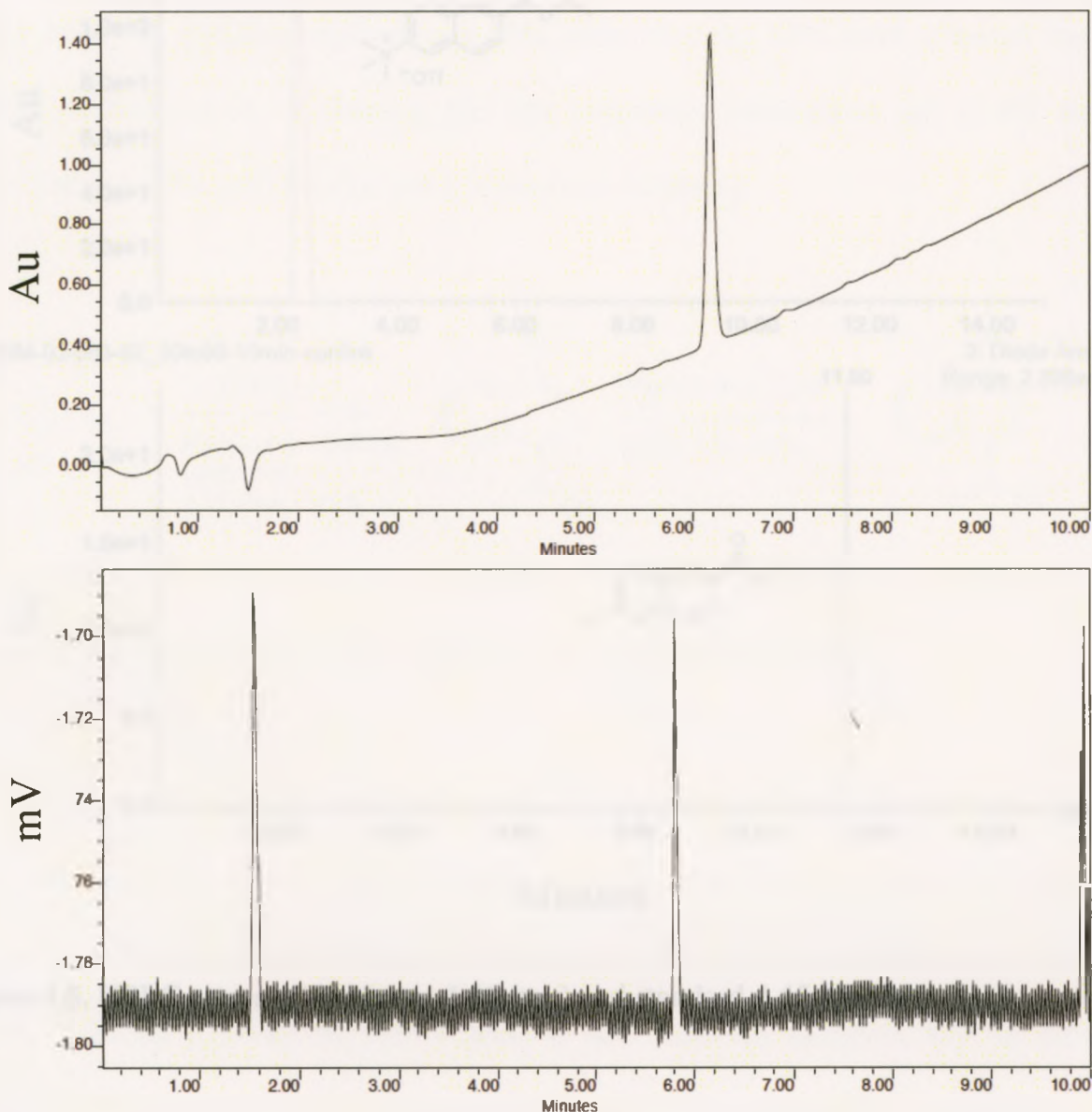


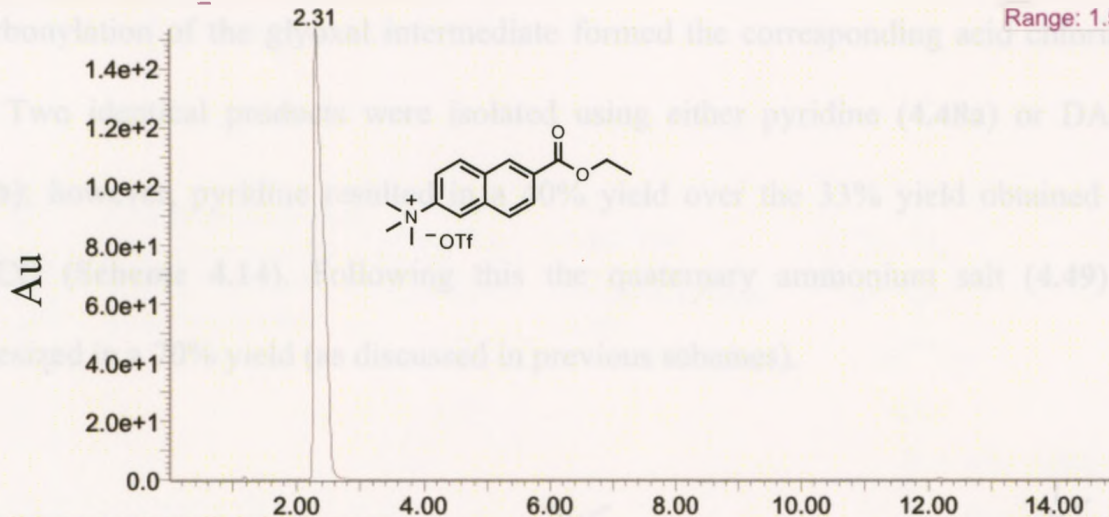
**Figure 4.4.** HPLC UV trace of non-radioactive standard 4.45 (top) and gamma trace of fluorine-18 labelled product 4.46 (bottom).

## Default file

MM-03-064-02-SM\_30to90-10min-sunfire

2: Diode Array

Range: 1.541e+2



MM-03-063-02\_30to90-10min-sunfire

2: Diode Array

Range: 2.395e+1

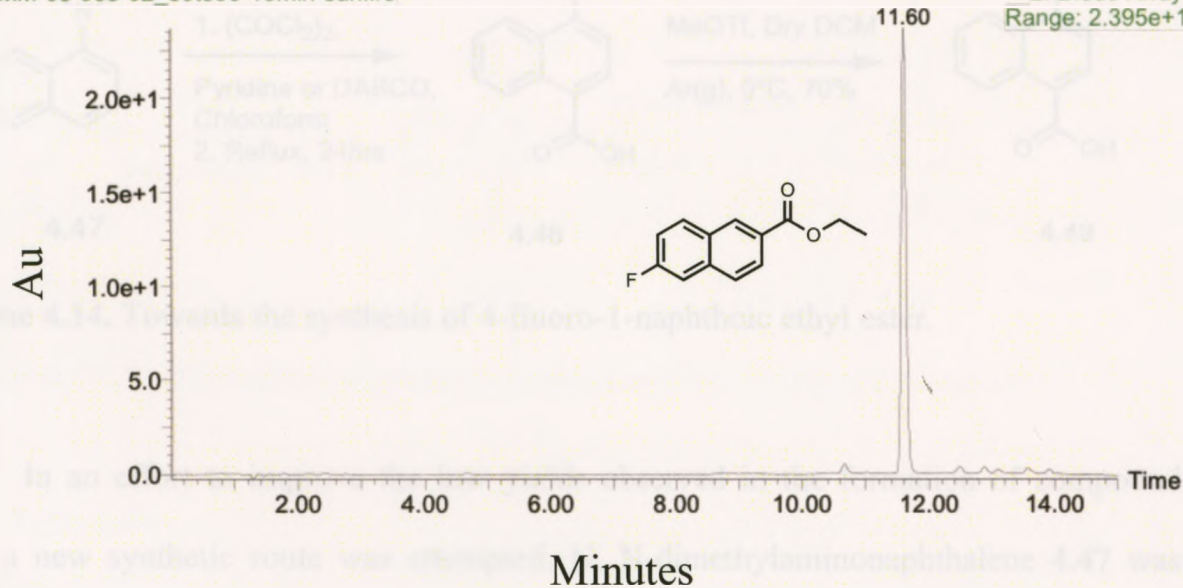
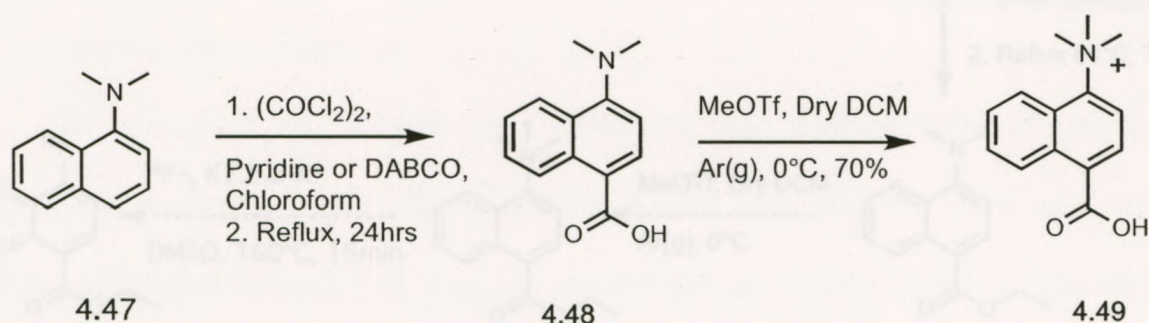


Figure 4.5. HPLC traces of precursor 4.41 (top) and standard 4.45 (bottom).

#### 4.2.4 Other Attempts at Designing Non-Radioactive Standards

In addition to fluorinating the opposing ring as in compound 4.41, we are investigating the radio-chemical synthesis of 4-fluoro-2-naphthoic acid (4.54). This target

has the most resemblance to that of benzene as both the EWG and leaving group are on the same ring. Starting from N, N-dimethylaminonaphthalene (**4.47**), a glyoxal chloride intermediate was formed from the addition of oxalyyl chloride and base (**Scheme 4.14**). Decarbonylation of the glyoxal intermediate formed the corresponding acid chloride of **4.48**. Two identical products were isolated using either pyridine (**4.48a**) or DABCO (**4.48b**); however, pyridine resulted in a 40% yield over the 33% yield obtained from DABCO (**Scheme 4.14**). Following this the quaternary ammonium salt (**4.49**) was synthesized in a 70% yield (as discussed in previous schemes).

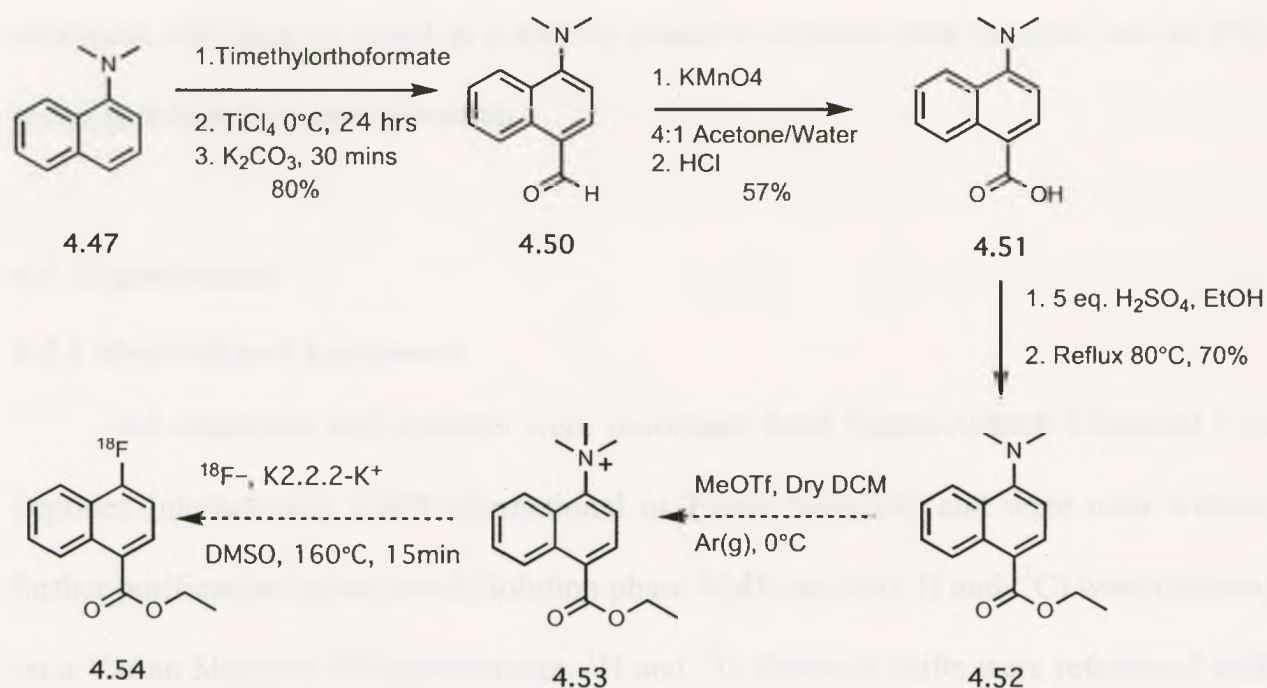


**Scheme 4.14.** Towards the synthesis of 4-fluoro-1-naphthoic ethyl ester.

In an effort to improve the low yields observed in the formation of compound **4.48**, a new synthetic route was attempted. N, N-dimethylaminonaphthalene **4.47** was added to a cold solution of trimethylorthoformate. The drop-wise addition of titanium chloride, a strong hygroscopic Lewis acid, to **4.47** afforded aldehyde **4.50** in 80%. Oxidation of aldehyde **4.50** to corresponding acid **4.51** was initially attempted in a peroxide solution however, based on NMR spectroscopy the aldehyde peak was still present. A method using a silver nitrate catalyst in acetonitrile was attempted, which also failed to work<sup>136</sup>. The addition of potassium permanganate, a strong oxidizing agent,



afforded acid **4.51** in a 57% yield. The acid **4.51** was then protected under acidic conditions to yield ethyl ester **4.52** by the method previously discussed. Subsequent reaction steps are described in Scheme 4.15 which are proposed to ultimately form fluorine-18 labelled naphthoic ethyl **4.54**.



**Scheme 4.15.** An alternative approach to synthesizing 4-fluoro-2-naphthoic acid.

### 4.3 Conclusions

The synthesis of 18-mer and 8-mer ghrelin analogues with modified  $\text{Ser}^3$  side chains have been investigated based on their binding affinities to the GHSR. The synthesized ghrelin analogues have demonstrated high affinity towards the GHSR even when incorporating bulky fluorinated aromatic substituents. This has led to the development of a radiolabelling strategy for incorporating fluorine-18 into a naphthalene prosthetic group. It proved to be difficult to synthesize a fluorine-18 naphthalene ring, when situating fluorine next to the electron withdrawing substituent. However when



placing fluorine on the opposing ring, a nucleophilic aromatic substitution can occur. This is the first example of the design, synthesis, and characterization of a radiolabelled naphthalene analog used as a prosthetic group for the molecular imaging of disease. The next step in the integrated design is to optimize conditions needed for integrating the radiolabelled prosthetic group into the low molecular weight ghrelin analogues. These analogues will then be tested in a murine model to validate their potential use as PET imaging probes for cancer detection.

## 4.4 Experimental

### 4.4.1 Materials and Equipment

All chemicals and solvents were purchased from Sigma-Aldrich Chemical Co., Peptides International, VWR international or Fisher Scientific and were used without further purification unless noted. Solution phase NMR spectra ( $^1\text{H}$  and  $^{13}\text{C}$ ) were obtained on a Varian Mercury 400 spectrometer.  $^1\text{H}$  and  $^{13}\text{C}$  chemical shifts were referenced with the residual solvent resonances relative to trimethylsilane. High-resolution mass spectra were obtained on a Finnigan MAT 8400 Mass Spectrometer (EI) and Micromass LCT Mass Spectrometer (ESI). Low-resolution mass spectra were obtained on a Micromass Quattro Micro API (MS-ESI and LC-MS-ESI). Anhydrous DCM was prepared by distillation from CaH under argon. Oven-dried or flame dried glassware was used in water sensitive reactions under a flow of argon. The radiolabelling synthesis was done using the Lawson Health Research Institute cyclotron facility at St. Joseph's Hospital. All fluorine-18 reactions took place in a Tracer-Lab FX-FE (General Electric) automated synthesis unit, using tracer lab software. A Waters symmetry, 4.6 x 150 mm, 5 Å, C-18 column was used and coupled to a gamma detector. This system employed a Waters 1525

Binary HPLC pump, Waters 2487 dual  $\lambda$  absorbance detector, Waters In-Line degasser and Breeze software (version 3.30). Flash chromatography was performed using a Merk Silica gel 60 (230-400 mesh). Reactions were followed by TLC analysis, which were carried out on EMD Silica Gel 60-F(254) plates. Analytical HPLC was performed using a Grace Vydac Protein/Peptide RP-C18 column 4.6 x 250 mm, 5  $\mu$ m or a Sunfire RP-C18 column 4.6 x 250 mm, 5  $\mu$ m. Preparative HPLC was performed using a Grace Vydac Peptide/Protein SP-C18 column 22.0 x 250 mm, 10  $\mu$ m or a Sunfire SP-C18 column 22.0 x 250 mm, 10  $\mu$ m. A gradient system was used: ACN + 0.1% TFA (solvent A) and water + 0.1% TFA (Solvent B). The absorbance was detected in the 200 nm to 500 nm wavelength range.

#### ***4.4.2 General Procedure for Peptide Assembly***

Fully protected resin bound peptides were synthesized manually according to the general procedures in Fmoc solid phase peptide synthesis. Fmoc protected rink amide MBHA resin (loading 0.56 or 0.47 meq/ g) was used as the solid support. N-Fmoc amino acids with strong acid labile protecting groups for side chain functional groups, were used in general, and Boc-Gly was used for the N-terminus. Fmoc-(Dpr), with the  $\beta$ -amine protected through an allyloxycarbonyl (alloc) group, was used for residue-3. Fmoc removal was achieved by adding 20% piperidine in DMF for 5 and 15 minutes, followed by washes with DMF and DCM after each treatment. For each amino acid coupling, resin was treated twice with 3 eq. of Fmoc or Boc amino acids, 3 eq. of 3-[bis(dimethylamino)methyl]-3H-benzotriazol-1-oxide hexafluorophosphate (HBTU) and 6 eq. of N,N-diisopropylethylamine (DIPEA) in 2 mL of DMF for 30

minutes to 2 hours. Couplings were followed by multiple washes with DMF, and CH<sub>2</sub>Cl<sub>2</sub>. Using this general procedure, peptides were prepared on resin.

#### ***4.4.3 General Procedure for Selective Deprotection and Resin Cleavage***

Selective deprotections were carried out using an orthogonal deprotection strategy for Dpr<sup>3</sup>. The β-amine protected with allyloxycarbonyl (alloc) was selectively removed by treating the resin with 0.35 eq. of tetrakis(triphenylphosphine)palladium (Pd(PPh<sub>3</sub>)<sub>4</sub>), and 20 eq. of phenylsilane (PhSiH<sub>3</sub>) in 2 mL of anhydrous DCM. This treatment was repeated twice, followed by successive washes with DMF and DCM. The Kaiser test was used to monitor the presence or absence of a free amine. After further modifications to the β-amine of Dpr<sup>3</sup> were complete, the peptide was deprotected and cleaved from the resin using 95% TFA, 2.5% TIS, and 2.5% water for 3-6 hours. The resin was filtered and rinsed with a small amount of TFA. Cold tert-butyl methyl ether (TBME) was added to the filtrate to form a precipitate. Following the addition of TBME, the slurry was centrifuged and decanted. The peptide was rinsed with TBME and collected again. The solid was dissolved in water with the addition of acetonitrile (ACN) when needed, froze, and lyophilized to obtain a crude peptide as a powder. Purification was carried out using preparative HPLC, and the purity of the isolated product was determined by analytical HPLC.

#### ***4.4.4 General Procedure for Fluorine Bearing Ghrelin(1-18), and [Tyr<sup>8</sup>]Ghrelin(1-8) Analogues***

Analogues 4.21, 4.22 and 4.24-4.27 were made on resin following a general procedure similar to the synthesis of 2.16. Selective removal of alloc located off the β-



amine of Dpr<sup>3</sup> was deprotected according to the general procedure for selective deprotections. Side Chains **A** (4-fluoro-1-naphthoic acid), **B** (fluorobenzoic acid), and **C** (6-fluoro-2-naphthoic acid) were coupled to the peptide according to the general procedure in peptide assembly. Successful couplings were washed and rinsed with DMF and DCM. Following this, a final cleavage and deprotection was conducted according to the general procedure to obtain the crude peptide.

#### 4.4.5 [Dpr<sup>3</sup>(fluorobenzoic acid)]Ghrelin(1-18)-amide (4.21) and [Dpr<sup>3</sup>(4-fluoro-1-naphthoic acid)]Ghrelin(1-18)-amide (4.22)

Purification was performed by HPLC (gradient 30-80% solvent A in B) to obtain 4.21 and 4.22 with yields of 8.5% (18 mg), and 7% (16 mg) as white powders (ESI-MS and purity reported in Table 4.5.)

#### 4.4.6 [Dpr<sup>3</sup>(fluorobenzoic acid)]/[Tyr<sup>8</sup>]Ghrelin(1-8)-amide (4.24), [Dpr<sup>3</sup>(4-fluoro-1-naphthoic acid)]/[Tyr<sup>8</sup>]Ghrelin(1-8)-amide (4.25), [Dpr<sup>3</sup>(6-fluoro-2-naphthoic acid)]/[Tyr<sup>8</sup>]Ghrelin(1-8)-amide (4.26) and [Tyr<sup>8</sup>]Ghrelin(1-8)-amide (4.27)

Purification was performed by HPLC (gradient 30-60% solvent A in B) to obtain 4.24, 4.25, 4.26 and 4.27 with yields of 10%, 9.7%, 4% and 15% as white powders (ESI-MS and purity reported in Table 4.7.

#### 4.4.7 General Procedure for Protecting Carboxylic Acids

In a 250 mL three neck round bottom flask, 90 mL of ethanol was added to the unprotected acid (1 eq.), while stirring under argon gas. Five eq. of 12M sulfuric acid (H<sub>2</sub>SO<sub>4</sub>) was added drop wise to the red solution while stirring in an ice bath. Following the addition of sulfuric acid, the reaction was heated and refluxed between 85-90 °C for 24 hours. The reaction mixture was concentrated under reduced pressure. The resulting red residue was extracted with dichloromethane and washed with a 0.1 molar solution of



sodium bicarbonate. The combined organic fractions were dried over  $\text{MgSO}_4$  followed by concentration *in vacuo*.

#### 4.4.8 2-Ethyl 3-aminonaphthoate (4.32)

Green solid, 0.27 g (75%).  $R_f$  0.31 (12% EtOAc/Hexanes);  $^1\text{H-NMR}$  (400 MHz,  $\text{DMSO-d}_6$ ):  $\delta$  8.43 (s, 1H), 7.78 (dd,  $J = 8.2, 3.0$  Hz, 1H), 7.52 (dd,  $J = 8.3, 3.0$  Hz, 1H), 7.38 (ddd,  $J = 8.3, 6.8, 1.3$  Hz, 1H), 7.12 (ddd,  $J = 8.1, 6.8, 1.2$  Hz, 1H), 7.03 (s, 1H), 6.45 (s, 2H), 4.35 (q,  $J = 7.1$  Hz, 2H), 1.36 (t,  $J = 7.1$  Hz, 3H).  $^{13}\text{C-NMR}$  (101 MHz;  $\text{DMSO-d}_6$ ):  $\delta$  167.4, 147.1, 137.2, 132.8, 129.3, 128.9, 124.9, 124.9, 122.0, 114.2, 109.0, 60.7, 14.4. HRMS (EI)  $m/z$  calc for:  $\text{C}_{13}\text{H}_{13}\text{NO}_2$ : 215.0952; found: 215.0950.

#### 4.4.9 2-Ethyl 6-aminonaphthoate (4.39)

White solid, 0.15 g (89%).  $R_f$  0.25 (5% EtOAc/Hexanes);  $^1\text{H-NMR}$  (400 MHz,  $\text{DMSO-d}_6$ ):  $\delta$  8.43 (d,  $J = 1.3$  Hz, 1H), 7.94-7.92 (m, 1H), 7.84 (dd,  $J = 8.6, 1.7$  Hz, 1H), 7.725-7.704 (m, 1H), 7.52 (br s, 2H), 7.17-7.16 (m, 2H), 4.33 (q,  $J = 7.1$  Hz, 2H), 1.34 (t,  $J = 7.1$  Hz, 3H). HRMS (EI)  $m/z$  calc for:  $\text{C}_{13}\text{H}_{13}\text{NO}_2$ : 215.0952; found: 215.0946.

#### 4.4.10 2-Ethyl 6-fluoronaphthoate (4.45)

White solid, 0.36 g (80%).  $R_f$  0.50 (10% EtOAc/Hexanes);  $^1\text{H-NMR}$  (400 MHz,  $\text{CDCl}_3$ ):  $\delta$  8.59-8.55 (m, 1H), 8.10-8.08 (m, 1H), 7.95 (dd,  $J = 9.01, 5.63$  Hz, 1H), 7.81 (d,  $J = 8.65$  Hz, 1H), 7.48 (dd,  $J = 9.63, 2.48$  Hz, 1H), 7.34-7.7.29 (m, 1H), 4.45 (q,  $J = 7.13$  Hz, 2H), 1.45 (t,  $J = 7.13$  Hz, 3H). HRMS (EI)  $m/z$  calc for:  $\text{C}_{13}\text{H}_{11}\text{FO}_2$ : 218.0743; found: 218.0740.

#### 4.4.11 1-Ethyl 4-dimethylaminonaphthoate (4.52)

Yellow solid, 0.50 g, (70%).  $R_f$  0.10 (10% EtOAc/Hexanes);  $^1\text{H-NMR}$  400 MHz,  $\text{CDCl}_3$ ):  $\delta$  8.95-8.91 (m, 1H), 8.37-8.35 (m, 1H), 8.21-8.19 (m, 1H), 7.89-7.87 (m, 1H), 7.81-7.71 (m, 2H), 4.46 (q,  $J = 7.1$  Hz, 2H), 3.52 (s, 6H), 1.47 (t,  $J = 7.1$  Hz, 3H).

#### 4.4.12 General Procedure for Reductive Amination of Aromatic Amines

A modified literature procedure was followed<sup>135</sup>. To a solution containing an aromatic amine (1 eq.) in 20 mL of methanol, was added sodium cyanoborohydride (10 eq.) and formaldehyde (37% in water, 20 eq.). To this solution, 99.8% acetic acid was added drop wise until the solution reached a pH of 3-5. The mixture was stirred at room temperature and monitored by TLC until completion. The reaction mixture was concentrated under reduced pressure. The resulting yellow residue was extracted with dichloromethane and washed with a 0.1 molar solution of sodium bicarbonate. The combined organic fractions were dried over  $\text{MgSO}_4$  followed by concentration *in vacuo*.

#### 4.4.13 3-Dimethylamino-2-naphthoic acid (4.31)

Green solid, 0.25 g (50%).  $R_f$  0.2 (10% MeOH/DCM)  $^1\text{H-NMR}$  (400 MHz,  $\text{CDCl}_3$ ):  $\delta$  8.549 (d,  $J = 0.33$  Hz 1H), 7.998 (dd,  $J = 8.68, 1.45$  Hz, 1H), 7.876-7.853 (m, 1H), 7.713-7.692 (m, 1H), 7.04-6.94 (br s, 1H), 3.131 (s, 6H).

#### 4.4.14 2-Ethyl 3-dimethylaminonaphthoate (4.33)

Yellow solid, 0.27 g (75%).  $R_f$  0.18 (5% EtOAc/Hexanes);  $^1\text{H-NMR}$  (400 MHz,  $\text{DMSO-d}_6$ ):  $\delta$  8.48 (m, 1H), 8.09-8.07 (m, 1H), 7.95-7.70 (m, 1H), 7.65-7.63 (m, 1H), 7.56 (s,

1H), 7.50-7.47 (m, 1H), 4.41 (q,  $J = 7.1$  Hz, 2H), 3.15 (s, 6H), 1.39 (t,  $J = 7.1$  Hz, 3H).

HRMS (EI)  $m/z$  calc for:  $C_{15}H_{17}NO_2$ : 243.1259; found: 243.1137.

#### 4.4.15 6-Dimethylamino-2-naphthoic acid (4.37)

Orange solid, 0.73 g (64%).  $R_f$  0.5 (10% MeOH/DCM);  $^1H$ -NMR (400 MHz,  $CDCl_3$ ):  $\delta$  8.55 (d,  $J = 0.3$  Hz, 1H), 8.00 (dd,  $J = 8.7, 1.4$  Hz, 1H), 7.84 (m,  $J = 9.1$  Hz, 1H), 7.68 (m,  $J = 8.7$  Hz, 1H), 7.25-7.20 (m, 1H), 7.04-6.94 (m, 1H), 3.13 (s, 6H). HRMS (EI)  $m/z$  calc for:  $C_{13}H_{13}NO_2$ : 215.0946; found: 215.0945.

#### 4.4.16 2-Ethyl 6-dimethylaminonaphthoate (4.40)

Yellow solid, 0.27 g (75 %).  $R_f$  0.20 (10% EtOAc/Hexanes);  $^1H$ -NMR (400 MHz,  $CDCl_3$ ):  $\delta$  8.47 (d,  $J = 1.3$  Hz, 1H), 7.97 (dd,  $J = 8.6, 1.7$  Hz, 1H), 7.79 (d,  $J = 9.1$  Hz, 1H), 7.64 (d,  $J = 8.7$  Hz, 1H), 7.15 (dd,  $J = 9.1, 2.5$  Hz, 1H), 6.88 (m, 1H), 4.42 (q,  $J = 7.1$  Hz, 2H), 3.07 (s, 6H), 1.44 (t,  $J = 7.1$  Hz, 3H).  $^{13}C$ -NMR (101 MHz;  $CDCl_3$ ):  $\delta$  167.4, 150.1, 137.6, 131.0, 130.5, 126.11, 125.99, 125.5, 123.6, 116.4, 105.6, 60.8, 40.6, 14.7. HRMS (EI)  $m/z$  calc for:  $C_{15}H_{17}NO_2$ : 243.1259; found: 243.12560.

#### 4.4.17 2-Ethyl 3-methylaminonaphthoate (4.34)

Yellow Solid, 0.14 g (50 %).  $R_f$  0.5 (15% EtOAc/Hexanes);  $^1H$ -NMR (400 MHz,  $CDCl_3$ ):  $\delta$  8.54 (s, 1H), 7.74 (m, 1H), 7.65 (m, 1H), 7.45 (ddd,  $J = 7.6, 1.1, 1.1$  Hz, 1H), 7.22 (ddd,  $J = 7.5, 0.8, 0.8$  Hz, 1H), 7.03 (s, 1H), 4.41 (q,  $J = 7.1$  Hz, 2H), 3.01 (s, 3H), 1.45 (t,  $J = 7.2$  Hz, 3H).



#### 4.4.18 General Procedure for Forming a Quaternary Ammonium Salt

To a 25 mL round bottom flask placed in an ice bath, the desired tertiary aromatic amine (1 eq.) was dissolved in 5 mL of dry dichloromethane and cooled to 0 °C using an ice bath. While stirring under argon gas, methyl trifluoromethanesulfonate (4 eq.) was added drop wise to the reaction mixture. The mixture was stirred for 30 minutes at 0 °C. At this time a white precipitate formed and the solution was allowed to stir for an additional 30 minutes. The white precipitate was filtered off, and dried under vacuo.

#### 4.4.19 6-(*N, N, N*-trimethylammonium trifluoromethansulfonyl)-2 naphthoic acid (4.38)

White solid, 0.18 g (50%). <sup>1</sup>H-NMR (400 MHz, DMSO-d<sub>6</sub>): δ 8.73 (m, 1H), 8.62-8.60 (m, 1H), 8.45-8.43 (m, 1H), 8.38-8.37 (m, 1H), 8.24-8.20 (m, 2H), 3.72 (s, 9H). ESI-MS calc for: C<sub>14</sub>H<sub>16</sub>NO<sub>2</sub>: 230.3; found [M+H]<sup>+</sup>: 231.0.

#### 4.4.20 2-ethyl 6-(*N, N, N*-trimethylammonium trifluoromethansulfonyl)-naphthoate (4.41)

White solid, 0.18 g (56%). <sup>1</sup>H-NMR (400 MHz, DMSO-d<sub>6</sub>): δ 8.75 (m, 1H), 8.63 (m, 1H), 8.45 (m, 1H), 8.26-8.21 (m, 2H), 8.15 (m, 1H), 4.40 (q, J = 7.1 Hz, 2H), 3.74 (s, 10H), 1.38 (t, J = 7.1 Hz, 3H). <sup>13</sup>C-NMR (101 MHz; dmsO): δ 14.40, 56.54, 56.58, 61.43, 119.35, 119.57, 122.52, 125.73, 126.80, 129.45, 129.75, 130.19, 131.89, 132.13, 134.50, 146.33, 165.67. ESI m/z calc for: C<sub>16</sub>H<sub>20</sub>NO<sub>2</sub>: 258.15; found [M+H]<sup>+</sup>: 258.20.

#### 4.4.21 4-(*N, N, N*-trimethylammonium trifluoromethansulfonyl)-1-naphthoic acid (4.49)

White solid, 0.27 g (70%). <sup>1</sup>H-NMR (400 MHz, DMSO-d<sub>6</sub>): δ 13.84 (bs, 1H), 8.87-8.85 (m, 1H), 8.73-8.71 (m, 1H), 8.20 (d, J = 8.5 Hz, 1H), 8.13 (d, J = 8.4 Hz, 1H), 7.88-7.85 (m, 2H), 3.95 (s, 9H). ESI m/z calc for: C<sub>14</sub>H<sub>16</sub>NO<sub>2</sub><sup>+</sup>: 230.11; found: 230.10.



#### 4.4.22 4-dimethylamino-1-napthoic acid (4.48)

In a 100 mL three necked round bottom flask, 1,4-diazabicyclo[2.2.2]octane (1.12 g, 0.01 mol) was dissolved in 15 mL dry chloroform. While stirring at 0 °C, oxalyl chloride (1.71 g, 0.01 mol) was added dropwise to the reaction mixture. Upon the formation of a yellow precipitate, dimethyl naphthalene **4.47** dissolved in 30 mL dry chloroform, was added dropwise using an addition funnel over the course of one hour. The reaction mixture was refluxed at 75 °C overnight and monitored by thin layer chromatography. The reaction mixture was concentrated under reduced pressure. The resulting orange residue was extracted with chloroform and acidified water at pH 3-4. The combined organic fractions were dried over MgSO<sub>4</sub> followed by concentration *in vacuo* yielding 0.71 g (33%) of an orange precipitate. R<sub>f</sub> 0.05 (100% CHCl<sub>3</sub>); <sup>1</sup>H-NMR (400 MHz, DMSO-d<sub>6</sub>): δ 12.70 (s, 1H), 9.01-8.99 (m, 1H), 8.18-8.11 (m, 1H), 7.61-7.51 (m, 3H), 7.08-7.06 (m, 1H), 2.88 (s, 6H). HRMS (EI) m/z calc for: C<sub>13</sub>H<sub>13</sub>NO<sub>2</sub>: 215.0946; found: 215.0943.

#### 4.4.23 4-dimethylamino-1-naphthaldehyde (4.50)

N, N-Dimethyl-1-naphthylamine (1.6 mL, 10 mmol) and trimethyl orthoformate (1.62 mL, 15 mmol) were stirred at 0 °C in anhydrous DCM (40 mL) under nitrogen. Titanium tetrachloride (4.4 mL TiCl<sub>4</sub>, 20 mmol) in 20 mL anhydrous DCM, was added dropwise over 4 hours to the stirring solution. The reaction was then warmed to room temperature and stirred overnight. Saturated K<sub>2</sub>CO<sub>3</sub> solution (30 mL) was added to the reaction and stirred for 1 hour. The reaction mixture was filtered through a Buchner funnel. The resulting red solution was concentrated *in vacuo* and then extracted with DCM. The combined organic fractions were dried over MgSO<sub>4</sub> followed by concentration *in vacuo* yielding 1.3 g (80%) of a red precipitate. R<sub>f</sub> 0.10 (5% EtOAc/Hexanes); <sup>1</sup>H-NMR (400

MHz, CDCl<sub>3</sub>):  $\delta$  10.17 (s, 1H), 9.37-9.35 (m, 1H), 8.19-8.17 (m, 1H), 7.83 (d,  $J = 7.93$  Hz, 1H), 7.67-7.62 (m, 1H), 7.55-7.52 (m, 1H), 7.03 (d,  $J = 7.93$  Hz, 1H), 3.03 (s, 6H). HRMS (EI)  $m/z$  calc for: C<sub>13</sub>H<sub>13</sub>NO: 199.0997; found: 199.1000.

#### 4.4.24 4-dimethyl-1-naphthoic acid (4.51)

In a 100 mL double neck round bottom flask, 4-dimethylamino-1-naphthaldehyde 4.50 (1 eq., 0.82 mmol) was dissolved in a 4:1 solution of acetone/water. Potassium Permanganate (KMnO<sub>4</sub>, 5 eq., 4.1 mmol) was dissolved in 8 mL acetone/water (4:1) and then added dropwise to the stirring solution over 30 minutes. The reaction was then refluxed at 60 °C and monitored by thin layer chromatography. The resulting red solution was concentrated *in vacuo* and then filtered through a Buchner funnel. The combined aqueous solution was acidified with 6 M HCl and then extracted in DCM. The combined organic fractions were dried over MgSO<sub>4</sub> followed by concentration *in vacuo* yielding 0.10g (57%) of a yellow precipitate.  $R_f$  0.20 (7.5% MeOH/DCM); <sup>1</sup>H-NMR (400 MHz, CDCl<sub>3</sub>):  $\delta$  9.14-9.12 (m, 1H), 8.31 (d,  $J = 8.11$  Hz 1H), 8.20 (dd,  $J = 8.47, 0.75$  Hz 1H), 7.58-7.48(m, 2H), 6.98 (d,  $J = 8.15$  Hz 1H), 2.96 (s, 6H).

#### 4.4.25 F-18 radiolabelling procedure 2-Ethyl 6-<sup>18</sup>fluoronaphthoate (4.46)

Nucleophilic fluorine-18 was prepared by passing a solution of <sup>18</sup>F/H<sub>2</sub>O (0.5 mL) through an anion exchange column and eluting with a 2 mL solution of K<sub>2</sub>CO<sub>3</sub>/Kryptofix 2.2.2. Azeotropic removal of water was achieved by adding 500  $\mu$ L of anhydrous ACN and heating (55 °C) the solution while under nitrogen. A second portion of 500  $\mu$ L of anhydrous ACN was added followed by heating (55 °C) under nitrogen. The quaternary ammonium salt **4.41** dissolved in 1 mL of anhydrous DMSO was then added to the dried

$K^{18}F$ -Kryptofix 2.2.2 complex. The reaction mixture was stirred and heated to 160 °C for 15 minutes. Product **4.46** was then analyzed using RP-HPLC coupled to a gamma detector and compared to the UV trace of non-radioactive standard **4.45**.

## Chapter Five: Conclusions

In 2008, it was estimated that 12.7 million new cases and 7.6 million deaths occurred worldwide from cancer related diseases<sup>137</sup>. The World Health Organization has recently estimated deaths from cancer to continue to rise to 11 million by 2030, even though it was reported that 30% of cancers could be avoided by reducing high risk factors such as tobacco use, physical inactivity and urban air<sup>137</sup>. More importantly, new approaches in diagnosing and treating cancer at its initial stages may result in a decrease in cancer related deaths.

The development of molecular imaging agents serves as a non-invasive approach to diagnosing cancer related diseases. Molecular imaging can be defined as the “visualization representation, characterization and quantification of a biological process occurring at the cellular and sub cellular levels”<sup>3</sup>. Today, much of the existing research focuses on the design, synthesis and characterization of new imaging agents targeting a variety of cancers. In one approach, an imaging probe is designed and synthesized in order to target a highly overexpressed cancer-specific receptor. In general, this agent consists of two parts: (a) a biomolecular vehicle and (b) a signalling source. In addition to selecting the appropriate targeting vehicle and receptor-ligand, various modifications must be made to ensure the probe displays high specificity and affinity towards the receptor of interest. Following this step, the synthesized probe is then evaluated in a number of in vitro and in vivo assays, to confirm the effectiveness in targeting a cancer-specific receptor.

In this thesis, a molecular imaging agent targeting a highly overexpressed cancer-specific receptor was designed and synthesized. Ghrelin is a 28-amino acid peptide



hormone and is the endogenous ligand for the growth hormone secretagogue receptor (GHSR). Our initial design feature used truncated ghrelin analogues as the biomolecular vehicle, based on evidence suggesting the GHSR was highly overexpressed in a number of tumour models. As an initial study, the objective was to design a non-radioactive imaging probe that could target the GHSR with high affinity and specificity. It was evident from past structure activity relationship studies, that ghrelin's unique Ser-3 lipophilic side chain, N-terminal amine and Phe4 residue were critical for receptor recognition. Thus, the location of the signalling source was positioned towards the C-terminus, off a pendent lysine side chain to avoid interference with ghrelin's N-terminal binding region. Additional modifications by replacing both Ser3 with Dpr3 and the C-terminal carboxylic acid with an amide moiety ensured additional *in vivo* stability.

The design and synthesis of fluorescein-ghrelin **2.21** was accomplished by using an orthogonal protecting group strategy. This ensured the selective addition of both the unique octanoylated side chain and fluorescein isothiocyanate at residues 3 and 19. To our knowledge, this is the first reported design and synthesis of a ghrelin optical imaging agent. Fluorescein-ghrelin **2.21** displayed a 9.5 nM IC<sub>50</sub> value, similar to that of native ghrelin's 8.1 nM affinity for the GHSR. In addition, the half-life of fluorescein-ghrelin **2.21** incubated in rat serum was 33 minutes, which was similar to that of native ghrelin's 27 minute half-life. Thus, the C-terminal addition of a bulky substituent confirms the use of **2.21** to be stable for future *in vivo* imaging studies. Furthermore, **2.21** displayed high uptake in both PC3 and LNCaP cells as well as *ex vivo* prostate cancer tissue. Importantly, preferential uptake was found in prostatic intraepithelial neoplasia (PIN) and prostate cancer (PCa), as compared to normal prostate and benign prostatic hyperplasia (BPH). In an additional study, we looked at GHSR expression in a murine model by

western blot analysis and found the GHSR-1a was overexpressed in the heart and brain. To confirm the expression of the GHSR-1a present within the heart, our fluorescein-ghrelin **2.21** was incubated in ex vivo murine heart tissue. Using confocal microscopy, **2.21** displayed high uptake noted by the bright fluorescence observed within heart tissue. These results suggest an additional use of our fluorescein-ghrelin **2.21** in monitoring heart disease in patients with cardiomyopathy. Both of these studies validated our probes effectiveness in both in vitro and ex vivo imaging studies. More importantly, the design and synthesis of **2.21** allowed us to modify native ghrelin while still maintain potent receptor recognition to the GHSR-1a. These modifications supported the development of positron emission tomography (PET) agents.

The next step in developing an imaging agent was to create a radioactive analogue for PET nuclear imaging. Two different approaches were used to incorporate either gallium-68 or fluorine-18 into the backbone of modified ghrelin.

In the first approach (chapter three), tris-t-butyl-DOTA, a radio-metal chelate, was incorporated into a pendent lysine side chain on the C-terminus of a modified 18-mer ghrelin analogue. A similar orthogonal protecting group strategy as for the synthesis of **2.21** allowed for addition of tris-t-butyl-DOTA. Binding affinities of 2.29 nM and 9.1 nM was observed for both unlabelled **3.6** and gallium labelled **3.7** modified ghrelin, demonstrating the ability to incorporate a radio-metal chelate while still maintaining receptor recognition. The development of a radiolabelling strategy yielded the  $^{68}\text{Ga}$  modified ghrelin **3.8** in a 75% radiochemical yield. To our knowledge, the design and synthesis of a gallium-68 ghrelin analogue used for PET nuclear imaging hasn't been achieved up until now. The effectiveness of **3.8** will be evaluated by imaging a small animal with localized prostate tumours using PET nuclear imaging.

In the second approach (chapter four), non-radioactive fluorine labelled ghrelin analogues were synthesized based on previous results suggesting other bulky, hydrophobic groups could replace ghrelin's unique lipophilic side chain. Initially 18-mer modified ghrelin analogues were synthesized to incorporate either fluorobenzoic acid **4.21** or fluoronaphthoic acid **4.22** into the Dpr3 side chain. Binding assays confirmed the non-radioactive fluorine labelled ghrelin(1-18)-amide analogues had better binding affinity than native ghrelin. Interestingly, incorporating the bulkier naphthyl substituent as in **4.22** provided enhanced binding affinity over benzene **4.21**. This supported the additional design and synthesis of analogues containing naphthyl substituents.

The design and synthesis of lower molecular weight nonradioactive fluorine compounds helped determine the minimal binding sequence capable of binding to the GHSR. Truncated ghrelin(1-8)-amide analogues were synthesized with the addition of Tyr-8 replacing Glu-8, based on previous structure-activity relationships. Modified ghrelin with the less bulky benzene side chain as in **4.24**, reported a 440 nM binding affinity. However, when replacing the native octanoylated side chain with a naphthyl aromatic ring as in **4.25**, the binding affinity drastically improved to 9.9 nM.

Based on the low nM binding affinities, a prosthetic group approach for incorporating radioactive fluorine-18 into the low molecular weight [Tyr8]ghrelin(1-8)-amide analogues was designed. A fluorine-18 labelled naphthalene ring was synthesized using nucleophilic aromatic substitution. To our knowledge this is the first synthesis of a radiolabelled naphthalene ring used as a prosthetic group. Additional methodologies for incorporating this prosthetic group into the Dpr3 side chain need to be evaluated prior to using this agent for PET nuclear imaging.



The development of novel ghrelin-based imaging agents has been discussed for their use in PET nuclear imaging. This project has progressed through the design, synthesis and in vitro evaluation of truncated ghrelin analogues, resulting in fluorine and gallium labelled peptides with high receptor potency. The lead analogues are ready to be evaluated for in vivo stability and specificity. Numerous optimization studies will be needed in order to carry this probe into a pre-clinical study. Nonetheless, the future of ghrelin as a molecular imaging probe for diagnosing early stage prostate cancer looks very promising.



## Chapter Six: References

---

- <sup>1</sup> Lee, S.; Xie, J.; Chen, X. *Chemical Reviews* **2010**, *110*, (5), 3087-3111.
- <sup>2</sup> Hoffmann, J. M.; Gambhir, S. S. *Radiology* **2007**, *244*, (1), 39-47.
- <sup>3</sup> Massoud, T. F.; Gambhir, S. S. *Genes and Development* **2003**, *17*, 545-580.
- <sup>4</sup> Willmann, J. K.; Bruggen, N. V.; Dinkeborg, L. M.; Gambhir, S. S. *Nature Reviews in Drug Discovery* **2008**, *7*, 591-607.
- <sup>5</sup> Jadvar, H. *Nature Reviews in Urology* **2009**, *6*, 317-323.
- <sup>6</sup> Langner, L. **2006**, <http://en.wikipedia.org/wiki/File:PET-MIPS-anim.gif>.
- <sup>7</sup> Wu, A. M.; Olafsen, T. *The Cancer Journal* **2008**, *14*, (3), 191-197.
- <sup>8</sup> Reubi, J. C.; Maecke, H. R. *Journal of Nuclear Medicine* **2008**, *49*, 1735-1738.
- <sup>9</sup> Lee, S.; Xie, J.; Chen, X. *Biochemistry* **2010**, *49*, 1364-1376.
- <sup>10</sup> Reubi, J. C. *Endocrinology Reviews* **2003**, *24*, 389-427.
- <sup>11</sup> Cassoni, P.; Papotti, M.; Ghe, C.; Catapano, F.; Sapino, A.; Graziani, A.; Deghenghi, R.; Reissmann, T.; Ghigo, E.; Muccioli, G. *The Journal of clinical endocrinology and metabolism* **2001**, *86*, (4), 1738-1745.
- <sup>12</sup> Jeffery, P.L.; Herington, A.C.; Chopin, L.K. *The Journal of endocrinology* **2002**, *172*, (3), R7-11.
- <sup>13</sup> Gaytan, F.; Morales, C.; Barreiro, M. L.; Jeffery, P.; Chopin, L. K.; Herington, A. C.; Casanueva, F. F.; Aguilar, E.; Dieguez, C.; Tena-Sempere, M. *The Journal of clinical endocrinology and metabolism* **2005**, *90*, (3), 1798-1804.
- <sup>14</sup> Chan, W. C.; White, P. D. *Fmoc solid phase peptide synthesis: a practical approach*; Oxford University Press, **2000**.
- <sup>15</sup> Haldemann, A. R.; Rosler, H.; Barth, A.; Waser, B.; Geiger, L.; Godoy, N.; Markwalder, R. V.; Seiler, R.; Sulzer, M.; Reubi, J. C. *Journal of Nuclear Medicine* **1995**, *36*, 403-410.
- <sup>16</sup> Benedetti, E.; Morelli, G.; Accardo, A.; Mansi, R.; Tesauro, D.; Aloj, L. *BioDrugs* **2004**, *18*, 279-295.

- 
- <sup>17</sup> Jacobsen, O.; Zhu, L.; Ma, Y.; Weiss, I. D.; Sun, X.; Niu, G.; Kiesewetter, D. O.; Chen, X. *Bioconjugate Chemistry* **2011**, *22*, (3), 422-428.
- <sup>18</sup> Aloj, L.; Morelli, G. *Current Pharmaceutical Design* **2004**, *10*, 3009-3031.
- <sup>19</sup> Merrifield, R. B.; *Journal of the American Chemical Society* **1963**, *85*, 2149-2154.
- <sup>20</sup> Mitchell, A. R. *Peptide Science* **2008**, *90*, (3), 175-184.
- <sup>21</sup> Santini, R.; Griffith, M. C.; Qi, M. *Tetrahedron Letters* **1998**, *39*, 8951-8954.
- <sup>22</sup> Kaiser, E.; Colescot, R. L.; Bossinge, C. D.; Cook, P. I. *Analytical Biochemistry* **1970**, *34*, 595-598.
- <sup>23</sup> West, C. M.; Jones, T.; Price, P. *Nature Review Chemistry* **2004**, *4*, 457-469.
- <sup>24</sup> Cai, L.; Lu, S.; Pike, V. *European Journal of Organic Chemistry* **2008**, *17*, 2843-2853.
- <sup>25</sup> Synder, S.; Kilbourn, M. R. *Chapter 6. Chemistry of Fluorine-18 radiopharmaceuticals*, Wiley and Sons, **2003**.
- <sup>26</sup> Orit, J.; Chen, X. *Current Topics in Medicinal Chemistry* **2010**, *10*, 1048-1059.
- <sup>27</sup> Lau, E. Y.; Greig, J. T. *Biophysics* **1997**, *73*, 1579-1592.
- <sup>28</sup> Van Oosten, E. *Synthesis of Fluorine-19 Labeled Radiopharmaceuticals for Positron Imaging Tomography*, Thesis, **2009**.
- <sup>29</sup> Le Bars, D. *Journal of Fluorine Chemistry* **2006**, *127*, 1488-1493.
- <sup>30</sup> Okarvi, S. M. *European Journal of Nuclear Medicine* **2001**, *28*, 929-938.
- <sup>31</sup> Nickles, R.; Daube, M.; Ruth, T. *The International Journal of Applied Radiation and Isotopes* **1984**, *35*, 117-122.
- <sup>32</sup> Bartholoma, M. D.; Louie, A. S.; Valliant, J. F.; Zubieta, J. *Chemical Reviews* **2010**, *110*, 2903-2920.
- <sup>33</sup> Lambrecht, R.; Sajjid, M. *International Journal for Chemical Aspects of Nuclear Science and Technology* **1998**, *43*, 171-179.
- <sup>34</sup> Rao, J.; Dragulescu-Andrasi, A.; Yao, H. *Current Opinion in Biotechnology* **2007**, *18*, 17-25.

- 
- <sup>35</sup> Cheong, W. F.; Prahl, S. A.; Welch, A. J. *IEEE Journal of Quantum Electronics* **1990**, *26*, 2166-2195.
- <sup>36</sup> Frangioni, J. *Current Opinion in Chemical Biology* **2003**, *7*, 626-634.
- <sup>37</sup> Litchman, J. W.; Conchello, J. A. *Nature Methods* **2005**, *2*, (12), 910-919.
- <sup>38</sup> Willmann, J. K.; Bruggen, N. V.; Dinkelborg, L. M.; Gambhir, S. S. *Nature Reviews* **2008**, *7*, 591-607.
- <sup>39</sup> Rosita, D.; Dewitt, M. A.; Luyt, L. G. *Journal of Medicinal Chemistry* **2009**, *52*, (8), 216-2203.
- <sup>40</sup> Jemal, A.; Seigel, R.; Xu, J.; Ward, E. *A Cancer Journal for Clinicians* **2010**, *60*, (5), 277-300.
- <sup>41</sup> Rosser, C. J. *BMC Urology* **2008**, *8*, (20), 1-3.
- <sup>42</sup> National cancer institute. 2011, [www.cancer.gov/cancertopics/factsheet/detection/PSA](http://www.cancer.gov/cancertopics/factsheet/detection/PSA).
- <sup>43</sup> Thompson, I. M.; Pauler, D. K.; Goodman, P. J.; Catherine, M.; Tangen, P. H.; Lucia, M. S.; Howard, L.; Parnes, M. D.; Minasian L. M; Leslie, G. F.; Lippman, S. M.; Crawford, E. D.; Crowley, J. J.; Coltman, C. A. *New England Journal of Medicine* **2004**, *350*, (22), 2239-2246.
- <sup>44</sup> Smith, D. D.; Humphrey, P. A.; Catalona, W. J. *American Cancer Society: Communication* **1997**, *80*, (9), 1852-1856.
- <sup>45</sup> Schroder, F. H.; Hugrosson, J.; Roobol, M. J.; Tammela, T. L.; Ciatto, S.; Nelen, V.; Kwiatkowski, M.; Lujan, H.; Zappa, M.; Denis, L. J.; Recker, F.; Berenguer, A.; Maattanen, L.; Bangma, C. H.; Aug, G.; Villers, A.; Rebillard, X.; Van-der Kwast, T.; Blijenberg, B. G.; Moss, S. M.; de Koning, H. J.; Auvinen, A. *New England Journal of Medicine* **2009**, *360*, (13), 1320-1328.
- <sup>46</sup> Van Leeuwen, P. J.; Connolly, D.; Gavin, A.; Roobol, M. J.; Black, A.; Bangma, C. H.; Schroder, F. H. *European Journal of Cancer* **2010**, *46*, (2), 377-383.
- <sup>47</sup> Hricak, H.; Choyke, P. L.; Eberhardt, S. C.; Leibel, S. A.; Scardino, P. T. *Radiology* **2007**, *243*, (1), 28-53.
- <sup>48</sup> Fricke, E.; Machtens, S.; Hofmann, M.; Van Den Hoff, J.; Bergh, S.; Brunkhorst, T.; Meter, G. J.; Karstens, J. H.; Knapp, W. H.; Boerner, A. R. *European Journal of Nuclear Medicine and Molecular Imaging* **2003**, *30*, (4), 607-611.
- <sup>49</sup> Hofer, C.; Laubenbacher, C.; Block, T.; Breul, J.; Hartung, R.; Schwaiger, M. *European Journal of Urology* **1999**, *36*, (1), 31-35.



- 
- <sup>50</sup> Koa, P. F.; Chou, Y. H.; Lai, C. W. *Clinical Nuclear Medicine* **2008**, *33*, (4), 308-310.
- <sup>51</sup> Effert, P. J.; Bares, R.; Handy, S.; Wolff, J. M.; Bill, U.; Jakse, G. *The Journal of Urology* **1996**, *155*, 994-998.
- <sup>52</sup> Mohler, J.; Bahnon, R. R.; Botton, B.; Busby, J. E.; D'Amico, A.; Eastham, J. A.; Enke, C. A.; George, D.; Horwitz, E. M.; Huben, R. P.; Kantoff, P.; Kawachi, M.; Kuettel, M.; Lange, P. H.; Macvicar, G.; Plimack, E. R.; Pow-Sang, J. M.; Roach, M.; Rohren, E.; Roth, B. J.; Shrieve, D. C.; Smith, M. R.; Srinivas, S.; Twardowski, P.; Walsh, P. C. *NCCN Clinical Practice Guidelines in Oncology* **2010**, *8*, (2), 162-200.
- <sup>53</sup> Thompson, I.; Thrasher, J. B.; Aus, G.; Burnet, A. L.; Canby-Hagino, E. D.; Cookson, M. S.; D'Amico, A. V.; Dmochowski, R. R.; Eton, D. T.; Forman, J. D.; Goldenberg, S. L.; Hernandez, J.; Higano, C. S.; Kraus, S. R.; Moul, J. W.; Tangen, C. M. *The Journal of Urology* **2007**, *177*, (6), 2106-2131.
- <sup>54</sup> Mustafi, D.; Palczewski, K. *Molecular Pharmacology* **2009**, *75*, 1-12.
- <sup>55</sup> Kroeze, W. K.; Sheffler, D. J.; Roth, B. L. *Journal of Cell Science* **2003**, *116*, (24), 4867-4869.
- <sup>56</sup> Lander, E. S *et al. Nature* **2001**, *409*, 1-12.
- <sup>57</sup> Flower, D. R. *Biochimica et Biophysica Acta* **1999**, *1422*, 207-234.
- <sup>58</sup> Kristiansen, K. *Pharmacology Therapeutics* **2004**, *103*, 21-80.
- <sup>59</sup> Smith, R. G.; Vanderploeg, L. H.; Howard, A. D.; Feighner, S. D.; Cheng, K.; Hickey, G. J.; Wyvratt, M. J.; Fisher, M. H.; Nargund, R. P. Patchett, A. A. *Endocrine Reviews* **1996**, *18*, 621-245.
- <sup>60</sup> Jeffery, P. L.; Herrington, A. C.; Chopin, L. K. *Cytokine and Growth Factor Reviews* **2003**, *14*, 113-122.
- <sup>61</sup> Guan, X. M.; Yu, H.; Palyha, O. C.; McKee, K. K.; Feighner, S. D.; Sirinathsinghji, D. J.; Smith, R. G.; Ploeg, L. H.; Howard, A. D. *Molecular Brain Research* **1997**, *48*, 23-29.
- <sup>62</sup> Petersenn, S.; Rasch, A. C.; Penschorn, M.; Beil, F. U.; Schulte, H. M. *Endocrinology* **2011**, *142*, 2649-2659.
- <sup>63</sup> Ueberberg, B.; Unger, N, Saeger, W.; Mann, K.; Petersenn, S. *Hormone Metabolism Research* **2009**, *41*, 814-21.



- 
- <sup>64</sup> Gnanapavan, S.; Kola, B.; Bustin, S. A.; Morris, D. G.; McGee, P.; Fairclough, P.; Bhattacharya, S.; Carpenter, R.; Grossman, A. B.; Korbonits, M. *The Journal of clinical endocrinology and metabolism* **2002**, *87*, (6), 2988-2991
- <sup>65</sup> Gaytan, F.; Barreiro, M. L.; Caminos, J. E.; Chopin, L. K.; Herington, A. C.; Morales, C.; Pinilla, L.; Paniagua, R.; Nistal, M.; Casanueva, F. F.; Aguilar, E.; Dieguez, C.; Tena-Sempere, M. *The Journal of Clinical Endocrinology and Metabolism* **2004**, *89*, (1), 400-409.
- <sup>66</sup> Volante, M.; Allia, E.; Gugliotta, P.; Funaro, A.; Broglio, F.; Deghenghi, R.; Muccioli G.; Ghigo, E.; Papotti, M. *The Journal of Clinical Endocrinology and Metabolism* **2002**, *87*, (3), 1300-1308.
- <sup>67</sup> Papotti, M.; Cassoni, P.; Volante, M.; Deghenghi, R.; Muccioli, G.; Ghigo, E. *The Journal of Clinical Endocrinology and Metabolism* **2001**, *86*, (10), 5052-5059.
- <sup>68</sup> Kojima, M.; Hosoda, H.; Date, Y.; Nakazato, M.; Matsui, H.; Kangawa, K. *Nature* **1999**, *402*, 656-660.
- <sup>69</sup> Veldhuis, J. D.; Bowers, C. Y. *International Journal of Peptides* **2010**, *2010*, 1-40.
- <sup>70</sup> Nikolopoulos, D.; Theocharis, S.; Kouraklis, G. *Regulatory Peptides* **2010**, *163*, 7-17.
- <sup>71</sup> GroBauer, J.; Kosol, S.; Schrank, E.; Zangger, K. *Bioorganic and Medicinal Chemistry* **2010**, *18*, 5483-5488.
- <sup>72</sup> Howard, A. D.; Feighner, S. D.; Cully, D. F.; Arena, J. P.; Liberatore, P. A.; Rosenblum, C. L.; Hamelin, M.; Hreniuk, D. L.; Palyha, O. C.; Anderson, J.; Paress, P. S.; Diaz, C.; Chou, M.; Liu, K. K.; McKee, K. K.; Pong, S. S.; Chung, L. Y.; Elbrecht, A.; Dashkevich, M.; Heavens, P.; Rigby, M.; Sirinathsighji, D. J.; Dean, D. C.; Melillo, D. G.; Patchett, A. A.; Nargund, R.; Griffin, P. R.; DeMartino, J. A.; Gupta, S. K.; Schaeffer, J. M.; Smith, R. G.; Van der Ploeg, L. H. *Science* **1996**, *273*, 974-977.
- <sup>73</sup> Matsumoto, M.; Hosoda, H.; Kitajima, Y.; Morozumi, N.; Minamitake, Y.; Tanaka, S.; Matsuo, H.; Kojima, M.; Hayashi, Y.; Kangawa, K. *Biochemical and Biophysical Communications* **2001**, *287*, 142-146.
- <sup>74</sup> Matsumoto, M.; Kitajima, Y.; Iwanami, T.; Hayashi, Y.; Tanaka, S.; Minamitake, Y.; Hosoda, H.; Kojima, M.; Matsuo, H.; Kangawa, K. *Biochemical and Biophysical Communications* **2001**, *284*, 655-659.
- <sup>75</sup> Van Craenenbroeck, M.; Gregoire, F.; De Neef, P.; Robberecht, P.; Perret, J. *Peptides* **2004**, *25*, 959-965.

- 
- <sup>76</sup> Bednarek, M. A.; Feighner, S. D.; Pong, S.; McKee, K. K.; Hreniuk, D. L.; Silva, M. V.; Warren, V. A.; Howard, A. D.; Van der Ploeg, L. H. Y.; Heck, J. V. *The Journal of Medicinal Chemistry* **2000**, *43*, 4370-4376.
- <sup>77</sup> Camina, J. P.; Carreira, M. C.; El Messari, S.; Llorens-Cortes, C.; Smith, R. G.; Casanueva, F. F. *Endocrinology* **2004**, *145*, 930-940.
- <sup>78</sup> Rosita, D.; Dewitt, M. A.; Luyt, L. G. *Journal of Medicinal Chemistry* **2009**, *52*, (8), 216-2203.
- <sup>79</sup> De Vriese, C.; Gregoire, F.; Lema-Kiskoka, R.; Waelbroeck, M.; Robberecht, P.; Delporte, C. *Endocrinology* **2004**, *145*, 4997-5005.
- <sup>80</sup> Montet, X.; Yaun, H.; Weissleder, R.; Josephson, L. *A Journal of Technical Methods and Pathology* **2006**, *86*, (5), 517-525.
- <sup>81</sup> Beiras-Fernandez, A.; Kreth, S.; Weis, F.; Ledderose, C.; Pottinger, T.; Dieguez, C.; Beiras, A.; Reichart, B. *Peptides* **2010**, DOI:10.1016/j.peptides.2010.08.019.
- <sup>82</sup> Lai, K. C.; Cheng, C. H.; Leung, P. S. *Pancreas* **2007**, *35*, 1-8.
- <sup>83</sup> McGirr, R.; McFarland, M. S.; McTavish, J.; Luyt, L. G.; Dhanvantari, S. *Regulatory Peptides* **2011**, *in press*.
- <sup>84</sup> Behnam Azad, B.; Rota, V. A.; Breadner, D.; Dhanvantari, S.; Luyt, L. G. *Bioorganic and Medicinal Chemistry* **2010**, *18*, 1265-72.
- <sup>85</sup> McGirr, R.; Hu, S.; Yee, S. P.; Kovacs, M. S.; Lee, T. Y.; Dhanvantari, S. *Molecular Imaging and Biology* **2010**, Epub ahead of print.
- <sup>86</sup> Lu, C.; McFarland, M. S.; Nesbitt, R.; Williams, A.; Chan, S.; Gomez-Lemus, J.; Autran, A.; Alzahrani, A.; Chin, J.; Izawa, J.; Luyt, L. G.; Lewis, J. *The Prostate* **2011**, *in press*.
- <sup>87</sup> Heppeler, A.; Froidevaux, S.; Eberle, A. N.; Maecke, H. R. *Current Medicinal Chemistry* **2000**, *7*, 971-994.
- <sup>88</sup> Behr, T. M.; Gotthardt, M.; Barth, A.; Behe, M. *The Quarterly Journal of Nuclear Medicine and Molecular Imaging* **2001**, *45*, 189-200.
- <sup>89</sup> Breeman, W. A.; de Jong, M.; Kwekkeboom, D. J. *et al. European Journal of Nuclear Medicine* **2001**, *28*, 1421-1429.
- <sup>90</sup> Okavari, S. M. *Nuclear Medicine Communications* **1999**, *20*, 1093-1112.
- <sup>91</sup> Weiner, R. E.; Thakur, M. L. *Applied Radiation and Isotopes* **2002**, *57*, 749-763.

- 
- <sup>92</sup> Forster, G. J.; Engelbach, M.; Brockmann, J. J.; Reber, H. J.; Buchholz, H. G.; Macke, H. R.; Rosch, F. R.; Herzog, H. R.; Bartenstein, P. R. *European Journal of Medicinal Chemistry* **2001**, *28*, 1743-1750.
- <sup>93</sup> Jamar, F.; Barone, R.; Mathieu, I.; Walrand, S.; Carlier, P.; de Camps, J.; Schran, H.; Chen, T.; Smith, M. C.; Bouterfa, H.; Valkema, R.; Krenning, E. P.; Kvols, L. K.; Pauwels, S. *European Journal of Nuclear Medicine and Molecular Imaging* **2003**, *30*, (4), 510-518.
- <sup>94</sup> Hofmann, M.; Maeck, H.; Borner, R.; Weckesser, E.; Schoffski, P.; Oei, L.; Schumacher, J.; Henze, M.; Heppeler, A.; Meyer, J.; Knapp, H. *European Journal of Nuclear Medicine* **2001**, *28*, (12), 1751-1757.
- <sup>95</sup> Henze, M.; Shumacher, T.; Hipp, P.; Kowalski, J.; Becker, D. W.; Doll, J.; Macke, H. R.; Hofmann, M.; Debus, J.; Haberkorn, U. *Journal of Nuclear Medicine* **2001**, *42*, (7), 1053-1056.
- <sup>96</sup> Ugur, O.; Kothari, P. J.; Finn, R. D.; Zanzonico, P.; Ruan, S.; Guenther, I.; Maecke, H. R.; Larson, S. M. *Nuclear Medicine and Biology* **2002**, *29*, (2), 147-157.
- <sup>97</sup> Khan, M. U.; Khan, S. El-Refaie, S.; Win, Z.; Rubello, D.; Al-Nahhas, A. *European Journal of Surgical Oncology* **2009**, *35*, 561-567.
- <sup>98</sup> Griffiths, G. L.; Chang, C.; McBride, W. J.; Rossi, E. A.; Sheerin, A.; Tejada, G. R.; Karacay, H.; Sharkey, R. M.; Horak, I. D.; Hansen, H. J.; Goldenberg, D. M. *Journal of Nuclear Medicine* **2004**, *45*, 30-39.
- <sup>99</sup> Fani, M.; Andre, J. P.; Maecke, H. R. *Contrast Media and Molecular Imaging* **2008**, *3*, 53-63.
- <sup>100</sup> Loc'h, C.; Maziere, B.; Comar, D. *Journal of Nuclear Medicine* **1980**, *21*, 171-173.
- <sup>101</sup> Hnarowich, D. J. *International Journal of Applied Radiation and Isotopes* **1977**, *28*, 169-181.
- <sup>102</sup> Hunatowich, D. J. *Progress in Nuclear Medicine* **1978**, *4*, 113-117.
- <sup>103</sup> Green, M. A.; Welch, M. J. *International Journal of Applied Radiation and Instrumentation* **1989**, *16*, 435-448.
- <sup>104</sup> Moerlein, S. M.; Welch, M. J. *International Journal of Nuclear Medicine and Biology* **1981**, *8*, 277-287.
- <sup>105</sup> Maecke, H. R.; Andre, J. P. *Ernst Schering Research Found Workshop* **2007**, *62*, 215-242.



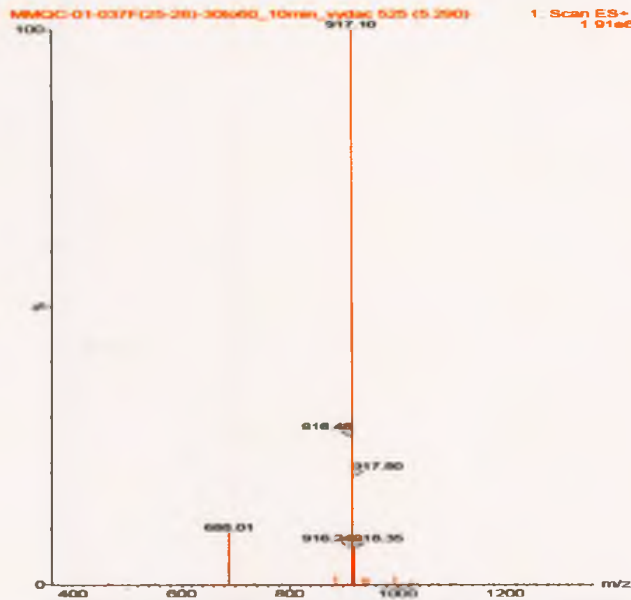
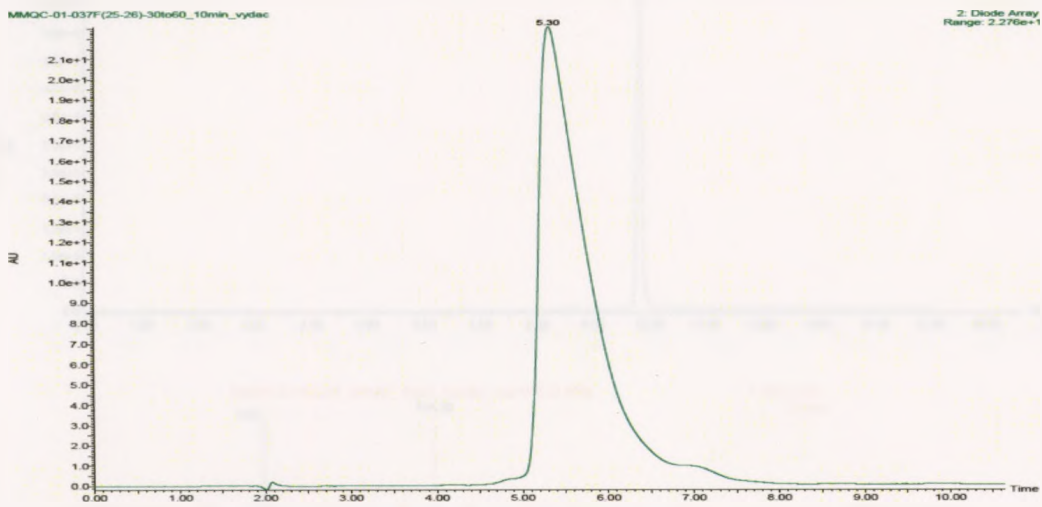
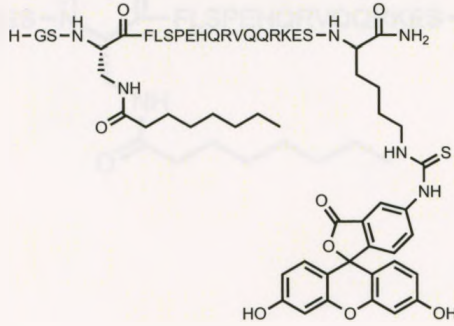
- 
- <sup>106</sup> Deutsch, E. *Journal of Nuclear Medicine* **1993**, *34*, 1132-1133.
- <sup>107</sup> Wadas, T. J.; Wong, E. H.; Weisman, G. R.; Anderson, C. J. *Chemical Reviews* **2010**, *110*, 2858-2902.
- <sup>108</sup> Koukouraki, S.; Strauss, L. G.; Georgoulas, V.; Schuhmacher, J.; Haberkorn, U.; Karkavitas, N.; Dimitrakopoulou-Strauss, A. *European Journal of Nuclear Medicine and Molecular Imaging* **2006**, *33*, 460-466.
- <sup>109</sup> Carpino, L. A. *Journal of the American Chemical Society* **1993**, *115*, 4379.
- <sup>110</sup> Carpino, L. A.; El-Faham, A. *Journal of Organic Chemistry* **1994**, *59*, 695.
- <sup>111</sup> Albericio, F.; Abdelmoty, I.; Bofill, J. M.; Carpino, L. A.; El-Faham, A.; Foxman, D. F.; Gairi, M.; Griffin, G. W.; Kates, S. A.; Lloyd-Williams, P.; Scarmoutzos, L. M.; Shroff, H.; Triolo, S. A.; Wenschuh, H. *In Peptides 1994: Proceedings of the Twenty-Third European Peptide Symposium; Maia, H. L. S., Ed.; ESCOM; Leiden, 1995*, 60-61.
- <sup>112</sup> De Goeij, J. J. M.; Bonardi, M. L. *Journal of Radioanalytical and Nuclear Chemistry* **2005**, *263*, (1), 13-18.
- <sup>113</sup> Jalilian, A. R.; Tabatabai, S. A.; Shafiee, A.; Afarideh, H.; Najafi, R.; Bineshmarvasti, M. *Journal of Labeled Compounds and Radio-Pharmaceuticals* **2000**, *43*, 545-555.
- <sup>114</sup> Nickels.; Pham, W. *IFMBE Proceedings* **2010**, *27*, 35-38.
- <sup>115</sup> Smart, B. E. *Journal of Fluorine Chemistry* **2001**, *109*, 3-11.
- <sup>116</sup> M. J. Welch, C. S. Redvanly (Eds.), *Hand Book of Radiopharmaceuticals: Radiochemistry and Applications*, John Wiley & Sons, Ltd, **2003**.
- <sup>117</sup> Wester, H. J.; Herz, M.; Weber, P.; Heiss, R.; Senekowitsch-Schmidtke, R.; Schwaiger, M.; Stocklin, G. *Journal of Nuclear Medicine* **1999**, *40*, (1), 205-212.
- <sup>118</sup> Fowler, J. S.; Finn, R. D.; Lambrecht, R. M.; Wolf, A. P. *Journal of Nuclear Medicine* **1973**, *14*, (1), 63-64.
- <sup>119</sup> Tomiyoshi, K.; Amed, K.; Muhammad, S.; Huguchi, T.; Inoue, T.; Endo, K.; Yang, D. *Nuclear Medicine Communications* **1997**, *18*, 169-175.
- <sup>120</sup> Lim, J. L.; Zheng, L.; Berridge, M. S.; Tewson, T. J. *Nuclear Medicine and Biology* **1996**, *23*, 911-915.
- <sup>121</sup> Lemaire, C.; Cantineau, R.; Guillaume, M.; Plenevaux, A.; Chrstiaens, L. *Journal of Nuclear Medicine* **1991b**, *32*, (12), 2266-2272.

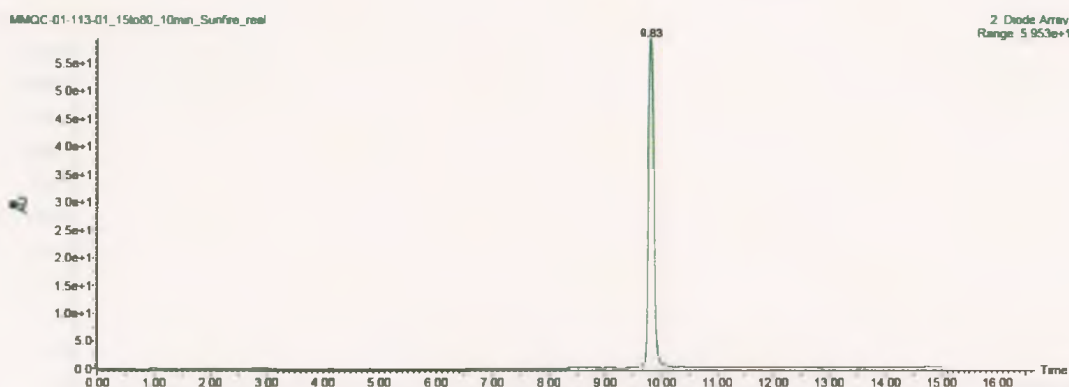
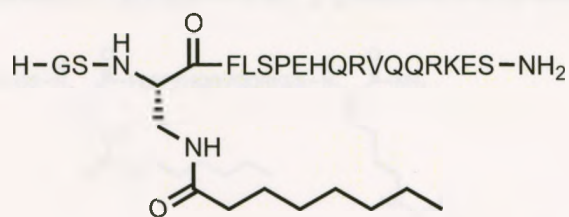


- 
- <sup>122</sup> Ding, Y. S.; Fowler, J. S.; Gatley, S. J.; Dewey, S. L.; Wolf, A. P. *Journal of Medicinal Chemistry* **1991a**, *34*, 767-771.
- <sup>123</sup> Som, P.; Atkins, H. L.; Bandoypadhyay, D.; Fowler, J. S.; MacGregor, R. R.; Matsui, K.; Oster, Z. H.; Sacker, D. F.; Shiue, C. Y.; Turner, H.; Wan, C. N.; Wolf, A. P.; Zabinksi, S. V. *Journal of Nuclear Medicine* **1980**, *21*, 670-675.
- <sup>124</sup> Shen, B. *Studies on the Nucleophilic Aromatic <sup>18</sup>F-Fluorination*, Thesis Dissertation, **2008**.
- <sup>125</sup> Le Bars, D. *Journal of Fluorine Chemistry* **2006**, *127*, (11), 1688-1493.
- <sup>126</sup> Miller, P. W.; Long, N. J.; Vilar, R.; Gee, A. D. *Angewandte Chemie International Edition* **2008**, *47*, 8998-9033.
- <sup>127</sup> Ehrenkaufer, R. E.; Potocki, J. F.; Jewett, D. M. *Journal of Nuclear Medicine* **1984**, *25*, 333.
- <sup>128</sup> Cai, L.; Lu, S.; Pike, V. W. *European Journal of Organic Chemistry* **2008**, *17*, 2841-3024.
- <sup>129</sup> Lin, Y. C.; Hung, G. H.; Luo, T. Y.; Tsai, S. C.; Sun, S. S.; Hsia, C. C.; Chen, S. L.; Lin, W. Y. *Annals of Nuclear Medicine* **2007**, *21*, (1), 79-83.
- <sup>130</sup> Marik, J.; Sutcliffe, J. L. *Applied Radiation and Isotopes* **2007**, *65*, 199-203.
- <sup>131</sup> Lane, C. F. *Synthesis* **1975**, 135-146.
- <sup>132</sup> Shen, B. *Studies on the Nucleophilic Aromatic <sup>18</sup>F-fluorination* **2008**, dissertation.
- <sup>133</sup> Seimbille, Y.; Phelps, M. E.; Czernin, J.; Silverman, D. H. S. *Journal of Labeled Compounds and Radiopharmaceuticals* **2005**, *48*, 829-843.
- <sup>134</sup> Sowmiah, S.; Srinivasadeskan, V.; Tseng, M.; Chu, Y. *Molecules* **2009**, *128*, 806-812.
- <sup>135</sup> Okamoto, A.; Tainaka, K.; Saito, I. *Bioconjugate Chemistry* **2005**, *16*, 1105-1111.
- <sup>136</sup> Chakraborty, D.; Gowda, R. R.; Malik, P. *Tetrahedron Letters* **2009**, *50*, 6553-6556.
- <sup>137</sup> Ferlay, J.; Shin, H. R.; Bray, F.; Forman, D.; Mathers, C.; Parkin, D. M. GLOBOCAN 2008, v1.2, Cancer Incidence and Mortality Worldwide: IARC CancerBase No. 10 [Internet]. Lyon, France: International Agency for Research on Cancer; 2010. Available from: <http://globocan.iarc.fr>, accessed on 15/07/2011.

**Appendix A:  $^1\text{H-NMR}$ , HPLC and MS-ESI of selected compounds**

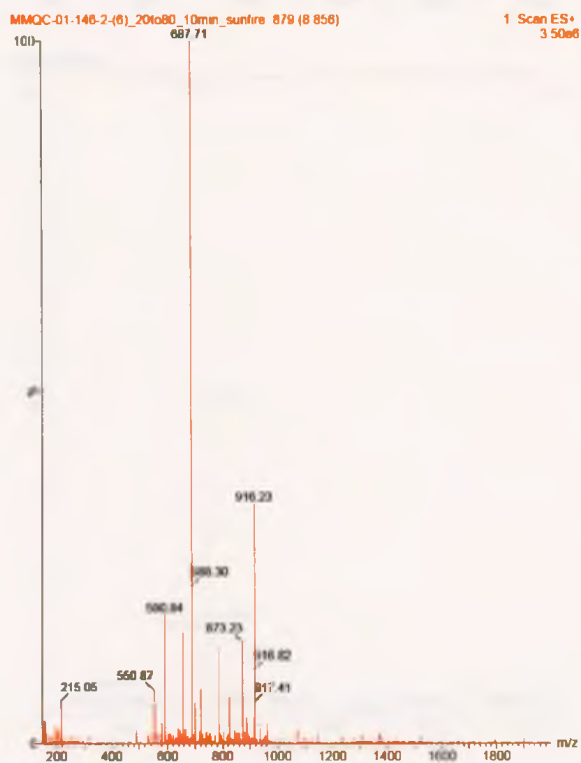
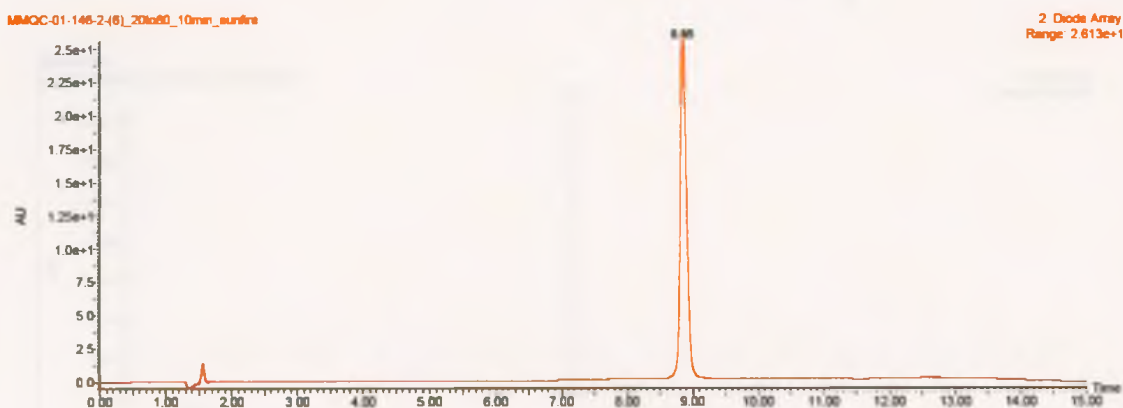
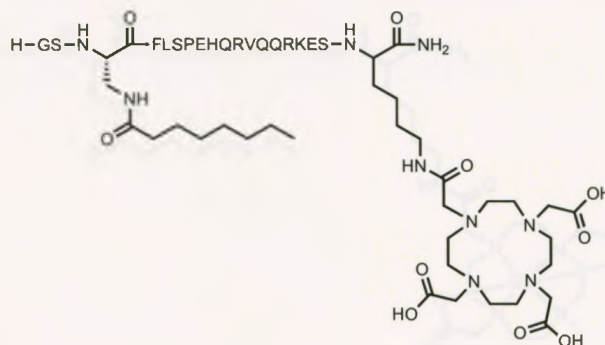
*HPLC and MS-ESI spectra of [Dpr<sup>3</sup> (Octanoicacid)][Lys<sup>19</sup> (Fluorescein)]ghrelin(1-19)-amide (2.21)*



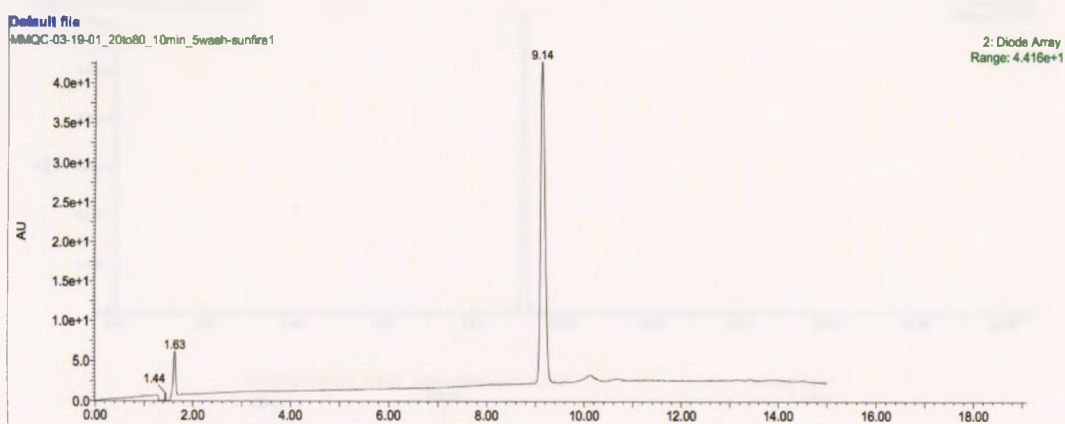
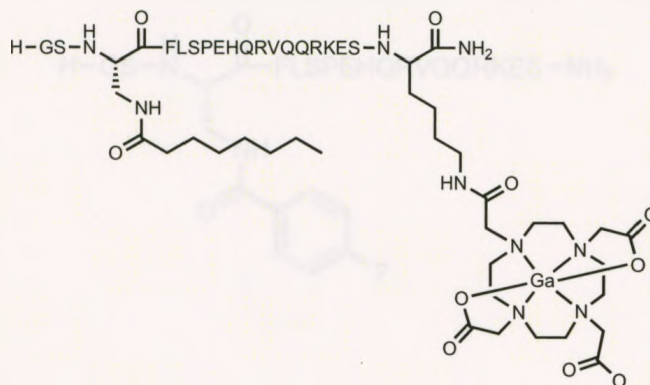
*HPLC and MS-ESI spectra of [Dpr<sup>3</sup> (Octanoic acid)] ghrelin(1-18)-amide (2.22)*



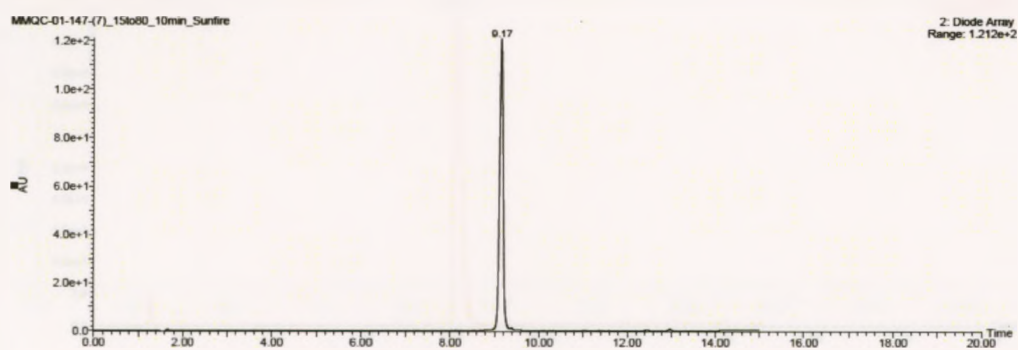
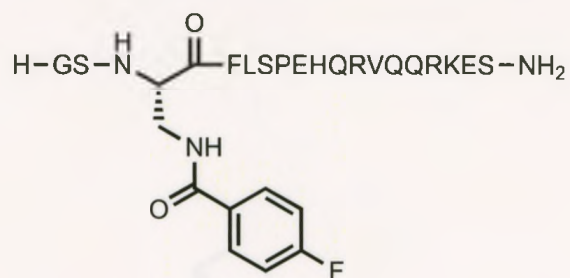
**HPLC and MS-ESI spectra of  
[Dpr(octanoyl)<sup>3</sup>, Lys(DOTA)<sup>19</sup>] ghrelin(1-19)-amide (3.6)**



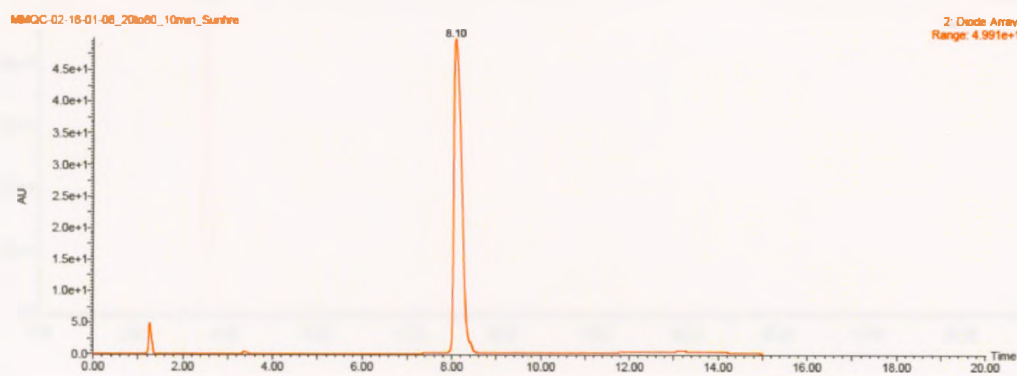
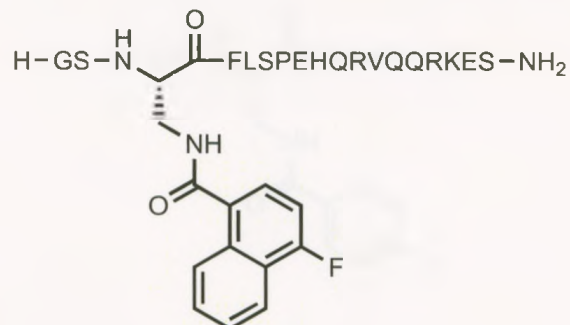
**HPLC and MS-ESI spectra of  
[Dpr(octanoyl)<sup>3</sup>, Lys(Ga<sup>69/70</sup>-DOTA)<sup>19</sup>] ghrelin(1-19)-amide (3.7)**



*HPLC and MS-ESI spectra of  
[Dpr<sup>3</sup>(fluorobenzoic acid)]Ghrelin(1-18)-amide (4.21)*

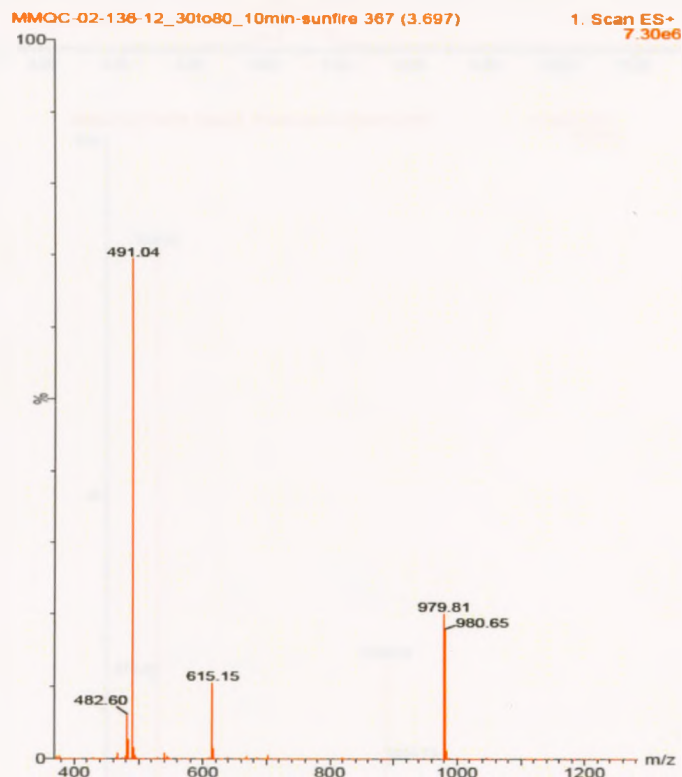
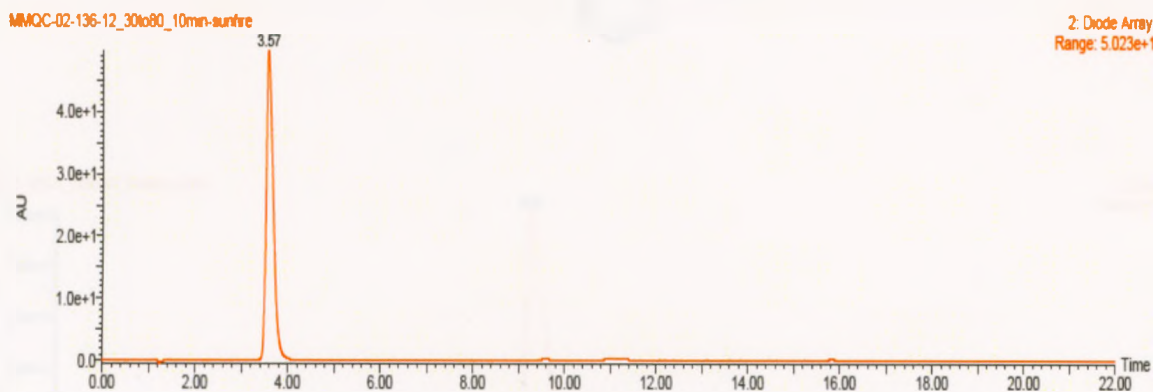
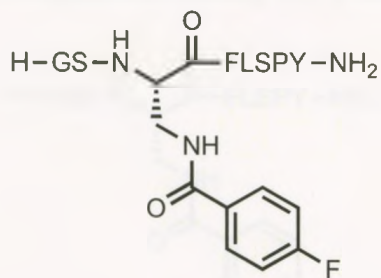


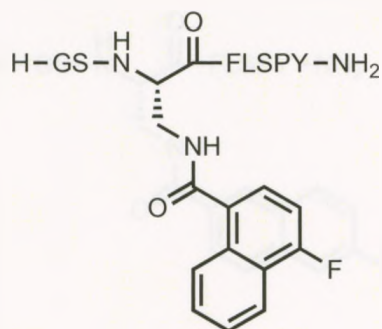
HPLC and MS-ESI spectra of  
[Dpr<sup>3</sup>(4-fluoro-1-naphthoic acid)]Ghrelin(1-18)-amide (4.22)



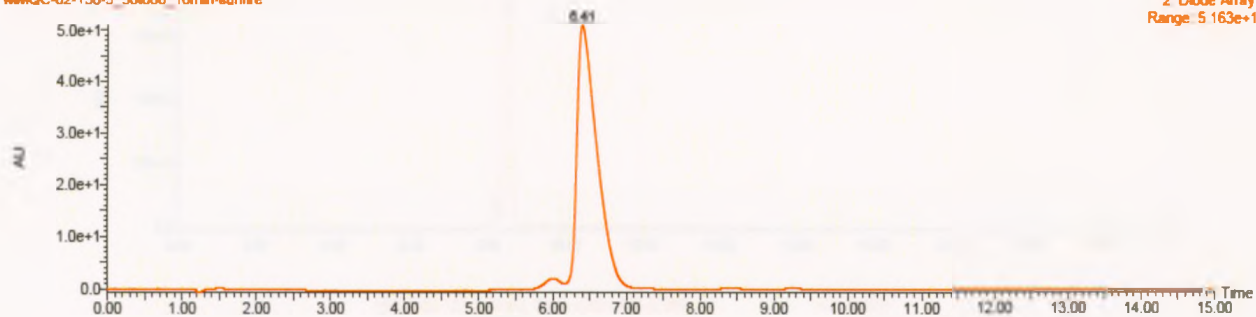


*HPLC and MS-ESI spectra of [Dpr<sup>3</sup>(fluorobenzoic acid)][Tyr<sup>8</sup>]Ghrelin(1-8)-amide (4.24)*

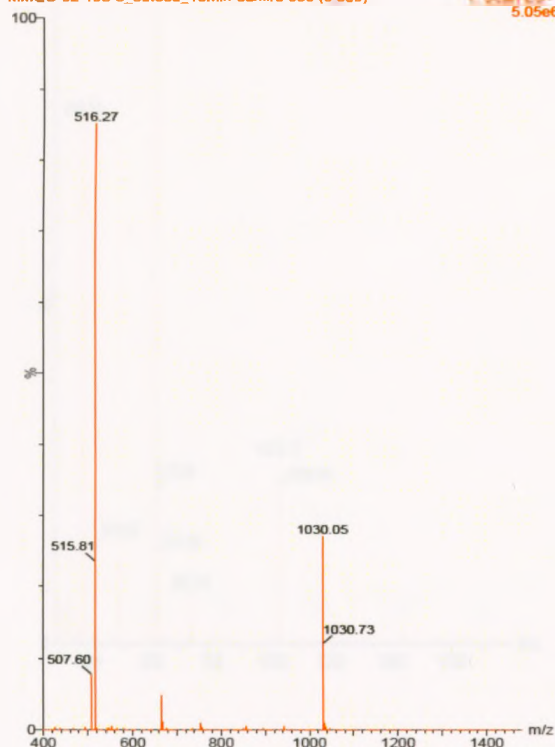


*HPLC and MS-ESI spectra of**[Dpr<sup>3</sup>(4-fluoro-1-naphthoic acid)][Tyr<sup>8</sup>]Ghrelin(1-8)-amide (4.25)*

MMQC-02-138-5\_30to80\_10min-sunfire

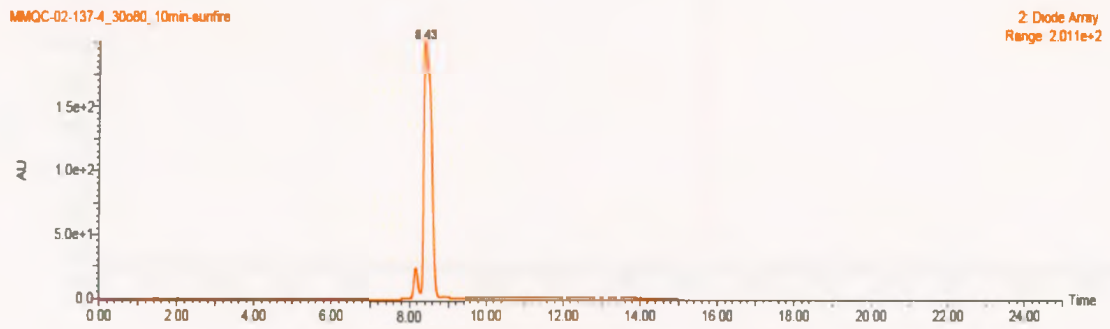
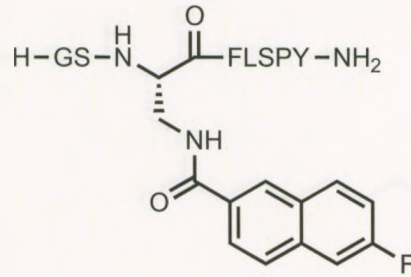


MMQC-02-138-5\_30to80\_10min-sunfire 656 (6.609)

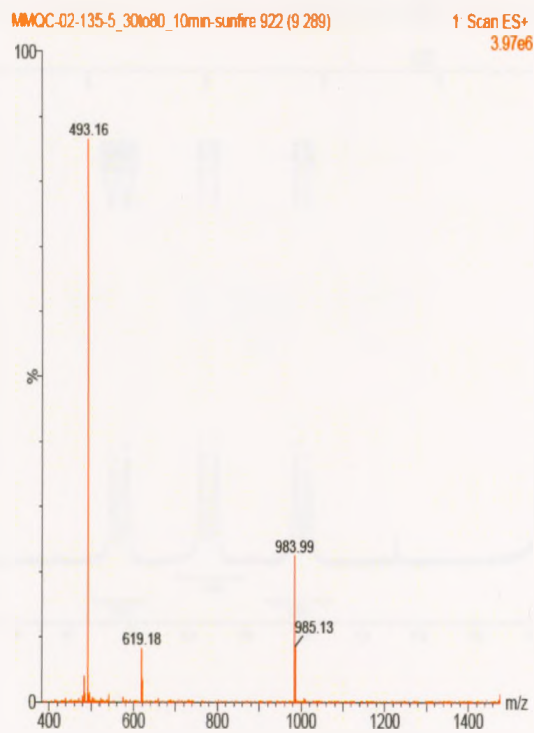
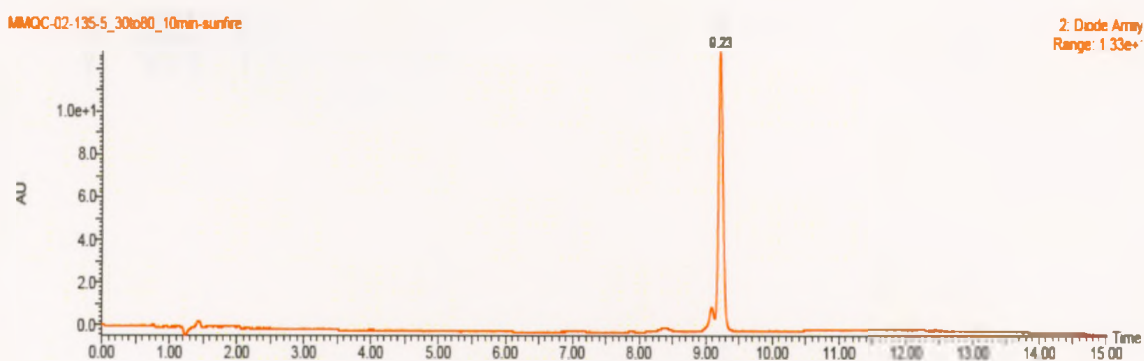
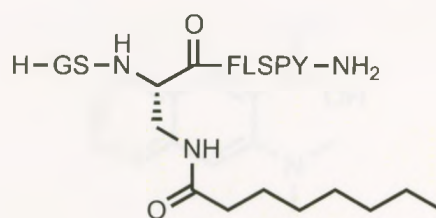
1. Scan 139  
5.05e6

*HPLC and MS-ESI spectra of*

*[Dpr<sup>3</sup>(6-fluoro-2-naphthoic acid)][Tyr<sup>8</sup>]Ghrelin(1-8)-amide (4.26)*

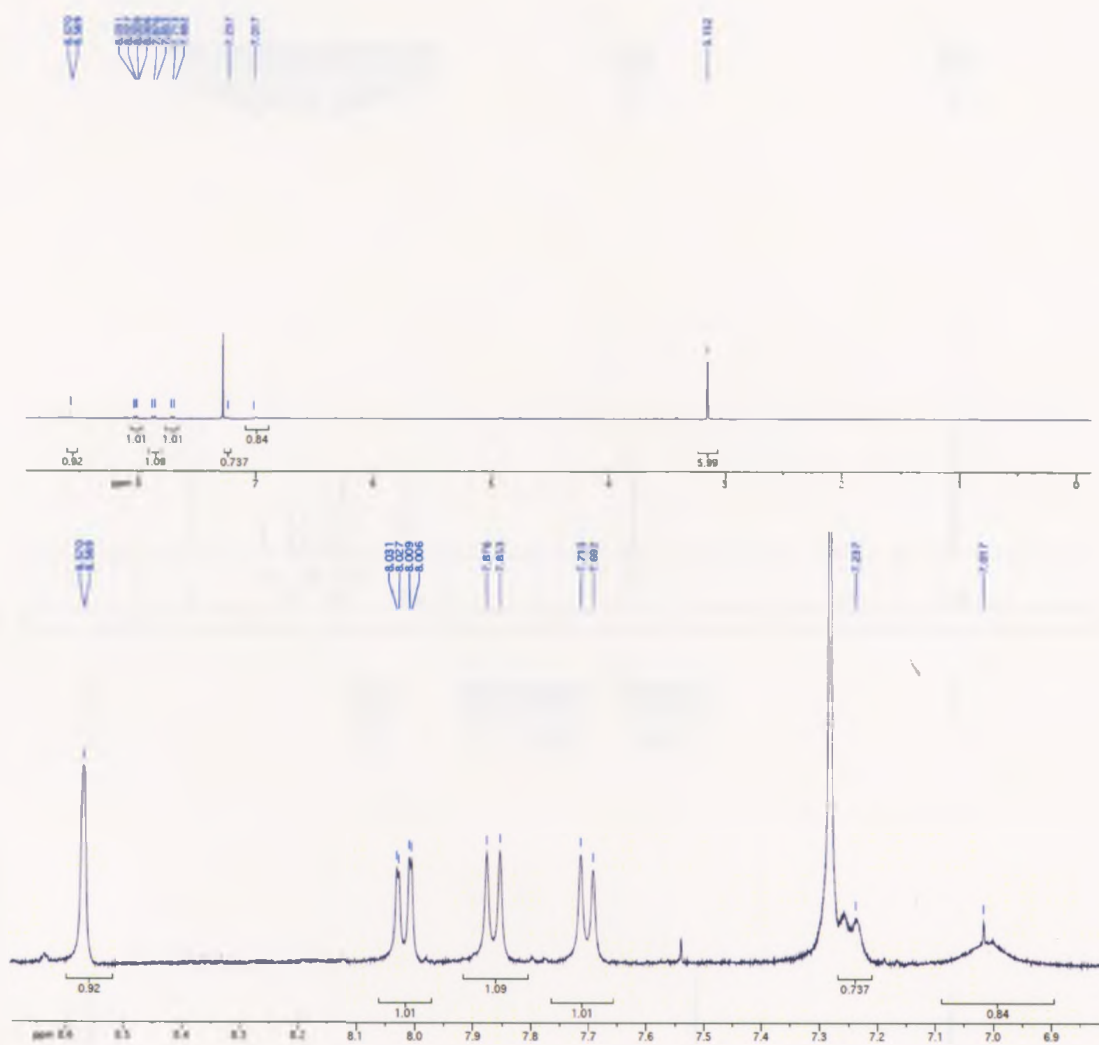
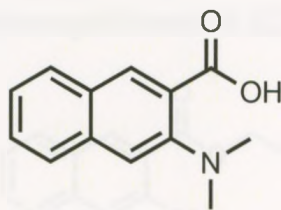


*HPLC and MS-ESI spectra of*  
*[Dpr<sup>3</sup>(Octanoic acid)] [Tyr<sup>8</sup>]Ghrelin(1-8)-amide (4.27)*



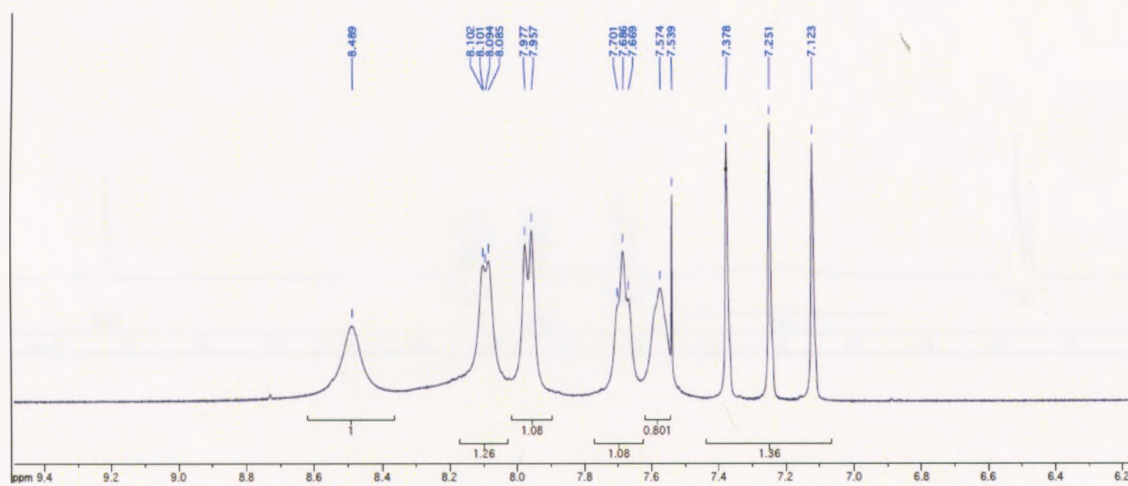
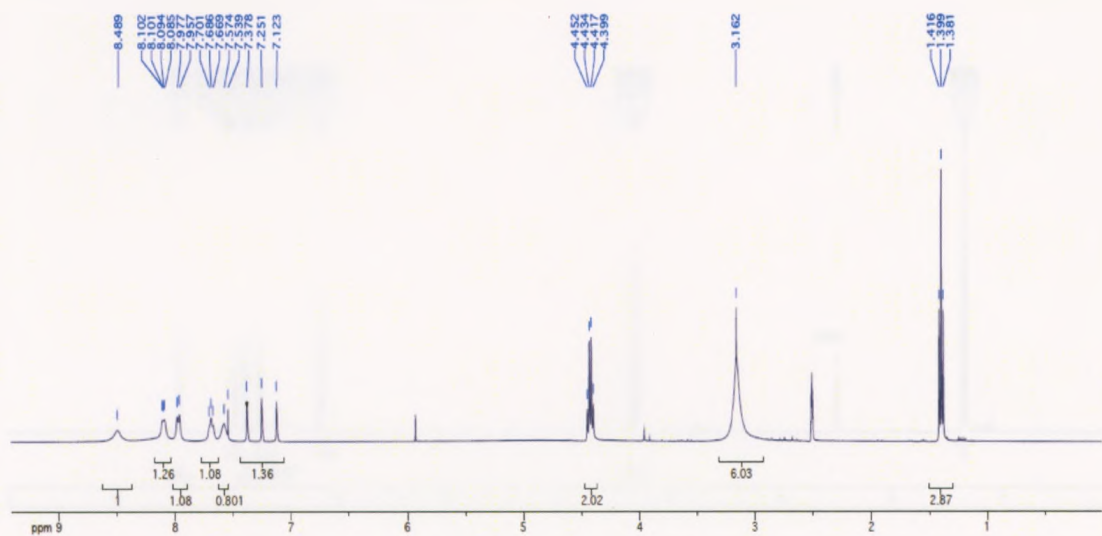
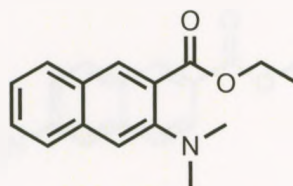


*<sup>1</sup>H-NMR spectrum of*  
*3-dimethylamino-2-naphthoic acid (4.31) in CDCl<sub>3</sub>*

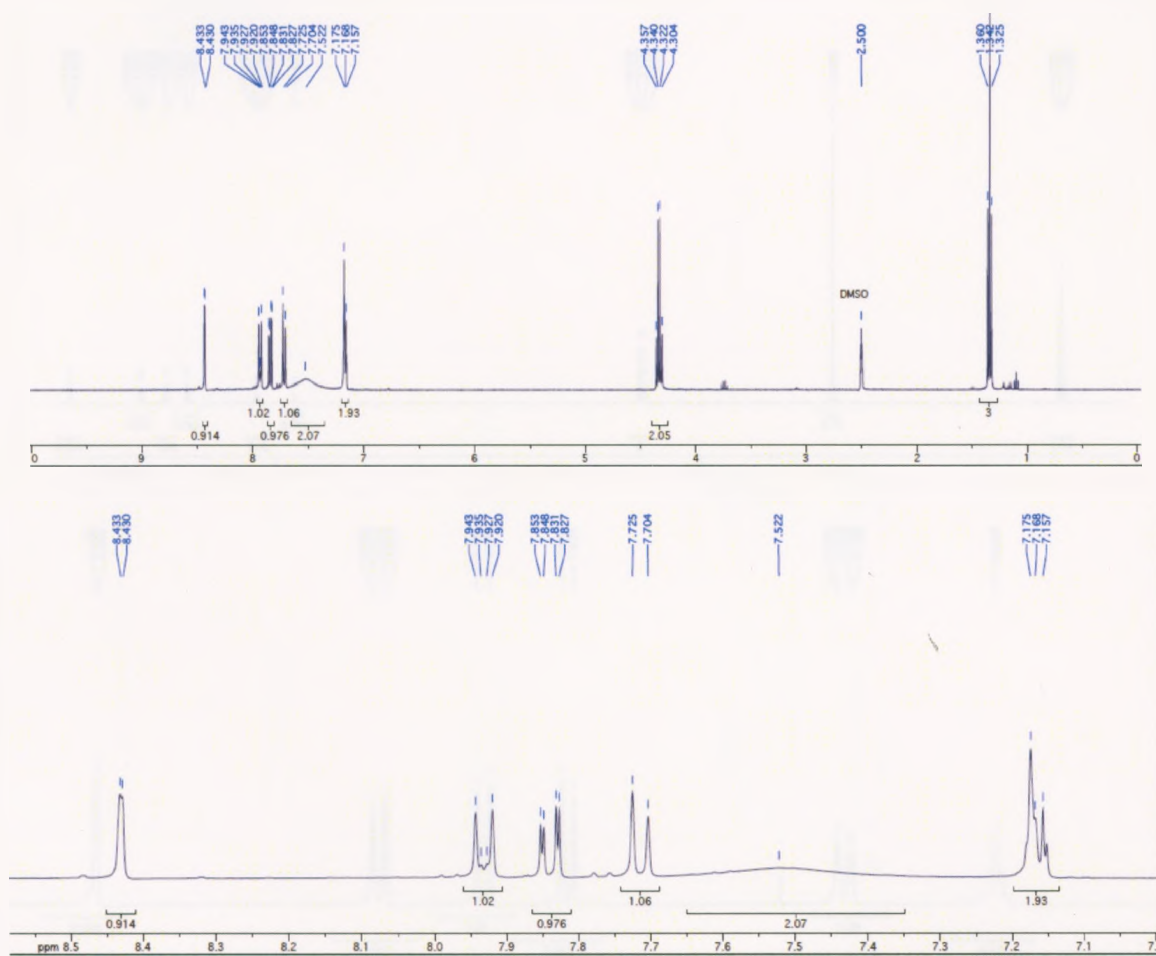
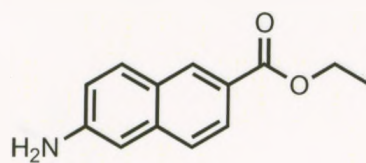




*<sup>1</sup>H-NMR spectrum of*  
**2-Ethyl 3-dimethylaminonaphthoate (4.33) in DMSO-d<sub>6</sub>**

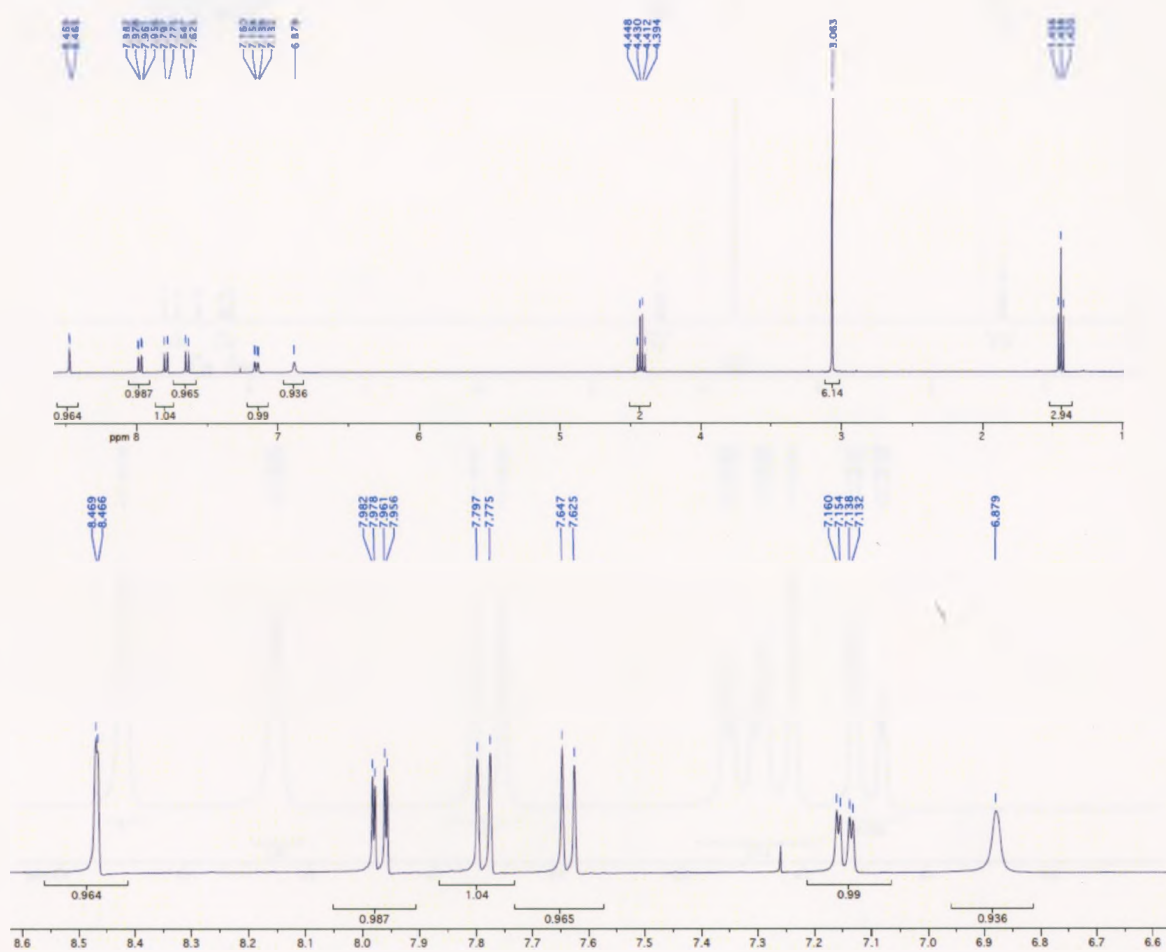
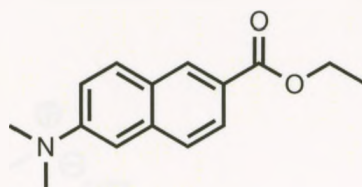


*<sup>1</sup>H-NMR spectrum of*  
*2-Ethyl 6-aminonaphthoate (4.39) DMSO-d<sub>6</sub>*

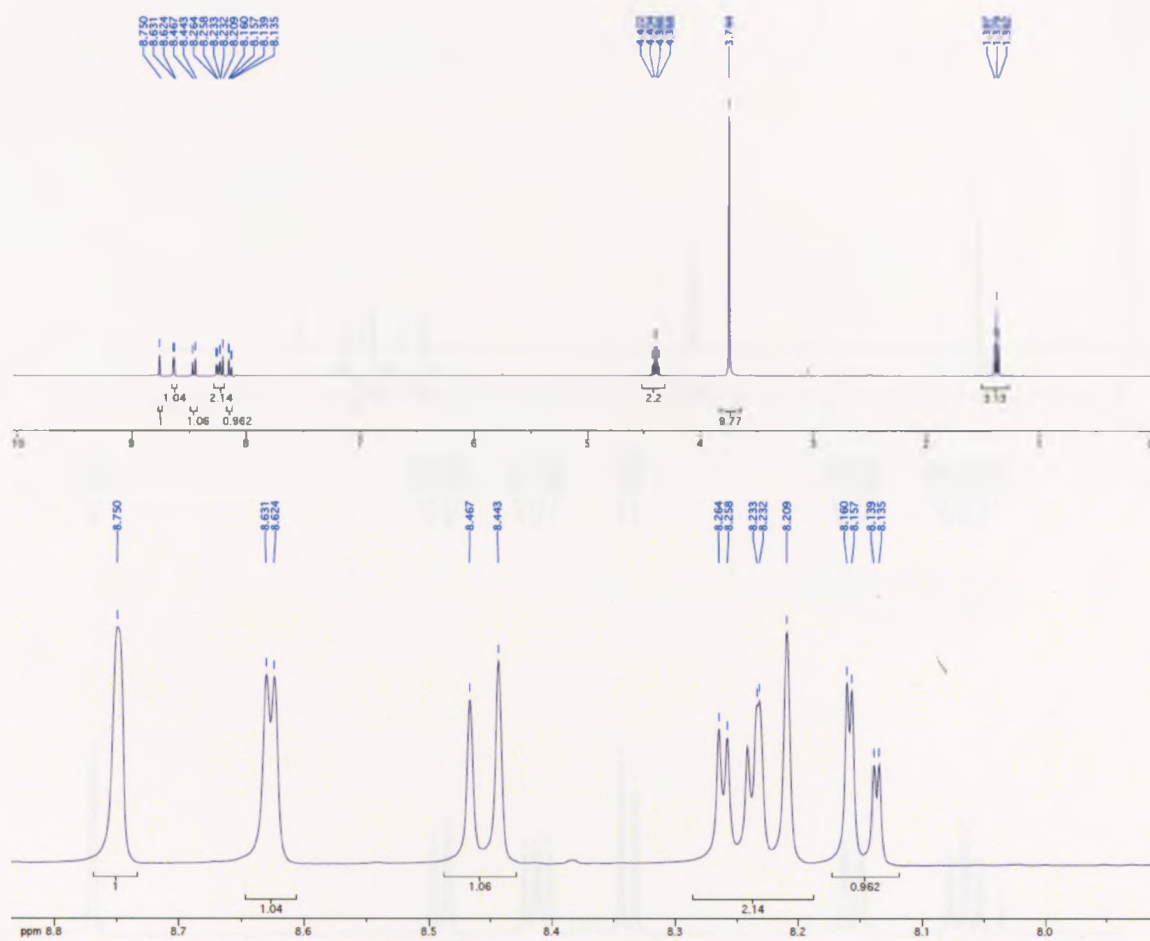
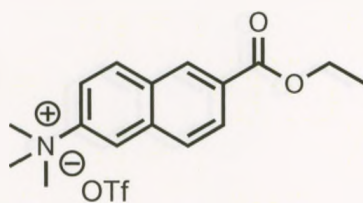




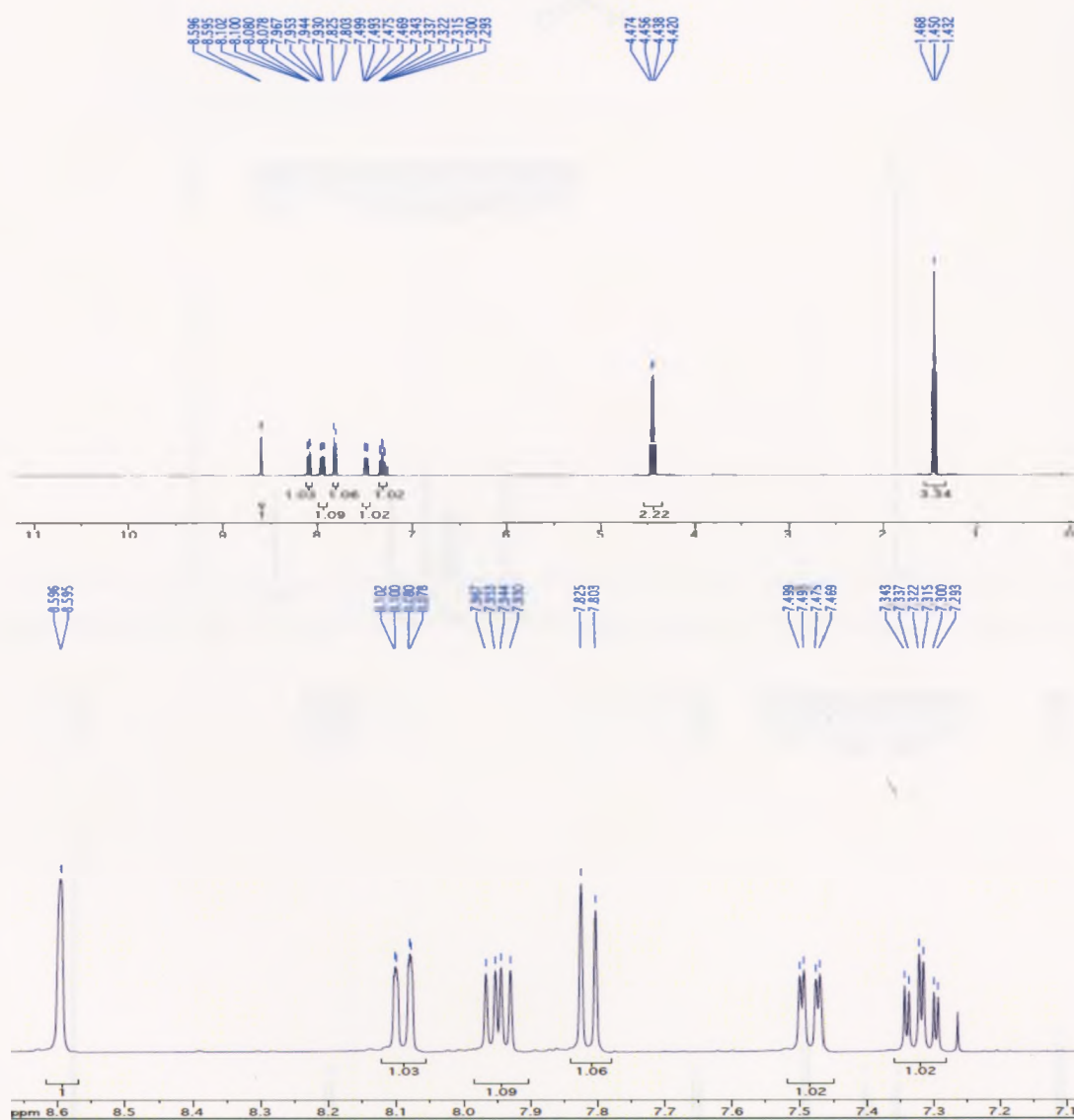
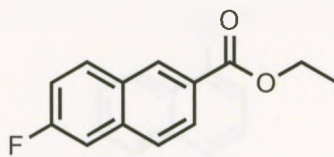
*<sup>1</sup>H-NMR spectrum of*  
*2-Ethyl 6-dimethylaminonaphthoate (4.40) in CDCl<sub>3</sub>*



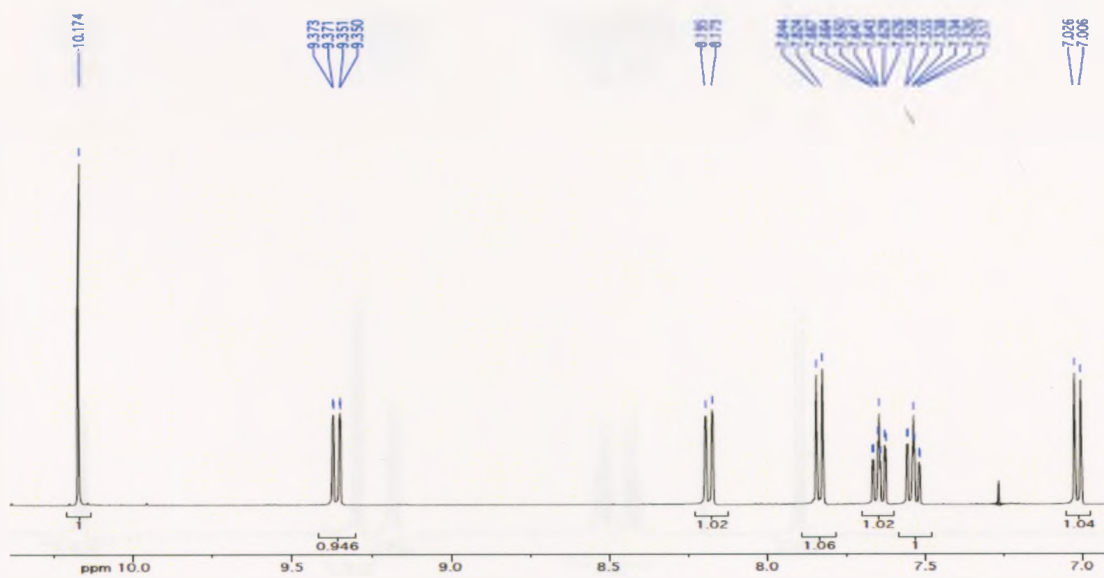
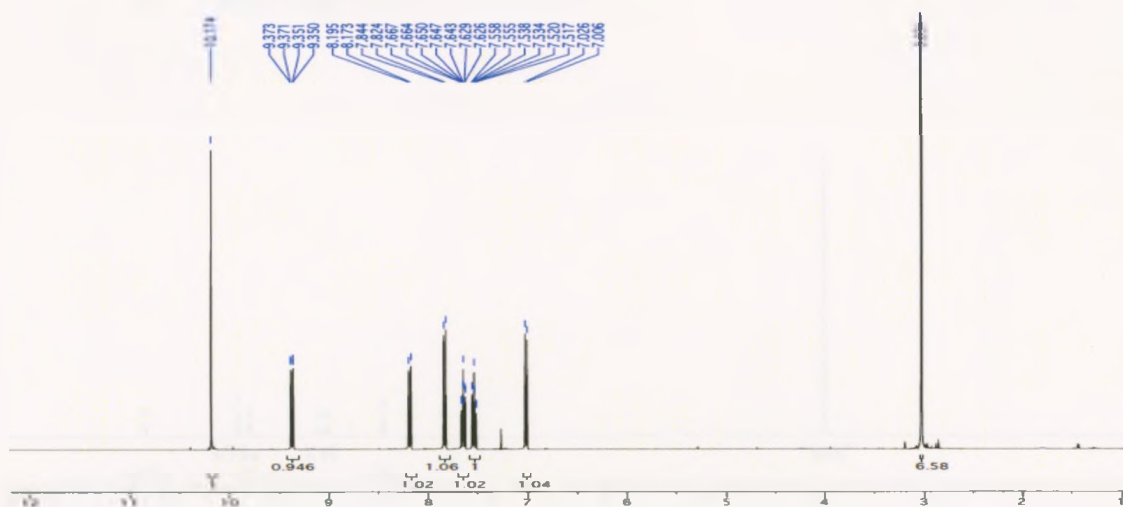
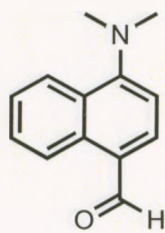
*<sup>1</sup>H-NMR spectrum of*  
*2-Ethyl 6-(N, N, N-trimethylammonium)-naphthoate (4.41) in DMSO-d<sub>6</sub>*



1.1.1  $^1\text{H-NMR}$  spectrum of  
2-Ethyl 6-fluoronaphthoate (4.45) in  $\text{CDCl}_3$

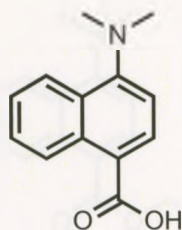


*<sup>1</sup>H-NMR spectrum of*  
*4-dimethylamino-1-naphthylaldehyde (4.51) in CDCl<sub>3</sub>*

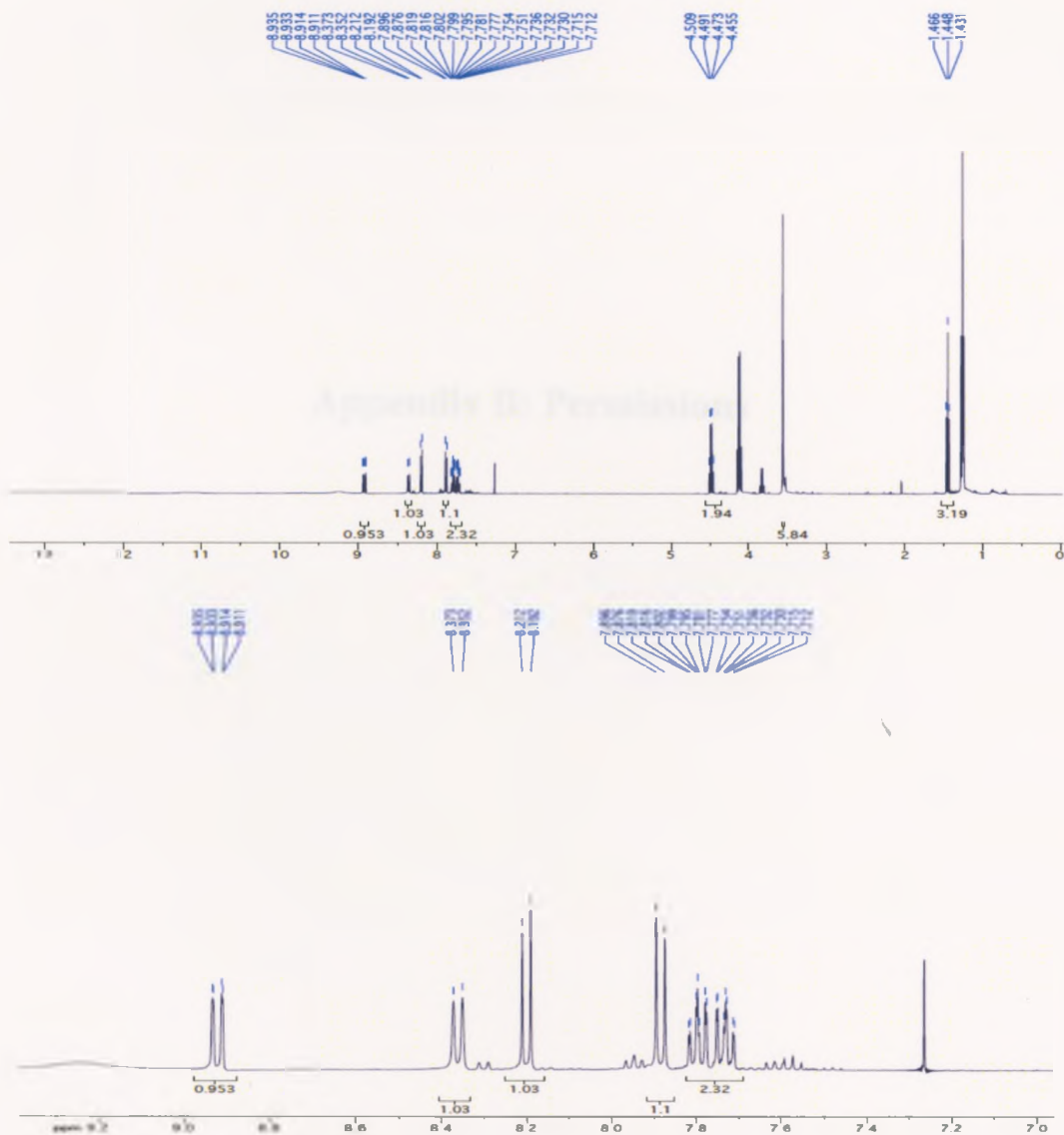
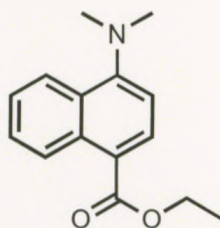




*<sup>1</sup>H-NMR spectrum of*  
*4-dimethylamino-1-naphthoic acid (4.51) in CDCl<sub>3</sub>*



*<sup>1</sup>H-NMR spectrum of*  
*1-Ethyl-4-dimethylamino-naphthoate (4.52) in CDCl<sub>3</sub>*



**Appendix B: Permissions**

Permission for parts of Chapter two:

Reproduced in part with permission from Regulatory Peptides and The Prostate,  
submitted for publication.